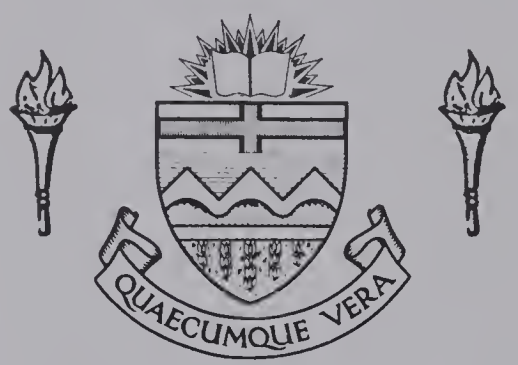

The University of Alberta
Printing Department
Edmonton, Alberta

THE UNIVERSITY OF ALBERTA

NUMERICAL SOLUTION FOR COMBINED FREE AND FORCED LAMINAR CONVECTION WITH AND WITHOUT HEAT SOURCES IN INCLINED TUBES

by

© SHUN-WU HONG, B.Sc.
(National Taiwan University)

A THESIS

SUBMITTED TO THE FACULTY OF GRADUATE STUDIES

IN PARTIAL FULFILMENT OF THE REQUIREMENTS FOR THE DEGREE

OF MASTER OF SCIENCE

DEPARTMENT OF MECHANICAL ENGINEERING

EDMONTON, ALBERTA

Spring, 1971

THE UNIVERSITY OF ALBERTA

FACULTY OF GRADUATE STUDIES

The undersigned certify that they have read, and recommend to the Faculty of Graduate Studies for acceptance, a thesis entitled "NUMERICAL SOLUTION FOR COMBINED FREE AND FORCED LAMINAR CONVECTION WITH AND WITHOUT HEAT SOURCES IN INCLINED TUBES" submitted by SHUN-WU HONG in partial fulfilment of the requirements for the degree of Master of Science.

ABSTRACT

A theoretical study is presented for hydrodynamically and thermally fully developed combined free and forced laminar convection with upward flow in inclined tubes subjected to a uniform wall heat flux. The case with uniform internal heat generation within the fluid is also studied. A numerical solution using a combination of boundary vorticity method and a line iterative relaxation method is employed, and a comparison is made between the numerical analysis and the small amount of analytical data available in the literature. The numerical solution converges up to a reasonably high value of the characteristic parameter where generally an asymptotic behavior for flow and heat transfer results already appears, and further results can be obtained by a linear extrapolation.

The results of the present investigation show that the perturbation analysis in terms of power series of Rayleigh number has a rather limited range of applicability for the present problem, and reveal further that a maximum value for Nusselt number does not exist for any tube inclination angle with given values of the dimensionless parameters which is clearly contrary to the result from perturbation solution. The tube inclination angle, or body-force orientation effects on flow and heat transfer characteristics are clarified for upward laminar flow configuration, and show that in high Rayleigh number regime the tube orientation effect has considerable influence on the results in the neighborhood of horizontal direction. Typical graphical results for velocity and temperature

profiles, flow and heat transfer parameters are presented. The influence of each parameter such as Re, Ra, Pr, F and α on flow and heat transfer results is clarified in this study.

ACKNOWLEDGEMENTS

The author wishes to extend his appreciation to

- Dr. K.C. Cheng for his supervision of this thesis,
- Dr. G.J. Hwang and Mr. M. Akiyama for their valuable suggestions,
- The University of Alberta for computer calculation,
- Mrs. E.S. Buchanan for her patience in typing this thesis,
- National Research Council of Canada for research assistantship through grant NRC A-1655,
- his mother and friends for their constant encouragement.

TABLE OF CONTENTS

LIST OF FIGURES

LIST OF TABLES

NOMENCLATURE

A = axial pressure gradient in fluid, $-(\partial P/\partial Z+\rho_w g \sin \alpha)$

$\underline{A}$ = matrix

A_r = cross section area, πa^2

a = radius of tube

a_i, b_i, c_i, d_i = element of vector

C = axial temperature gradient, $\partial T/\partial Z$

C_p = constant pressure specific heat

$\underline{d}$ = vector form

F = heat source parameter, $aQ/\rho C_p \nu C$

f = friction factor, $2\tau_w/(\rho \bar{W}^2)$, or a dummy variable, see equation (2.12)

$\underline{f}$ = vector form

g = gravitational acceleration

G = function defined in equation (2.12)

$\bar{h}$ = average heat transfer coefficient

k = thermal conductivity

M = number of divisions in R-direction

N = number of divisions in ϕ-direction

Nu = Nusselt number, $\bar{h}(2a)/k$

P = pressure

Pr = Prandtl number, ν/κ

Q = volume heat source rate

R,ϕ,Z = cylindrical coordinates

Ra = Rayleigh number, $\beta g C a^4/\nu\kappa$

Re = Reynolds number, $A\ a^3/4\rho\nu^2$

r = dimensionless radial coordinate, R/a

S = pipe circumference, $2\pi a$

T = local temperature

U,V,W = velocity components in R, ϕ and Z directions

u,v,w = dimensionless velocity components in R, ϕ and Z directions

| | = absolute value

$\sum$ = summation

[ ] = matrix

GREEK LETTERS

α = angle of tube inclination, see Fig. 1

β = coefficient of thermal expansion

ε = a prescribed error

θ = dimensionless temperature difference, $(T_w-T)/Re\ C\ a\ Pr$

κ = thermal diffusivity, $k/\rho\ C_p$

μ = viscosity

ω = relaxation factor, see equation (2.19)

ν = kinematic viscosity, μ/ρ

ξ = vorticity function defined by equation (2.8)

ρ = density

τ = shear stress

ψ = dimensionless stream function

∇^2 = dimensionless Laplacian operator, $\partial^2/\partial r^2+\partial/r\partial r+\partial^2/r^2\partial\phi^2$

SUBSCRIPTS

b = value at boundary

c = characteristics value

i,j = space subscripts of grid point in R and ϕ directions

M = bulk mean value

0 = condition for pure forced convection without heat source in horizontal tube

s = integration along circumference of tube

w = value at wall

SUPERSCRIPTS

(n) = nth iteration

$\overline{}$ = average value

CHAPTER I

INTRODUCTION

1.1 Review of Pertinent Literature Relating to Laminar Forced Convection in Inclined Tubes with Buoyancy Effect.

Fully developed laminar convective heat transfer in various heated or cooled ducts with double helix secondary flow caused by such body forces as buoyancy forces in gravitational or rotating field, centrifugal or Coriolis forces acting in a cross-section normal to the main flow has been studied by many investigators in recent years. It is evident that in many practical problems the body forces cannot always be expected to act in a direction normal to the main flow. It is noted that the two limiting cases of combined free and forced laminar convections in vertical and horizontal tubes have been studied rather extensively in the past. Fully developed combined free and forced laminar convection in vertical tubes or channels leads to a linear partial differential equation and various classical analytical methods can be applied for the solution. In contrast for the case of combined free and forced laminar convection in horizontal tubes the classical analytical methods cannot be readily applied since the governing differential equations are nonlinear. Morton [1] approached the combined free and forced laminar convection in uniformly heated horizontal tubes at low Rayleigh numbers using a perturbation method. The perturbation method is of mathematical interest, but is now known to be applicable only for rather low characteristic parameter flow regime which is not important in design.

The influence of tube orientation on fully developed combined free and forced laminar convection was recently studied by Iqbal and Stachiewicz [2] using a perturbation method identical to Morton's [1]. In view of the fact that the perturbation method as demonstrated in the literature for convective heat transfer with secondary flow diverges quickly with the increase of the characteristic parameter, it is desirable to study tube inclination angle or body-force orientation effect on fully developed combined free and forced laminar convection in uniformly heated tubes by another method. It is of interest to point out that Mori and Futagami [3] presented a theoretical analysis for the problem treated by Morton [1] which is valid for high ReRa regime only by employing boundary-layer approximation. In an attempt to bridge the gap between the perturbation method and the boundary-layer approximation, Hwang and Cheng [4] approached the same problem numerically by using a combination of line iterative method and boundary vorticity method. It was pointed out therein that the newly developed boundary vorticity method is applicable to a general convective heat transfer with secondary flow.

The study of forced convection in tubes or channels with internal heat generation has also been carried out by many investigators in recent years because of possible applications in nuclear and chemical reactors. Fully developed combined free and forced laminar convection in vertical tubes [5] or channels [6,7,8,9] with uniform internal heat generation has been studied rather completely. In contrast, for the same problem in horizontal tubes, only one study [10] using a perturbation method is reported in the literature. In this study, combined free and forced laminar convection in inclined tubes with uniform internal heat generation will also be studied. The present study can be considered as an

extension or generalization of the combined free and forced laminar convection in vertical or horizontal tubes reported in the literature.

1.2 Purpose of Present Investigation.

The purpose of this investigation is to demonstrate the applicability of the boundary vorticity method [4,11] for a steady fully developed combined free and forced laminar convection in uniformly heated inclined tubes with and without uniform internal heat generation and present accurate numerical results for flow and heat transfer. Besides clarifying the flow and heat transfer characteristics in inclined tubes, comparisons with the available data in the literature will be made. In order to limit the scope of the present study, consideration will be given only to the case of fully developed upward laminar flow in the inclined tubes subjected to only one type of thermal boundary condition. It should be emphasized that the present study represents a generalization or extension of the previous studies dealing with vertical or horizontal tubes, and is an asymptotic case for the Graetz problem in inclined tubes which apparently has not been solved yet.

CHAPTER II

THEORETICAL ANALYSIS

2.1 Formulation of the Problem.

Consideration is given to a steady hydrodynamically and thermally fully developed forced laminar upward flow of viscous incompressible fluid with uniform internal heat generation in an inclined tube subjected to the thermal boundary conditions of axially uniform wall heat flux and peripherally uniform wall temperature at any axial position. The following assumptions are made to facilitate the theoretical analysis:

1. Physical properties of fluid are considered to be constant except density variation with temperature in buoyancy term (Boussinesq approximation).
2. Viscous dissipation is negligible.
3. Axial pressure gradient is constant.

Introducing cylindrical coordinates (R, ϕ, Z) as shown in Fig. 1, and applying the assumptions stated above, the governing equations for the present problem take the following forms:

Continuity equation

$$\frac{\partial(RU)}{\partial R} + \frac{\partial V}{\partial \phi} = 0 \tag{2.1}$$

Momentum equation in R-direction

$$\rho \left(U\frac{\partial U}{\partial R} + \frac{V}{R}\frac{\partial U}{\partial R} - \frac{V^2}{R}\right) = -\frac{\partial P}{\partial R} + \mu \left(\frac{\partial^2 U}{\partial R^2} + \frac{1}{R}\frac{\partial U}{\partial R}\right.$$

$$\left. + \frac{1}{R^2}\frac{\partial^2 U}{\partial \phi^2} - \frac{U}{R^2} - \frac{2}{R^2}\frac{\partial V}{\partial \phi}\right) - \rho g \cos\alpha \cos\phi \tag{2.2}$$

Momentum equation in ϕ-direction

$$\rho\left(U\frac{\partial V}{\partial R}+\frac{V}{R}\frac{\partial V}{\partial \phi}+\frac{UV}{R}\right)=-\frac{1}{R}\frac{\partial P}{\partial \phi}+\mu\left(\frac{\partial^2 V}{\partial R^2}+\frac{1}{R}\frac{\partial V}{\partial R}+\frac{1}{R^2}\frac{\partial^2 V}{\partial \phi^2}+\frac{2}{R^2}\frac{\partial U}{\partial \phi}-\frac{V}{R^2}\right)+\rho g\cos\alpha\sin\phi \tag{2.3}$$

Momentum equation in Z-direction

$$\rho\left(U\frac{\partial W}{\partial R}+\frac{V}{R}\frac{\partial W}{\partial \phi}\right)=-\frac{\partial P}{\partial Z}-\rho g\sin\alpha+\mu\left(\frac{\partial^2 W}{\partial R^2}+\frac{1}{R}\frac{\partial W}{\partial R}+\frac{1}{R^2}\frac{\partial^2 W}{\partial \phi^2}\right) \tag{2.4}$$

Energy equation

$$\rho C_p\left(U\frac{\partial T}{\partial R}+\frac{V}{R}\frac{\partial T}{\partial \phi}+W\frac{\partial T}{\partial Z}\right)=k\left(\frac{\partial^2 T}{\partial R^2}+\frac{1}{R}\frac{\partial T}{\partial R}+\frac{1}{R^2}\frac{\partial^2 T}{\partial \phi^2}\right)+Q \tag{2.5}$$

Applying the no-slip condition at the wall and peripherally uniform wall temperature at any axial position, the boundary conditions for equations (2.2) to (2.5) are:

$$U = V = W = T_w - T = 0 \qquad \text{at pipe wall}$$

It will be assumed that the density ρ in the buoyancy force term of the momentum equation takes the following form:

$$\rho = \rho_w[1+\beta(T_w - T)], \quad \text{where } \beta = -\frac{1}{\rho}\left(\frac{\partial \rho}{\partial T}\right)_p$$

In order to express the results in general terms, the following dimensionless dependent variables, constants, parameters, and a dimensionless stream function ψ are introduced:

Dimensionless radius, $r = \frac{R}{a}$

Dimensionless velocity,

$$u = \frac{U}{\nu/a}, \qquad v = \frac{V}{\nu/a}, \qquad w = \frac{W}{Re(\nu/a)}$$

Dimensionless temperature, $\theta = \dfrac{T_w - T}{Re\ C\ a\ Pr}$

Stream function,

$$u = \frac{1}{r}\frac{\partial \psi}{\partial \phi}, \qquad v = -\frac{\partial \psi}{\partial r} \tag{2.6}$$

Reynolds number,

$$Re = \frac{A\ a^3}{4\rho\nu^2}, \quad \text{where } A = -\left(\frac{\partial P}{\partial Z} + \rho_w\ g\ \sin\alpha\right)$$

Prandtl number, $Pr = \dfrac{\nu}{\kappa}$

Rayleigh number, $Ra = \dfrac{\beta\ g\ C\ a^4}{\nu\ \kappa}$

Heat generation parameter, $F = \dfrac{Q\ a}{\rho\ C_p\ \nu\ C}$

where $C = \dfrac{\partial T}{\partial Z}$ = constant

The momentum and energy equations can now be restated in the following dimensionless forms after eliminating pressure terms between equations (2.2) and (2.3) by cross-differentiation. The results are:

Momentum equation for secondary flow

$$\nabla^2\xi = u\frac{\partial \xi}{\partial r} + \frac{v}{r}\frac{\partial \xi}{\partial \phi} + ReRa\left(\frac{\partial \theta}{\partial r}\sin\phi + \frac{1}{r}\frac{\partial \theta}{\partial \phi}\cos\phi\right)\cos\alpha \tag{2.7}$$

Vorticity equation

$$\nabla^2\psi = \xi \tag{2.8}$$

Axial momentum equation

$$\nabla^2 w = u\frac{\partial w}{\partial r} + \frac{v}{r}\frac{\partial w}{\partial \phi} + Ra\ \theta\ \sin\alpha - 4 \tag{2.9}$$

Energy equation

$$\nabla^2\theta = Pr\ \left(u\frac{\partial \theta}{\partial r} + \frac{v}{r}\frac{\partial \theta}{\partial \phi}\right) - w + \frac{F}{Re} \tag{2.10}$$

Through symmetry it is required to consider only one-half of the circular region as shown in Fig. 1. The boundary conditions for equations (2.7) to (2.10) can be restated as follows:

$$\psi = \frac{\partial \psi}{\partial r} = w = \theta = 0 \qquad \text{at } r = 1$$

$$\psi = \xi = \frac{\partial \theta}{\partial \phi} = \frac{\partial w}{\partial \phi} = 0 \qquad \text{along } \phi = 0 \text{ and } \pi \tag{2.11}$$

The governing equations (2.7), (2.9), (2.10) are quasi-linear second-order partial differential equations of elliptic type, and the vorticity equation (2.8) is simply a Poisson's equation. If we substitute equation (2.8) into equation (2.7) we obtain the governing equation for secondary flow involving a biharmonic operator. The resulting set of governing equations for ψ, w and θ was solved by Iqbal and Stachiewicz [2] using a perturbation approach similar to Morton's [1] for the case without heat generation in inclined tubes and by Iqbal [10] with uniform internal heat generation in horizontal tubes.

However, the perturbation method as demonstrated in the literature for convective heat transfer with secondary flow is known to diverge quickly with the increase of the characteristic parameter such as ReRa for fully developed laminar flow in uniformly heated horizontal tubes. In view of the serious limitation of the applicability of the perturbation method, a numerical solution appears to be the only practical approach for an accurate solution of the present problem. But the numerical solution of the biharmonic equation in polar coordinates by the available conventional method [12] using an iterative technique with successive over (or under) relaxation is known to converge extremely slowly, and is not practical from the viewpoint of computing time. This

difficulty can be overcome readily by using a recently developed boundary vorticity method [4,11] for the equation (2.7) and (2.8).

2.2 Finite-Difference Approximation.

Using the three-point central-difference operators, equations (2.7) to (2.10) can be transformed into a set of algebraic finite-difference equations. The equations (2.7) to (2.10) can be regarded as having the following form:

$$\frac{\partial^2 f}{\partial r^2} + \frac{1}{r}\frac{\partial f}{\partial r} + \frac{1}{r^2}\frac{\partial^2 f}{\partial \phi^2} = u\frac{\partial f}{\partial r} + \frac{v}{r}\frac{\partial f}{\partial \phi} + G \qquad (2.12)$$

where f is a dummy variable, u and v are secondary velocity components, and G represents the remaining terms in each of the equations (2.7), (2.9) and (2.10). It is noted that if u = v = 0, equation (2.12) reduces to a Poisson's equation. Referring to a coordinate system and numerical grid shown in Fig. 1, the finite-difference formulation of equation (2.12) can be written as,

$$\frac{f_{i-1,j} + f_{i+1,j} - 2f_{i,j}}{(\Delta r)^2} + \frac{f_{i+1,j} - f_{i-1,j}}{2r_i\,\Delta r} + \frac{f_{i,j-1} + f_{i,j+1} - 2f_{i,j}}{(r_i\,\Delta\phi)^2}$$

$$= u_{i,j}\frac{f_{i+1,j} - f_{i-1,j}}{2\Delta r} + v_{i,j}\frac{f_{i,j+1} - f_{i,j-1}}{2r_i\,\Delta\phi} + G_{i,j} \qquad (2.13)$$

After multiplying by $(\Delta r)^2$ and rearranging equation (2.13) becomes

$$\left(1 - \frac{\Delta r}{2r_i} + \frac{\Delta r}{2}u_{i,j}\right) f_{i-1,j} - 2\left[1+\left(\frac{\Delta r}{r_i\Delta\phi}\right)^2\right] f_{i,j} + \left(1+\frac{\Delta r}{2r_i} - \frac{\Delta r}{2}u_{i,j}\right)$$

$$f_{i+1,j} = G_{i,j}(\Delta r)^2 - \left[\left(\frac{\Delta r}{r_i\Delta\phi}\right)^2 + \frac{(\Delta r)^2}{2r_i\Delta\phi}v_{i,j}\right] f_{i,j-1} - \left[\left(\frac{\Delta r}{r_i\Delta\phi}\right)^2\right.$$

$$\left. - \frac{(\Delta r)^2}{2r_i\Delta\phi}\,v_{i,j}\right] f_{i,j+1} \qquad (2.14)$$

Letting,

$$a_i = 1 - \frac{\Delta r}{2r_i} + \frac{\Delta r}{2} u_{i,j}$$

$$b_i = -2\left[1+\left(\frac{\Delta r}{r_i \Delta\phi}\right)^2\right]$$

$$c_i = 1 + \frac{\Delta r}{2r_i} - \frac{\Delta r}{2} u_{i,j}$$

$$d_i = G_{i,j}(\Delta r)^2 - \left[\left(\frac{\Delta r}{r_i\Delta\phi}\right)^2 + \frac{(\Delta r)^2}{2r_i\Delta\phi} v_{i,j}\right] f_{i,j-1} - \left[\left(\frac{\Delta r}{r_i\Delta\phi}\right)^2 - \frac{(\Delta r)^2}{2r_i\Delta\phi} v_{i,j}\right] f_{i,j+1}$$

equation (2.14) can be reduced to

$$a_i f_{i-1,j} + b_i f_{i,j} + c_i f_{i+1,j} = d_i \qquad (2.15)$$

Equation (2.15) is seen to be a general finite-difference expression applicable to equations (2.7) to (2.10). In computing the secondary velocity components using $u = \frac{1}{r}\frac{\partial\psi}{\partial\phi}$ and $v = -\frac{\partial\psi}{\partial r}$, a more accurate result can be obtained by employing a five-point central-difference formula such as

$$\frac{\partial f_{i,j}}{\partial r} = \frac{1}{12\Delta r}(f_{5,j} - 6f_{4,j} + 18f_{3,j} - 10f_{2,j} - 3f_{1,j}), \quad \text{for } i = 2$$

$$= \frac{1}{12\Delta r}(f_{i-2,j} - 8f_{i-1,j} - 8f_{i+1,j} + f_{i+2,j})$$

$$\text{for } i = 3,4,\ldots M-1$$

$$= \frac{1}{12\Delta r}(f_{M-3,j} - 6f_{M-2,j} + 18f_{M-1,j} - 10f_{M,j} - 3f_{M+1,j}), \quad \text{for } i = M$$

$$\frac{\partial f_{i,j}}{\partial\phi} = \frac{1}{12\Delta\phi}(-f_{i,2} + 8f_{i,3} - f_{i,4}), \quad \text{for } j = 2$$

$$= \frac{1}{12\Delta\phi}(f_{i,j-2} - 8f_{i,j-1} + 8f_{i,j+1} - f_{i,j+2}), \quad \text{for } j = 3,4,\ldots N-1$$

$$= \frac{1}{12\Delta\phi}\,(f_{i,N-2} - 8f_{i,N-1} + f_{i,N}), \qquad \text{for } j = N$$

It is noted that $\partial f_{i,j}/\partial\phi = 0$ at $j = 1$ and $N + 1$. In order to avoid the singularity at the origin of the cylindrical coordinates a finite-difference equation in Cartesian coordinates is employed at the origin.

2.3 Numerical Solution Using Line Iterative Technique and Boundary Vorticity Method.

The transformation of equations (2.7) to (2.10) into a general algebraic finite-difference equation (2.13) was mentioned in Section 2.2. The boundary conditions (equation (2.11)) can be written in finite-difference forms as,

$$\psi_{i,j} = w_{i,j} = \theta_{i,j} = u_{i,j} = v_{i,j} = 0 \qquad \text{for } i = M+1$$

$$\psi_{i,j} = \xi_{i,j} = 0 \qquad \text{for } j = 1 \text{ and } N + 1 \qquad (2.16)$$

$$\psi_{i-1,j} = \psi_{i+1,j} \qquad \text{for } i = M + 1$$

$$\theta_{i,j-1} = \theta_{i,j+1},\ w_{i,j-1} = w_{i,j+1} \qquad \text{for } j = 1 \text{ and } N + 1$$

Using the above boundary conditions, a set of finite-difference equations may be written in the following forms after applying equation (2.15) to the grid points along the radial line j:

$$b_1 f_{1,j} + c_1 f_{2,j} = d_1 \qquad i = 1$$

$$a_i f_{i-1,j} + b_i f_{i,j} + c_i f_{i+1,j} = d_i \qquad i = 2,3,4,\ldots M-1 \qquad (2.17)$$

$$a_M f_{M-1,j} + b_M f_{M,j} = d_M \qquad i = M$$

Furthermore, equation (2.17) can be written in matrix form as:

$$\underline{A}\,\underline{f} = \underline{d} \qquad (2.18)$$

or

$$\begin{bmatrix} b_1 & c_1 & & & & & & \\ a_2 & b_2 & c_2 & & & & 0 & \\ & a_3 & b_3 & c_3 & & & & \\ & & \cdot & \cdot & \cdot & & & \\ & & & \cdot & \cdot & \cdot & & \\ & & 0 & & \cdot & \cdot & \cdot & \\ & & & & & a_{M-1} & b_{M-1} & c_{M-1} \\ & & & & & & a_M & b_M \end{bmatrix} \begin{bmatrix} f_1 \\ f_2 \\ f_3 \\ \cdot \\ \cdot \\ \cdot \\ f_{M-1} \\ f_M \end{bmatrix} = \begin{bmatrix} d_1 \\ d_2 \\ d_3 \\ \cdot \\ \cdot \\ \cdot \\ d_{M-1} \\ d_M - c_{M+1} f_{M+1} \end{bmatrix}$$

Here $\underline{A}$ is seen to be a tridiagonal matrix and a Gaussian elimination method [13] may be used to solve $\underline{f}$. The following procedure using forward elimination and backward substitution is used.

$$h_1 = c_1/b_1$$

$$h_i = c_i/(b_i - a_i h_{i-1}) \qquad i = 2,3,.....M-1$$

$$q_1 = d_1/b_1$$

$$q_i = (d_i - a_i\, q_{i-1}) \,/\, (b_i - a_i h_{i-1}) \qquad i = 2,3,....M$$

and $f_M = q_M$

$$f_i = q_i - h_i f_{i+1} \qquad i = M-1,\ M-2,...1$$

It is noted that the numerical solution can be applied to equations (2.9) and (2.10) with the boundary conditions given in equation (2.16), but the boundary condition for equation (2.7) is unknown. On the other hand, two boundary conditions are available for equation (2.8). The success of the boundary vorticity method is based on the observation that a linear relationship exists between the vorticity $\xi_{M+1,j}$ and the

stream function $\psi_{M+1,j}$ at the boundary [4.11]. Using the boundary condition of $\psi_{i-1,j} = \psi_{i+1,j}$ for $i = M+1$, some elements of the matrix equation (2.18) such as a_M, b_M, f_M and $d_M - c_{M+1} f_{M+1}$ will now be replaced by $a_{M+1} + c_{M+1}$, b_{M+1}, f_{M+1} and d_{M+1}, respectively. Assuming arbitrary values $\xi_b^{(1)}$ and $\xi_b^{(2)}$ for $\xi_{M+1,j}$ and solving finite-difference equations for equations (2.7) and (2.8), the values for $\psi_b^{(1)}$ and $\psi_b^{(2)}$ can be obtained using the boundary condition $\frac{\partial \psi}{\partial r} = 0$ at wall. The boundary values for the vorticity $\xi_{M+1,j}$ and the stream function $\psi_{M+1,j}$ are related by the following linear equation:

$$\xi_b^{(3)} = \frac{\xi_b^{(2)} - \xi_b^{(1)}}{\psi_b^{(2)} - \psi_b^{(1)}} (\psi_b^{(3)} - \psi_b^{(2)}) + \xi_b^{(2)} \qquad (2.19)$$

Using this linear relation and noting that the correct stream function at the boundary is $\psi_b^{(3)} = 0$, $\xi_b^{(3)}$ can be computed. With the boundary vorticity numerically determined, the numerical solution of a set of equations (2.7) to (2.10) can be carried out by a line iterative relaxation procedure using the following equation:

$$f_{i,j}^{(n+1)} = f_{i,j}^{(n)} + \omega [f_{i,j}^{(n+1)} - f_{i,j}^{(n)}] \qquad (2.20)$$

where ω is a relaxation factor. The numerical solution of a set of equations (2.7) to (2.10) can be started by assuming initial values for $w_{i,j}$, $\theta_{i,j}$, $u_{i,j}$, and $v_{i,j}$ with the initial mesh size of M,N = 14. The numerical solution will be continued until the dependent variables $w_{i,j}$, $\theta_{i,j}$, $\psi_{i,j}$, and $\xi_{i,j}$ satisfy the following prescribed error:

$$\varepsilon = \Sigma_{i,j} | f_{i,j}^{(n+1)} - f_{i,j}^{(n)} | / \Sigma_{i,j} | f_{i,j}^{(n)} | < 10^{-5}$$

The secondary velocity components $u_{i,j}$ and $v_{i,j}$ can be obtained by using

the five-point finite-difference formula for the first derivatives. In order to obtain more accurate numerical results, the procedure is repeated by using the mesh size of M,N = 28 and iteration is continued until the prescribed error is reached.

The method of determining an optimum relaxation factor is not available for the present non-linear problem. However, it is found that the influence of overrelaxation ($\omega > 1$) or underrelaxation ($\omega < 1$) on computing time is not appreciable. Consequently, the relaxation factor of unity is used in most of the calculations. The rate of convergence for line iterative method depends on the values of the parameters Re, Ra, Pr, α and F. For given values of the parameters Re, Ra, Pr, α and F, it is possible to obtain flow and heat transfer results within 3 minutes in the low Rayleigh number regime on the IBM360/67 system. However, in high parameter regime such as $Ra \geq 4{,}000$, it takes around 5 minutes to complete one calculation for fixed values of the parameters Re, Ra, Pr, α and F. It is noted that in very high Rayleigh number regime the matrix cannot be inverted. In order to check the accuracy of the numerical results two different methods of obtaining the Nusselt number and the pressure-drop parameter are used. Since the prescribed error ε is set to be less than 10^{-5}, it is expected that the numerical results for the pressure drop parameter and Nusselt number will be valid up to four significant figures. This observation is confirmed by the agreement between the numerical results based on two alternative definitions for the flow and heat transfer results. Typical numerical results are given in Appendix C.

CHAPTER III

FLOW AND HEAT TRANSFER RESULTS WITHOUT HEAT SOURCES

3.1 Velocity Distributions.

For the present problem without heat sources, four independent parameters Re, Ra, Pr, and α appear in the governing equations, and it is not practical to carry out numerical computation for all possible cases. Consequently, consideration will be limited to a few typical cases to illustrate the effect of each parameter.

The axial velocity profile depends on Prandtl number, Rayleigh number, Reynolds number, and inclination angle. The effect of each parameter on axial velocity profile along $\phi = 0$ and π is illustrated in Fig. 2(a) to (d). The effect of Rayleigh number for Pr = 10, Re = 20, and $\alpha = 45°$ demonstrated in Fig. 2(a) shows that at Ra = 1,000, back flow already occurs from r = 0 to r = 0.25 along $\phi = \pi$. The Rayleigh number at which the back flow occurs is of considerable theoretical and practical interest, and the numerical result is given below for Pr = 0.75 and $\mathrm{ReRa} \leq 50{,}000$.

α	0°	10°	20°	30°	45°	60°	75°	90°
Ra	∞	3,800	1,950	1,350	930	780	690	670

It is noted that for pure forced convection with Ra = 0 the axial velocity profile is parabolic. As the Rayleigh number increases, the intensity of the secondary motion increases. This secondary motion is known to distort the parabolic velocity profile, and decreases the magnitude of the maximum velocity.

The effect of Reynolds number appears through a parameter ReRa in the momentum equation (2.7) for secondary flow, and the role of Reynolds

number on axial velocity profile is seen to be similar to that of ReRa for the limiting case of horizontal tube. Fig. 2(b) shows that the maximum axial velocity moves toward the direction $\phi = \pi$ as the Reynolds number increases.

For given values of Pr, Re and Ra, the effect of inclination angle α can be seen from axial momentum equation (2.9) using membrane analogy, and Fig. 2(c) confirms the well known axial velocity profiles for the horizontal ($\alpha = 0°$) and vertical tubes ($\alpha = 90°$).

The effect of Prandtl number appears in the convective terms of the energy equation (2.10). As the Prandtl number increases, the secondary motion decreases, and the axial velocity profile approaches that of Hagen-Poiseuille flow, as shown in Fig. 2(d). This observation is significant since it leads to the possibility for the numerical solution of Graetz problem with significant buoyancy effect. Fig. 2(d) shows the effect of Prandtl number on axial velocity profile for given values of ReRa, Ra and α. The magnitude of the maximum velocity is seen to increase as Prandtl number increases.

Typical streamlines are illustrated in Fig. 3 for $\alpha = 45°$ and the patterns are seen to be similar to those for horizontal tube $\alpha = 0°$ [4]. There are two symmetric streamline patterns for the secondary flow. One notes that at low Rayleigh number the centers of circulation first appear on the radial line $\phi = \frac{\pi}{2}$ or $-\frac{\pi}{2}$. With the increase of the Rayleigh number, they tend to move toward the wall radially, but circumferentially they move away from $\phi = \frac{\pi}{2}$ or $-\frac{\pi}{2}$ toward $\phi = \pi$. With further increase of Rayleigh number, they then move back toward the radial line $\phi = \frac{\pi}{2}$ or $-\frac{\pi}{2}$. For given values of Pr, Re and Ra, the location of the eye of the streamlines does not appear to be sensitive to the inclination

angle effect, but the absolute value of the stream function at the eye decreases with the increase of the inclination angle. Of course, the secondary flow disappears completely at $\alpha = 90°$. The distributions of the secondary flow velocity components u, v, will be discussed later in Chapter IV.

3.2 Temperature Distributions.

The effects of the parameters Ra, Re, α, and Pr, respectively, on the temperature profile along $\phi = 0$ and π are shown in Fig. 4(a) to (d) under the corresponding conditions as those for the axial velocity profiles discussed in Section 3.1. Qualitatively, the profiles for temperature and axial velocity are similar except the phenomenon of reverse flow. This observation is confirmed by the similarity of the respective governing equation.

Fig. 4(a) shows that at Ra = 1,000 with back flow (see Fig. 2(a)), the secondary flow is predominant and the temperature profile is flat in the central core region, indicating that the conduction terms are negligible as compared with the advective terms in the energy equation (2.10). Fig. 4(b) shows that the effect of Reynolds number on temperature profile is qualitatively similar to that of Reynolds number effect on axial velocity profile. As Reynolds number increases, the magnitude of the maximum temperature difference θ decreases, and its location shifts toward the lower wall. In addition, the temperature gradient at the bottom is seen to be higher than that at the top of the tube for high Reynolds number regime. For given values of the parameters Re, Ra, and Pr, the effect of inclination angle on temperature profile is shown in Fig. 4(c). For the limiting case of vertical tube, the temperature profile is symmetric. In

other words, the isotherms are concentric for the vertical tube case. The concentric isotherms will be gradually distorted as the tube inclination angle α varies from $\alpha = 90°$ to $\alpha = 0°$, and the center of the isotherms will move downward along the direction $\phi = \pi$. For given values of Re, Ra and α, the effect of Prandtl number on the temperature profile is qualitatively similar to that of Ra or Re as can be seen from the energy equation (2.10). This observation is also confirmed in Fig. 4(d). One sees that as Prandtl number increases, the symmetric temperature distribution is distorted gradually, and the magnitude of the maximum temperature difference decreases. Comparing the effects of Prandtl number on axial velocity and temperature profiles, it is clear that the effects of Prandtl number on axial velocity and temperature profiles are seen to be completely opposite.

The typical isotherms are illustrated in Fig. 3 for $\alpha = 45°$, and the pattern is seen to be similar to that for horizontal tube [4]. The temperature drops rather gradually from the value at the wall to the minimum value along the direction $\phi = 0$. Along the direction $\phi = \pi$, the temperature drops rapidly from the wall temperature to the same minimum value. A study of the isotherms in high Rayleigh number regime, for example at Ra = 4,000 with $\alpha = 45°$, reveals that the isotherms are nearly circular and concentric. This situation can also be seen from the temperature profile for Ra = 1,000 shown in Fig. 4(a), and is apparently related to back flow phenomenon shown in Fig. 2(a). Noting that the isotherms are concentric for the case without secondary flow, one sees that as the Rayleigh number increases from zero, the concentric isotherms will be gradually distorted and finally become concentric again at sufficiently large

Rayleigh number. It is noted that the pattern of the isotherms is closely related to the movement of the centers of circulation for the streamlines. When the centers of circulation return to the radial line $\phi = \frac{\pi}{2}$ or $-\frac{\pi}{2}$ again at sufficiently large Rayleigh number, the isotherms become nearly concentric circles. One should note that in discussing the Rayleigh number effect, the remaining parameters such as Pr, α and Re are held constant.

3.3 The Effects of Ra and Re on Flow and Heat Transfer Results.

The expressions for the product of friction factor and Reynolds number, f·Re, and Nusselt number, Nu, can be obtained by considering either the velocity and temperature gradients, respectively, along the tube wall or the overall force and energy balances, respectively, for the axial length dZ.

Following the usual definition for the product of friction factor and Reynolds number, we obtain

$$f\cdot Re = \frac{\bar{\tau}_w}{\frac{1}{2}\rho \bar{W}^2} \cdot \frac{\bar{W}\ 2a\ \rho}{\mu} = \frac{4a\ \bar{\tau}_w}{\mu\ \bar{W}} \tag{3.1}$$

where $\bar{\tau}_w$ can be obtained by considering the velocity gradient along the tube wall as,

$$\bar{\tau}_w = \frac{\mu \int_s \left(\frac{\partial W}{\partial R}\right)_w R\ d\phi}{\int_s R\ d\phi} = \mu \left(\frac{\overline{\partial W}}{\partial R}\right)_w \tag{3.2}$$

substituting equation (3.2) into equation (3.1), we have

$$(f\ Re)_1 = \frac{4 \left(\frac{\overline{\partial w}}{\partial r}\right)_w}{\bar{w}} \tag{3.3}$$

A force balance on a fluid element $A_r\, dZ$ gives

$$\bar{\tau}_w \cdot S = - A_r \left(\frac{\partial P}{\partial Z} + \bar{\rho}\, g \sin \alpha\right)$$

$$= A_r\, A\left(1 - \frac{1}{4} Ra\, \bar{\theta} \sin \alpha\right) \qquad (3.4)$$

Substituting equation (3.4) into equation (3.1) and using the dimensionless mean velocity $\bar{w}$, we obtain

$$(f \cdot Re)_2 = \frac{8}{\bar{w}} \left[\, 1 - \frac{\sin \alpha}{4}\, Ra\, \bar{\theta} \,\right] \qquad (3.5)$$

In the limiting case of horizontal tube $\alpha = 0$, equation (3.5) reduces to

$$(f\ Re)_2 = \frac{8}{\bar{w}}$$

Analogous to the resistance coefficient, the Nusselt number can be obtained in two ways. One way is to consider the temperature gradient at the wall, and the other way is to consider the overall energy balance for the axial length dZ. The Nusselt number is defined as

$$Nu = \frac{\bar{h}\ 2a}{k} \qquad (3.6)$$

Using the temperature gradient at wall, the average heat transfer coefficient $\bar{h}$ can be written as,

$$\bar{h}\ T_M\ S\ dZ = -k \left(\frac{\overline{\partial T}}{\partial R}\right)_w S\ dZ$$

or

$$\bar{h} = - \frac{k \left(\frac{\overline{\partial T}}{\partial R}\right)_w}{T_M}$$

where

$$T_M = \frac{\iint W\ (T_w - T)\ d\ A_r}{\iint W\ d\ A_r}$$

$$= Re\ C\ a\ Pr\ \frac{\overline{w\theta}}{\bar{w}}$$

So, the Nusselt number can be expressed as,

$$(Nu)_1 = \frac{2 \cdot \bar{w} \left(\frac{\overline{\partial \theta}}{\partial r}\right)_w}{\overline{w\theta}} \tag{3.7}$$

On the other hand, by considering the overall energy balance, we have

$$\rho C_p \frac{\partial T}{\partial Z} \bar{W} A_r = \bar{h} T_M S$$

or

$$\bar{h} = \frac{\rho C_p C A_r Re \nu}{T_M a S} \bar{w}$$

Consequently, equation (3.6) can be expressed as

$$(Nu)_2 = \frac{\bar{w}^2}{\overline{w\theta}} \tag{3.8}$$

For the present problem without heat sources, the parameters ReRa, Ra, Pr and α appear in the governing equations, and each parameter has its influence on flow and heat transfer results. Fig. 5 shows the ratio $fRe/(fRe)_0$ as a function of Rayleigh number with inclination angle α as a parameter for Pr = 0.75 and ReRa = 4,000. It is seen that after reaching approximately a value of 2 for $fRe/(fRe)_0$, an asymptotic behavior appears for each curve, and all the curves are seen to be parallel to each other. As the Rayleigh number increases, secondary motion increases, so does the $fRe/(fRe)_0$. Particularly at high Rayleigh number regime, the product fRe increases considerably as α varies from 0° to 45°. One notes that a slight deviation from the horizontal direction α = 0° introduces a substantial increase in friction factor in the high Rayleigh number regime. With Pr and α given, it is seen that the value of fRe depends on Ra only after reaching a certain value of Ra. This effect is clearly seen in Fig. 6, where the variation of $fRe/(fRe)_0$ with Ra is shown for Pr = 0.75

and $\alpha = 45°$ with ReRa as a parameter. After reaching say Ra = 200, the value for fRe is seen to be independent of Re and depends only on Ra. Note that the limiting value for Re is about 2,000 for laminar flow.

The effects of Rayleigh number on heat transfer results and flow results are known to be similar, and the heat transfer results are shown in Fig. 7 and Fig. 8. Fig. 7 shows that after reaching a certain value of Ra, the Nusselt number ratio $Nu/(Nu)_0$ is a function of Ra only for each α. The asymptotic behavior in the form of parallel straight lines for various α's in the high Rayleigh number regime as shown in Fig. 7 suggests that a new correlation is possible for heat transfer results, and this is demonstrated in Fig. 8 where all the heat transfer results in Fig. 7 are now replotted on the basis of $Nu/(Nu)_0$ versus Ra sin α. After reaching a value of say Ra sin $\alpha = 70$, all the heat transfer results for the range $0 < \alpha \leq 90°$ can be predicted by a single curve with sufficient accuracy. The tube orientation effect for Ra sin $\alpha < 70$ is of interest.

The effect of Reynolds number on heat transfer results is shown in Fig. 9 to Fig. 12. Fig. 9 shows that after reaching Ra = 450, the Nusselt number ratio $Nu/(Nu)_0$ is independent of Reynolds number, and is a function of Ra only. The curves for ReRa = 50,000 and 10,000 show that minimum value for $Nu/(Nu)_0$ exists at some value of Ra. An examination of the momentum equation (2.7) and the energy equation (2.10) shows that for horizontal tube case ($\alpha = 0°$), the flow and heat transfer results depend on Pr and ReRa. On the other hand, for the vertical case ($\alpha = 90°$), the flow and heat transfer results are independent of Re and Pr. This suggests that the Reynolds number effect is significant in the neighborhood of horizontal case. Figs. 10 to 12 show the effect of Reynolds number on

$Nu/(Nu)_0$ for $\alpha = 0°$, $30°$, and $60°$, respectively, with $Pr = 5$. It is clear that for the horizontal case shown in Fig. 10, the heat transfer rate increases with the increase of Reynolds number for a given value of Ra. Furthermore, for various values of Re, the curves are seen to be parallel to each other in the high Rayleigh number regime. Two curves for $Re = 5$ and $Re = 20$ in the case of $\alpha = 30°$ and $Pr = 5$ shown in Fig. 11 start significant deviation at around $Ra = 10$. This indicates that the Reynolds number effect appears after reaching around $Ra = 10$. However, after reaching say $Ra = 1{,}000$, the effect of Reynolds number is seen to be negligible. Fig. 12 shows that at $\alpha = 60°$ the influence of Reynolds number on heat transfer results is not appreciable for any Rayleigh number. It is seen that two curves for $Re = 5$ and $Re = 20$ in Fig. 12 coincide after reaching around $Ra = 700$. A comparison between Figs. 10 and 12 shows clearly that the effect of Reynolds number on heat transfer result is significant for the horizontal tube ($\alpha = 0°$) but insignificant at $\alpha = 60°$. It is expected that from $\alpha = 60°$ up to the limiting vertical case ($\alpha = 90°$) the heat transfer result will be independent of Reynolds number.

The numerical results from this study shown in Figs. 10 to 12 can be compared against the results from perturbation solution [14]. Figs. 10 to 12 show clearly that there is a significant difference between the present numerical solution and the perturbation solution. It should be pointed out that for the horizontal tube case the perturbation solution is known to diverge quickly with the increase of the parameter, and the rather sharp increase in the Nusselt number with the increase of Ra shown in Fig. 10 for $\alpha = 0°$ is typical of the perturbation solution. It is noted that for horizontal tube, the Nusselt number is dependent on the parameter ReRa. The trend of heat transfer results from perturbation

analysis for the inclination angles $\alpha = 30°$ and $60°$ shown in Fig. 11 and Fig. 12 respectively, also shows the same blow-up trend similar to that for $\alpha = 0°$.

3.4 The Effects of Prandtl Number and Tube Inclination Angle on Flow and Heat Transfer Results.

The Prandtl number effects on flow and heat transfer results for $\alpha = 45°$ and ReRa = 4,000 are shown in Fig. 13 and Fig. 14 respectively. Fig. 13 shows that the Prandtl number effect on $fRe/(fRe)_0$ is significant only in the low Rayleigh number regime. As Prandtl number increases, the ratio $fRe/(fRe)_0$ is seen to decrease in the low Rayleigh number region. After reaching about Ra = 2,000, the ratio $fRe/(fRe)_0$ is seen to be independent of Prandtl number. Fig. 14 shows $Nu/(Nu)_0$ versus Ra with Pr as a parameter. The Prandtl number effect is significant in the low Rayleigh number regime. Note the completely opposite effects of Prandtl number on flow and heat transfer results in the low Rayleigh number regime. It is noted that Prandtl number appears in the convective terms of the energy equation (2.10). Qualitatively, the effect of Prandtl number on heat transfer rate is similar to that of secondary motion. In other words, heat transfer rate increases with the increase of the Prandtl number in the low Rayleigh number region.

The effect of tube inclination angle on flow and heat transfer results is of considerable interest, and is shown in Figs. 15 to 18. It is seen that in the high Rayleigh number regime a slight variation of inclination angle introduces a substantial increase in $fRe/(fRe)_0$ and $Nu/(Nu)_0$. The practical implication of this effect is that the inclination angle effect cannot be neglected, for example, for helical tubes

in high Rayleigh number regime.

The variation of $fRe/(fRe)_0$ with α is shown in Fig. 15 for Pr = 0.75 and ReRa = 10,000 with Ra as a parameter. At Ra = 10, tube orientation for the range $\alpha = 0° \sim 30°$ is seen to be insensitive to the value of fRe, while at Ra = 4,000, tube inclination effect on the value of fRe is considerable in the range of $\alpha = 0° \sim 20°$. In Fig. 16, the ratio $Nu/(Nu)_0$ is plotted against α with Ra as a parameter for Pr = 0.75 and ReRa = 10,000. It is seen that the inclination angle effect on Nusselt number ratio in low Rayleigh number regime is opposite to that in the high Rayleigh number regime. The curves for Ra = 400 and 100 show that minimum value for $Nu/(Nu)_0$ exists at some value of α. At high Rayleigh number, say Ra = 4,000, heat transfer result changes significantly with slight deviation from horizontal direction $\alpha = 0°$ which suggests again that inclination angle effect cannot be neglected for certain helical tubes.

The problem under consideration was solved by Iqbal and Stachiewicz [2] using perturbation method and it is desirable to compare the results from this work with those of references [2] and [14]. Fig. 17 shows that there is a substantial difference between the present numerical solution and the analytical solution using perturbation method. The present numerical solution checks exactly with the known numerical results for horizontal tube ($\alpha = 0°$) [4] and the vertical tube ($\alpha = 90°$) [5], whereas the perturbation solution [2] covers the range $10° \leq \alpha \leq 50°$ only. The curves for ReRa = 3,000, 2,000, and 1,000 from perturbation solution do not appear to approach the value for $\alpha = 90°$. In view of the considerable discrepancy noted above, it is believed that the perturbation solution shown

in reference [2] is invalid. In particular, the suggestion [2] that for any combination of Rayleigh, Reynolds, and Prandtl numbers, there is an optimum value of tube inclination which gives the maximum value of Nusselt number for α ranging from 20 to 60 degrees appears to be erroneous. Fig. 18 further demonstrates the divergence of the perturbation solution. Once again, the suggestion of reference [14] that there is a maximum heat transfer result in the range of 20 to 60 degrees of inclination angle appears to be incorrect. Fig. 18 shows that even at Re = 4, 6, 8, the perturbation solution diverges for Pr = 5 and Ra = 100. It is reasonable to conclude that the perturbation solution for the present problem is valid only for very low Rayleigh number regime, say up to $Ra \leq 20$, and there is no optimum inclination angle for any given values of the Rayleigh, Reynolds, and Prandtl numbers.

CHAPTER IV

FLOW AND HEAT TRANSFER RESULTS WITH UNIFORM HEAT SOURCES

4.1 Influence of Heat Sources on Velocity and Temperature Profiles.

The axial velocity and temperature profiles depend on Prandtl number, tube inclination angle, Reynolds number, Rayleigh number and heat generation function. Since the effect of each parameter on axial velocity and temperature distributions is illustrated in Chapter III for the case without heat generation, for brevity, only the effects of heat generation and Rayleigh number will be considered here.

The effect of dimensionless heat generation parameter F on the dimensionless axial velocity and temperature profiles along $\phi = 0$ and π is shown in Fig. 19(a) and (b), respectively, for Pr = 0.75, $\alpha = 45°$, Re = 100, and Ra = 40. It can be seen that the velocity distribution near the wall becomes steeper with larger values of F. This fact agrees, for example, with the result for combined free and forced convection with uniform internal heat generation along a vertical flat plate reported in the literature. The shift of the location of the maximum velocity toward the direction $\phi = \pi$ shown in Fig. 19(a) for a given value of F is known to be caused by secondary flow. As the value of the heat sources parameter F increases, the maximum velocity increases and the location of the maximum velocity tends to shift back toward the pipe axis. It is expected that at a sufficiently high value of F, the velocity distribution will be parabolic. This trend is expected since with the increase of heat sources the temperature difference between the wall and fluid will decrease (see Fig. 19(b)). Noting the above observations, the increase of the

dimensionless axial velocity with increasing value of F can be seen qualitatively from the axial momentum equation (2.9). Fig. 19(b) shows that the dimensionless temperature difference θ is lower near the wall and elsewhere with larger values of F. The shift of the location of the maximum temperature difference is similar to that for the velocity profile and can be explained from the free convection or secondary flow effect. At F = 50, it is seen that the temperature difference θ becomes negative all around the wall (r = 1) indicating the reversed heat flow there. The behavior of the temperature profiles shown in Fig. 19(b) can also be seen from the relative contribution of the heat sources term and the axial convection term on the right hand side of the energy equation (2.10), keeping in mind that the secondary flow decreases with the increase of heat sources parameter F.

The effect of Rayleigh number on the axial velocity and temperature profiles along $\phi = 0$ and π is shown in Fig. 20(a) and (b) respectively, and is seen to be similar to the case without heat sources F = 0 which is shown in Chapter III. The trend of the Rayleigh number effect on the axial velocity profile shown in Fig. 20(a) suggests that at sufficiently high Rayleigh number the back flow may occur. At Ra = 1,000 the temperature distribution θ is already negative near the wall, indicating reversed heat flow situation. Of course this phenomenon cannot occur without heat sources. In Fig. 20(b) the shift of location and the magnitude of the maximum θ is apparently associated with the intensity of secondary flow. Fig. 20(a) also shows that the distortion from parabolic profile increases with the increase of Rayleigh number. The effects of heat sources parameter and Rayleigh number, respectively, on the velocity and

temperature profiles shown in Fig. 19 and Fig. 20 with all other parameters being held constant will be seen to be useful in interpreting the flow and heat transfer results.

In view of the fact that the secondary flow velocities are too small to be measured in experiment, the distributions of the secondary velocity components u, v are of some interest, and these are shown in Fig. 21(a) and (b) for several representative values of Ra with $\alpha = 45°$, Pr = 0.75, Re = 100 and F = 20. The trend of the effect of Rayleigh number on secondary velocity distribution indicates that boundary layer approximation does not appear to be possible even at high Rayleigh number for F = 20.

4.2 Heat Sources Effect on Flow and Heat Transfer Results.

The expressions for the product of friction factor and Reynolds number (fRe) and the Nusselt (Nu) are the same as those given in Chapter III for the case without heat generation except that the second definition for the Nusselt number must be modified. From the energy balance for the fluid element $A_r\, dZ$, we obtain

$$\int_{A_r} \rho\, C_p \frac{\partial T}{\partial Z}\, W\, dA_r - \int_{A_r} Q\, dA_r = \int_S \bar{h}\, T_M\, dS$$

or

$$\rho\, C_p\, C\, W_c\, \bar{w}\, A_r - Q\, A_r = \bar{h}\, T_M\, S,$$

where $W_c = Re\ (\nu/a)$

The average heat transfer coefficient is found to be,

$$\bar{h} = \frac{A_r}{T_M\, S} \left[\rho\, C_p\, C\, W_c\, \bar{w} - Q \right]$$

$$= \frac{k}{2a} \left[\frac{\bar{w}^2}{\overline{w\theta}} - \frac{F\, \bar{w}}{\overline{w\theta} Re} \right]$$

From the definition of Nusselt number the second definition of Nusselt number can now be written as

$$(Nu)_2 = \frac{\bar{h}\ 2a}{k}$$

$$= \frac{\bar{w}^2}{\overline{w\theta}} - \frac{F\ \bar{w}}{\overline{w\theta}\cdot Re} \qquad (4.1)$$

For the case without heat sources F = 0, equation (4.1) reduces to equation (3.8) which is

$$(Nu)_2 = \frac{\bar{w}^2}{\overline{w\theta}}$$

It is noted that the accuracy of the numerical results can be checked using two alternative expressions for the pressure-drop and heat transfer parameters.

The effect of heat sources parameter F on pressure-drop and heat transfer parameters is demonstrated in Fig. 22 for α = 45°, Pr = 0.75, Re = 100 and Ra = 40. At first glance the pressure-drop parameter in the form of fRe appears to be a linearly decreasing function of the heat-generation parameter F which is similar to that reported in [7] for a different definition of pressure-drop parameter for combined free and forced laminar convection in vertical rectangular channels with internal heat generation. The Nusselt number is seen to decrease appreciably with the increase of the heat sources parameter F. The difference in the relative influence of heat sources parameter on the parameters fRe and Nu can be explained from the velocity and temperature profiles shown in Fig. 19(a) and (b). It is noted that at F = 41.5 the heat transfer rate at wall is zero, and with the further increase of F, the Nusselt number becomes negative indicating reversed heat flow.

A comparison of the heat transfer results from this work with those obtained by a perturbation method for a limiting case of horizontal tube [10] is shown in Figs. 23 and 24. It should be noted that the Nusselt number reported in [10] is based on the mean temperature of the fluid with $(Nu)_0 = 6$ for Ra = 0 and F = 0; whereas the Nusselt number from this work is based on bulk temperature. It is expected that the difference between two results will be small when Ra is very small. However, some difference is observed for F = 10 in Fig. 23, and Pr = 5 in Fig. 24. In addition to the difference in the definition of Nusselt number, Fig. 23 clearly shows the typical blow-up trend of the heat transfer results with the increase of Rayleigh number obtained by the perturbation method. It can be expected that a significant difference in heat transfer predictions exists between the numerical method and perturbation method when Ra is large.

The effect of tube inclination angle on flow and heat transfer results is shown in Figs. 25 and 26 respectively, with heat sources function F as a parameter for Pr = 0.75, Re = 100 and Ra = 40. A close examination of the effect of F on fRe shown in Fig. 25 discloses that at any angle of tube inclination the value of fRe is not a linearly decreasing function of F. The straight-line relationship shown in Fig. 22 is caused by a rather compressed vertical scale.

The effect of Rayleigh number on pressure-drop parameter (fRe) and Nusselt number for $\alpha = 0°$, 45°, and 90° is shown in Figs. 27 and 28 respectively, for several representative values of F with Pr = 0.75 and Re = 100. In particular applications, the high Rayleigh number flow regime is of interest, and the effects of tube inclination and heat

sources are both seen to be significant. In particular, for $\alpha = 45°$ and $90°$, the heat sources effect is predominant when the Rayleigh number is large. Fig. 28 shows that for $F \neq 0$, the effect of Rayleigh number on heat transfer in horizontal tubes is completely different from that in inclined tubes within the range of F under investigation.

In order to see the Prandtl number effect, further flow and heat transfer results for $\alpha = 0°$, $45°$, and $90°$ are shown in Figs. 29 and 30 respectively, with F as a parameter for Pr = 5 and Re = 100. Note that the effect of Rayleigh number on fRe is quite small, even with heat sources for horizontal tube $\alpha = 0°$ with Pr = 5. On the other hand, the effect of Rayleigh number on Nu is significant for $\alpha = 0°$ at Pr = 5. This observation can be explained from the fact that when Prandtl number is large and the secondary flow is weak, the inertia terms in the momentum equations (2.7) and (2.9) can probably be neglected, whereas the convective terms in the energy equation (2.10) are important because of large Prandtl number for the case $\alpha = 0°$.

It should be noted that all the numerical results in Chapter III and IV are obtained by using a mesh size of M,N = 28 and a relaxation factor of unity. The numerical results indicate that generally the first four significant figures for the values of fRe and Nu check each other exactly for the two alternative expressions, confirming the accuracy of the numerical solution. The numerical results are listed in Tables 1 to 11 for future reference. Tables 10 and 11 list the numerical results for two alternative expressions for fRe and Nu.

The computing time required to obtain a complete solution for given values of the parameters Re, Ra, Pr, F, and inclination angle α ranges

from 2 to 3 minutes up to Ra $\doteq$ 400 on the IBM360/67 system. The required computing time increases with the further increase of Rayleigh number, and generally 5 to 6 minutes are required when Ra $\geq 10^3$.

CHAPTER V

CONCLUDING REMARKS

1. Based on the present numerical results it is now evident that the perturbation method [1, 2, 10, 14] as used in the literature diverges quickly with the increase of the characteristic parameter. The present numerical solution indicates that for any combination of Ra, Re, Pr, and F, the maximum value of Nusselt number does not exist for any tube inclination angle which is contrary to the result reported in [2, 14] using the perturbation method.
2. In high Rayleigh number regime, the tube orientation effect on flow and heat transfer results is significant in the neighborhood of $\alpha = 0°$. This implies that at high Rayleigh number the coupled effects of tube orientation, buoyancy forces, and centrifugal forces [16] must be considered for laminar forced convection heat transfer in helical tubes.
3. The numerical solution using a combination of boundary vorticity method and line iterative relaxation method proves to be very effective for combined free and forced laminar convection heat transfer in inclined tubes with or without internal heat generation. The convergence of the present numerical solution is ascertained by comparison with the known numerical results for the two limiting cases of horizontal tube ($\alpha = 0°$) and vertical tube ($\alpha = 90°$) for the case without heat generation. A comparison between this work and reference [5] for the vertical tube with uniform internal heat sources is

not possible because of the different definitions for heat-source parameter. For another limiting case of horizontal tubes with heat sources only qualitative comparison with reference [14] is possible in low Rayleigh number regime since the Nusselt number in [14] is based on mean temperature of fluid instead of bulk temperature used in the present investigation.

4. The present results for Pr = 5 without heat sources may be applied to the flat-plate solar collector tubes [15] for water heating. In view of the rather significant tube inclination angle effect with the increase of Rayleigh number, it appears that the determination of the suitable film heat-transfer coefficients in solar collectors based on theoretical and experimental data for horizontal tubes alone is inappropriate and unrealistic. However, the determination of the film heat-transfer coefficients in inclined solar collector tubes requires the solution of Graetz problem in inclined tubes.

5. The effects of heat sources on axial velocity and temperature profiles are seen to be considerable in inclined tubes. Reverse flow can occur at sufficiently high Rayleigh number, and reversed heat flow appears at a sufficiently high heat-source parameter. For given values of the parameters, both the Nusselt number and the pressure drop parameter (fRe) decrease with the increasing values of heat-source parameter F. For a given value of F ($F \neq 0$), the parameter (fRe) always increases with increasing values of Ra, whereas the Nusselt number generally decreases with increasing Ra in high Rayleigh number flow regime due to the counteracting effect between heat sources and impressed heat flux at the tube wall. In the case without heat generation ($F = 0$), both flow and heat

transfer parameters, fRe and Nu, increase with the increasing value of Rayleigh number.

6. The effect of Prandtl number is significant in low Rayleigh number regime. The Prandtl number effect is also seen to be significant when the inclination angle α is small. For any given value of the Prandtl number, an asymptotic behavior for flow and heat transfer results appears in high Rayleigh number regime.
7. The Reynolds number effect appears to be significant in the neighborhood of horizontal direction. In contrast, for the vertical tubes, the flow and heat transfer results are independent of Reynolds number. In high Rayleigh number regime, an asymptotic behavior appears for flow and heat transfer results for given values of Prandtl number, heat sources parameter, and tube inclination angle.
8. It is possible to apply the present numerical method to combined free and forced laminar convection problems where the body forces are caused by Coriolis forces or buoyancy forces in rotating field with a body force orientation effect. Furthermore, it is noted that the extension of the numerical technique to fully developed combined free and forced laminar convection in various noncircular inclined ducts or channels is obvious.

REFERENCES

1. Morton, B.R., "Laminar Convection in Uniformly Heated Horizontal Pipes at Low Rayleigh Numbers", Quarterly Journal of Mechanics and Applied Mathematics, vol. 12, 1959, pp. 410-420.

2. Iqbal, M., and Stachiewicz, J.W., "Influence of Tube Orientation on Combined Free and Forced Laminar Convection Heat Transfer", Journal of Heat Transfer, Trans. ASME, vol. 88, Series C, 1966, pp. 109-116.

3. Mori, Y., and Futagami, K., "Forced Convective Heat Transfer in Uniformly Heated Horizontal Tubes (2nd Report, Theoretical Study)," Int. J. Heat Mass Transfer, vol. 10, 1967, pp. 1801-1813.

4. Hwang, G.J., and Cheng, K.C., "Boundary Vorticity Method for Convective Heat Transfer with Secondary Flow-Application to the Combined Free and Forced Laminar Convection in Horizontal Tubes", Heat Transfer 1970 (Proc. Fourth International Heat Transfer Conference), vol. 4, NC 3.5, Elsevier Publishing Company, Amsterdam.

5. Hallman, T.M., "Combined Forced and Free-Laminar Heat Transfer in Vertical Tubes with Uniform Internal Heat Generation", Trans. ASME, vol. 78, 1956, pp. 1831-1841.

6. Ostrach, S., "Combined Natural and Forced-Convection Laminar Flow and Heat Transfer of Fluids with and without Heat Sources in Channels with Linearly Varying Wall Temperatures", NACA TN 3141, 1954.

7. Han, L.S., "Laminar Heat Transfer in Rectangular Channels", J. of Heat Transfer, Trans. ASME 81, 1959, pp. 121-128.

8. Lu, P.C., "Combined Free and Forced-Convection Heat-Generating Laminar Flow inside Vertical Pipes with Circular Sector Cross

Sections", J. of Heat Transfer, Trans. ASME 82, 1960, pp. 227-232.

9. Tao, L.N., "On Combined Free and Forced Convection in Chennels", Journal of Heat Transfer, Trans. ASME, Series C, vol. 82, 1960, pp. 233-238.

10. Iqbal, M., "Combined Free and Forced Convection in a Horizontal Tube with Uniform Internal Heat Generation", Nuclear Engineering and Design, vol. 7, 1968, pp. 49-48.

11. Hwang, G.J., "Thermal Instability and Finite Amplitude Convection with Secondary Flow", Ph.D. Thesis, Department of Mechanical Engineering, University of Alberta, 1970, Edmonton, Alberta, Canada.

12. Newell, J.H.Jr., and Bergles, A.E., "Analysis of Combined Free and Forced Convection for Fully Developed Laminar Flor in Horizontal Tubes", J. of Heat Transfer, Trans. ASME, Series C, vol. 92, 1970, pp. 83-93.

13. Young, D., "The Numerical Solution of Elliptic and Parabolic Partial Differential Equations", in Survey of Numerical Analysis, Todd, J., editor, McGraw-Hill, New York, 1962.

14. Iqbal, M., "Free-Convection Effects Inside Tubes of Flat-Plate Solar Collectors", Solar Energy 10, No. 4, 1966, pp. 207.

15. Baker, L.H., "Film Heat-Transfer Coefficient in Solar Collector Tubes at Low Reynolds Number", Solar Energy 11, No. 2, 78 (1967).

16. Akiyama, M., and Cheng, K.C., "Boundary Vorticity Method for Laminar Forced Convection Heat Transfer in Curved Pipes", To be published in Int. J. Heat Mass Transfer.

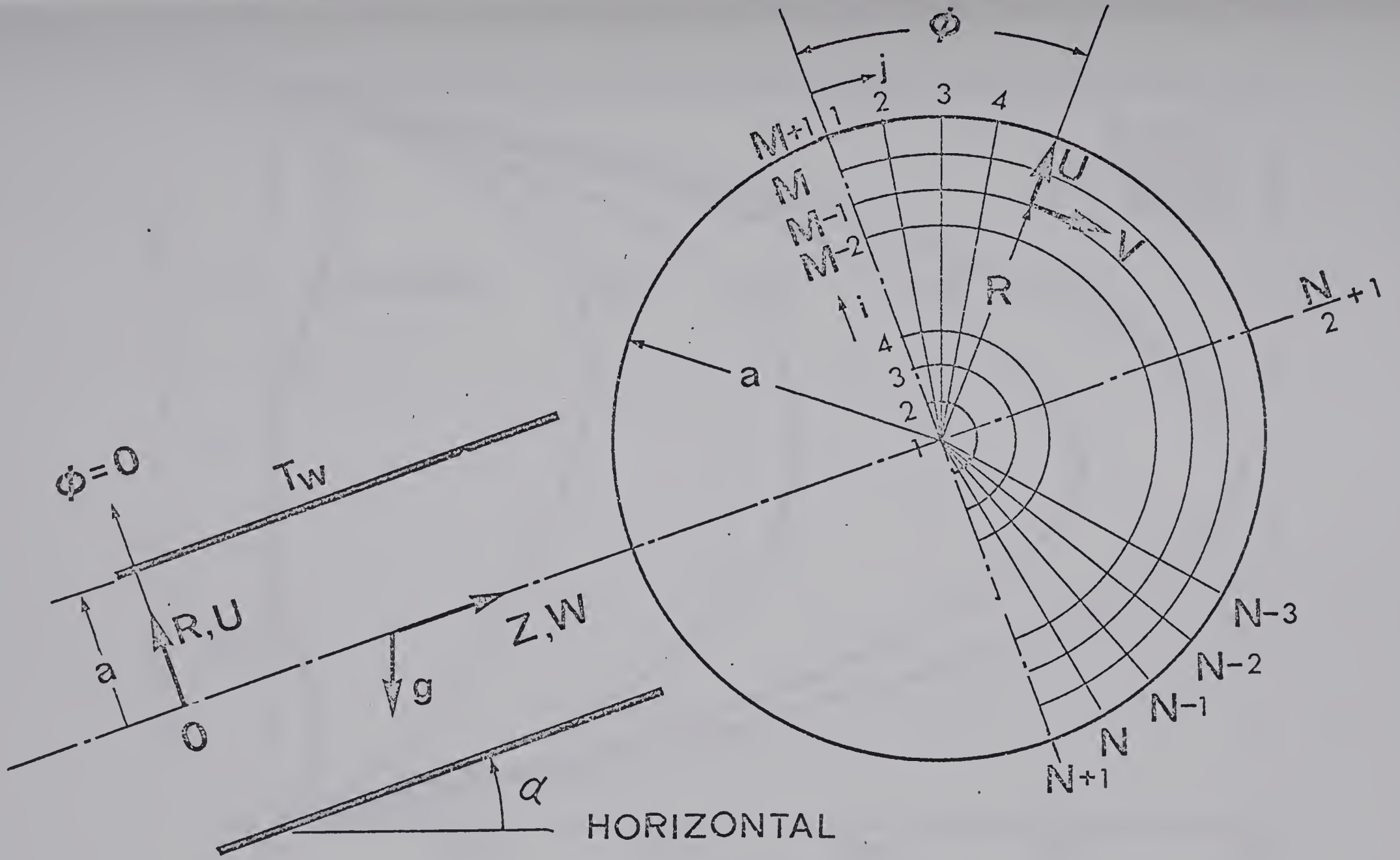

Fig.1 Coordinate system for inclined tube and numerical grid.

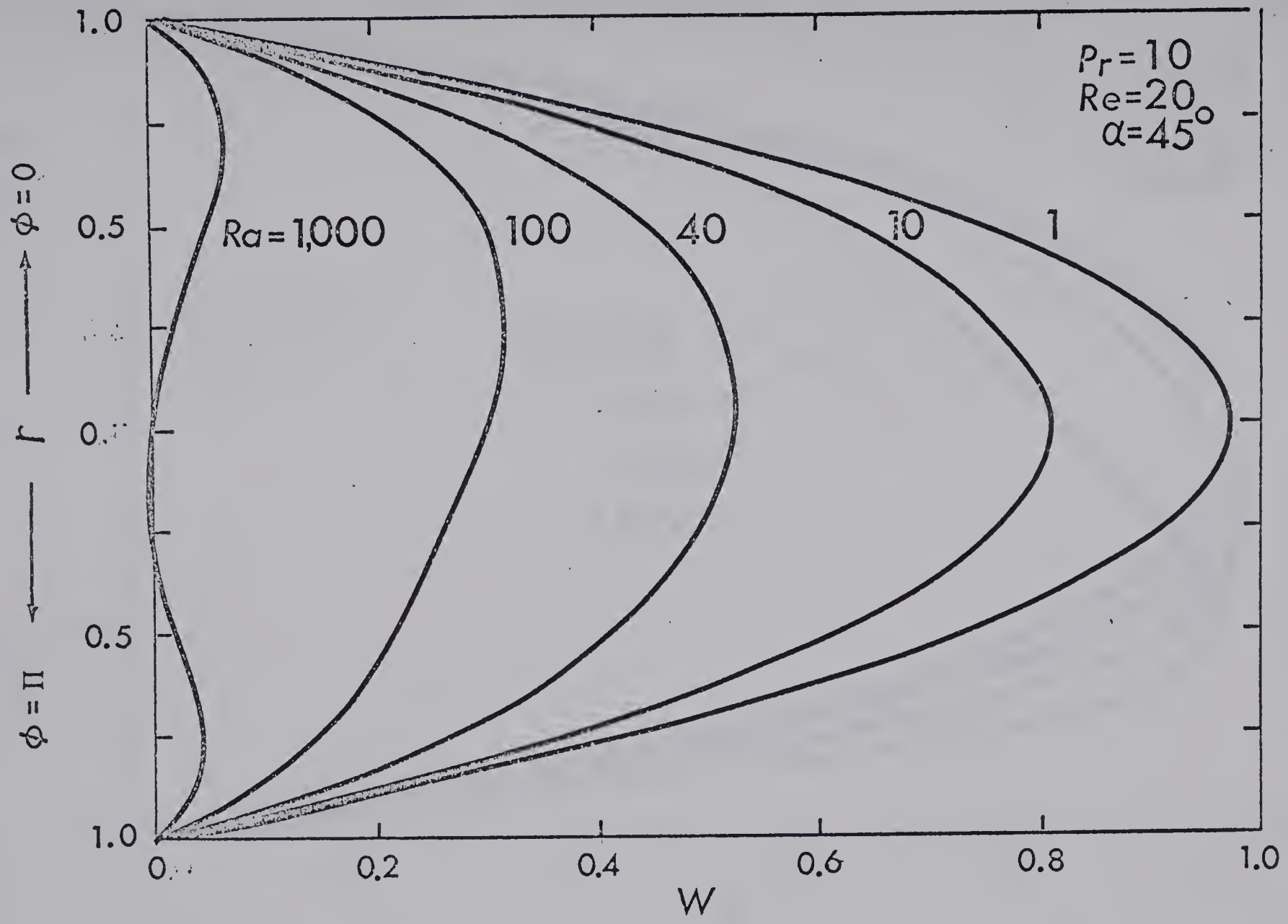

Fig.2(a) Effect of Ra on axial velocity profile along the directions $\phi = 0$ and π.

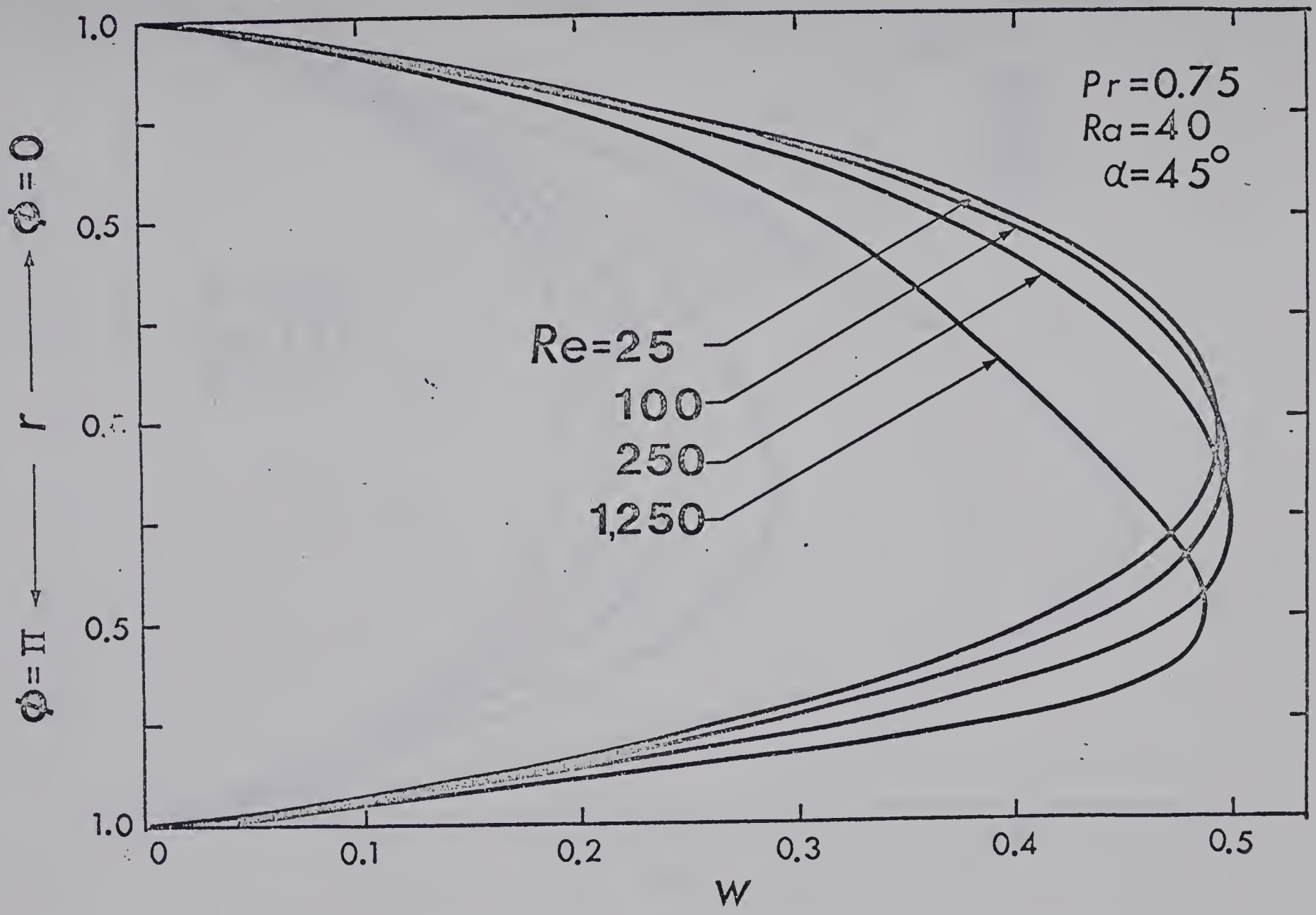

Fig.2(b) Effect of Re on axial velocity profile along the directions $\phi = 0$ and π.

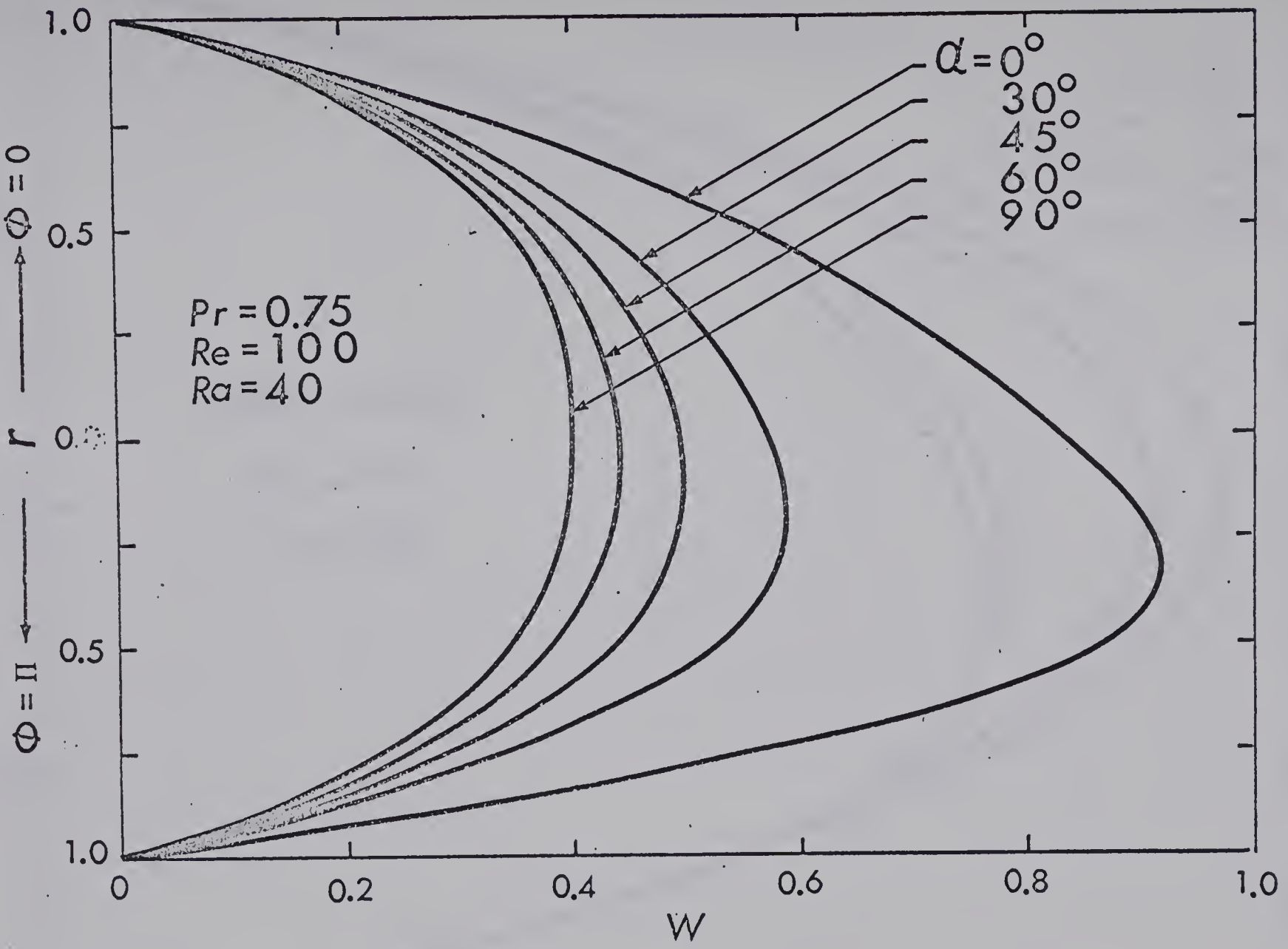

Fig.2(c) Effect of inclination angle on axial velocity profile along the directions $\phi = 0$ and π.

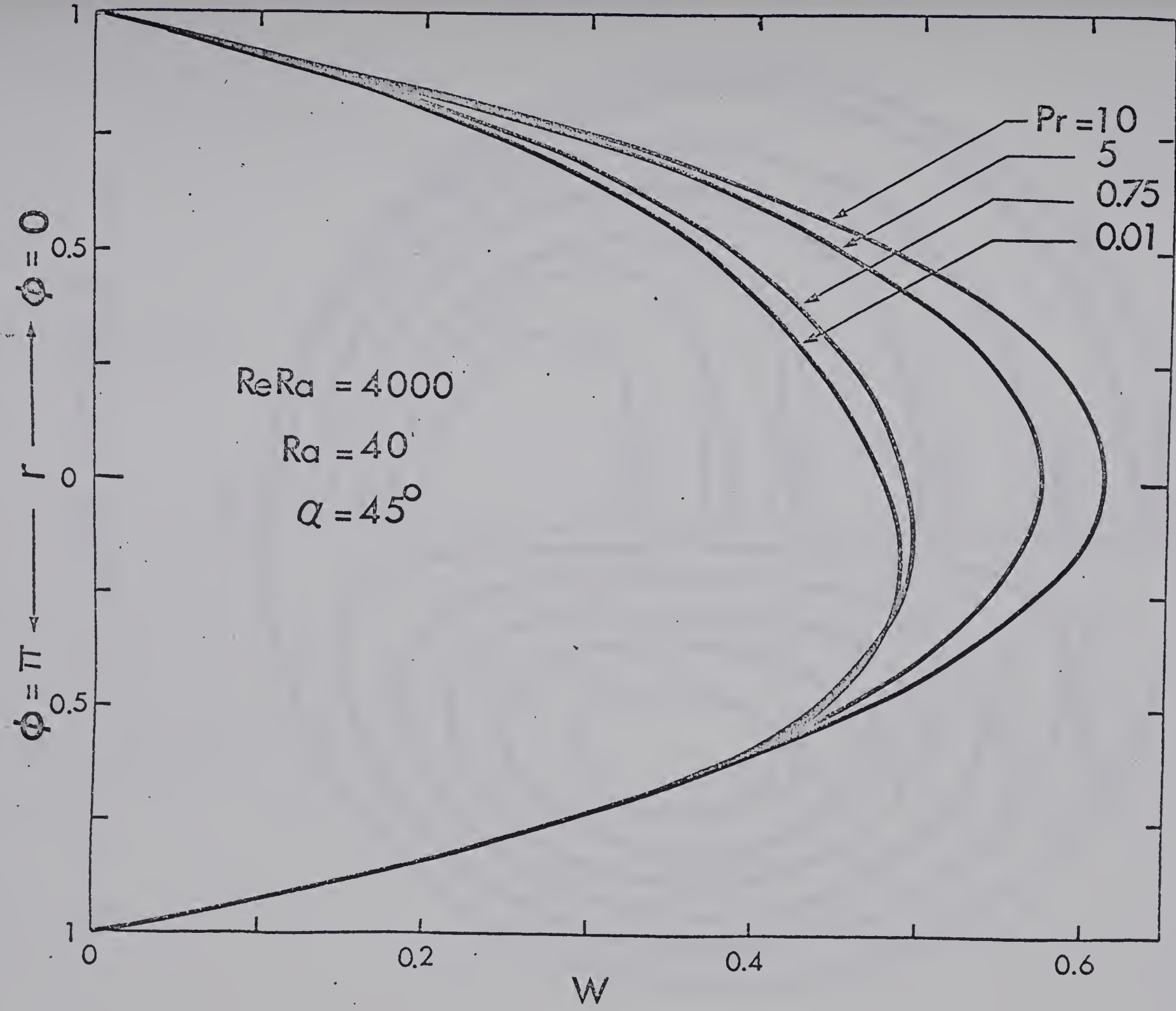

Fig.2(d) Effect of Prandtl number on axial velocity profile along the directions $\phi = 0$ and π

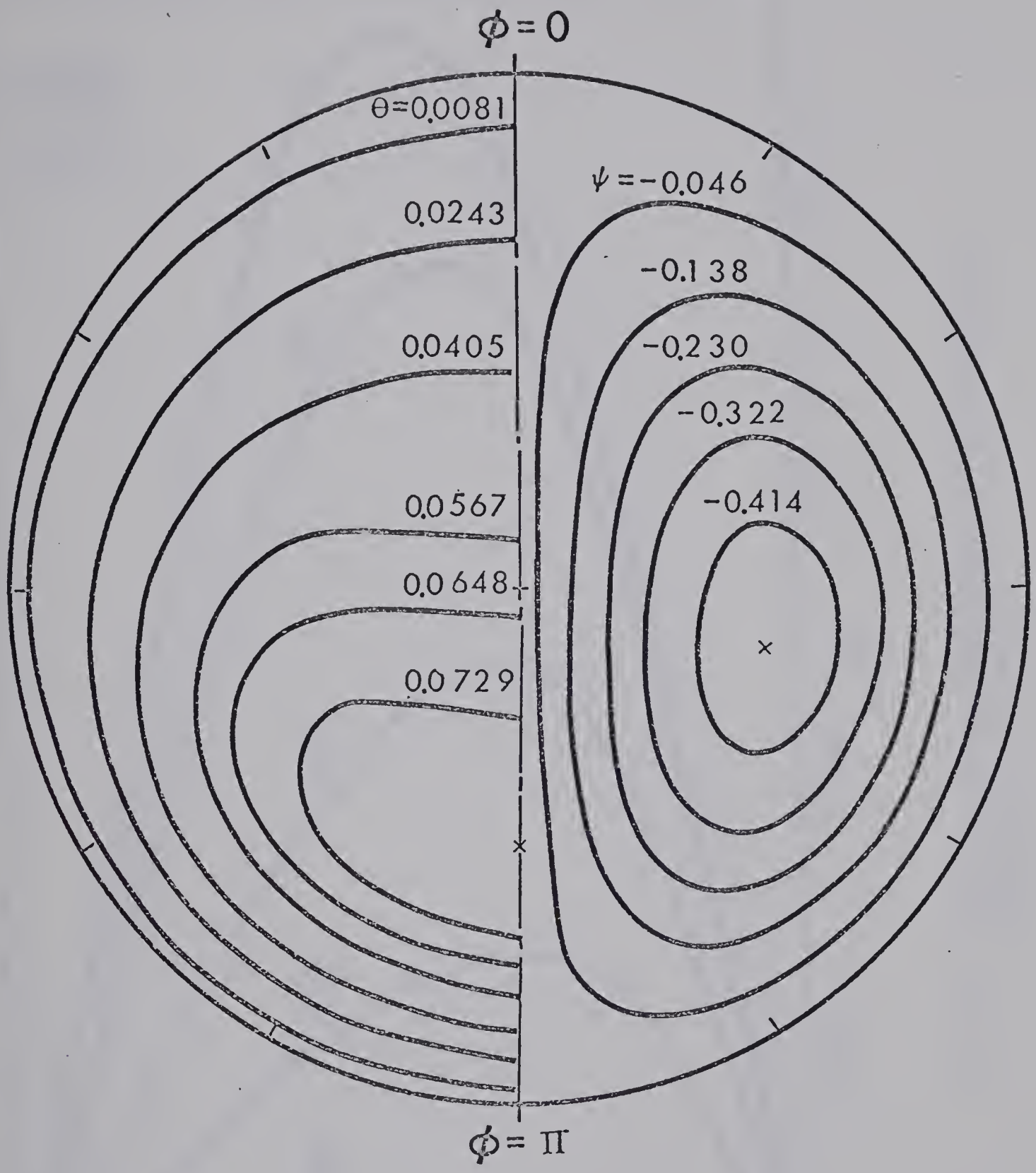

Fig.3 Streamlines and isothermals for Pr = 10, Re = 100, Ra = 40, and $\alpha = 45°$.

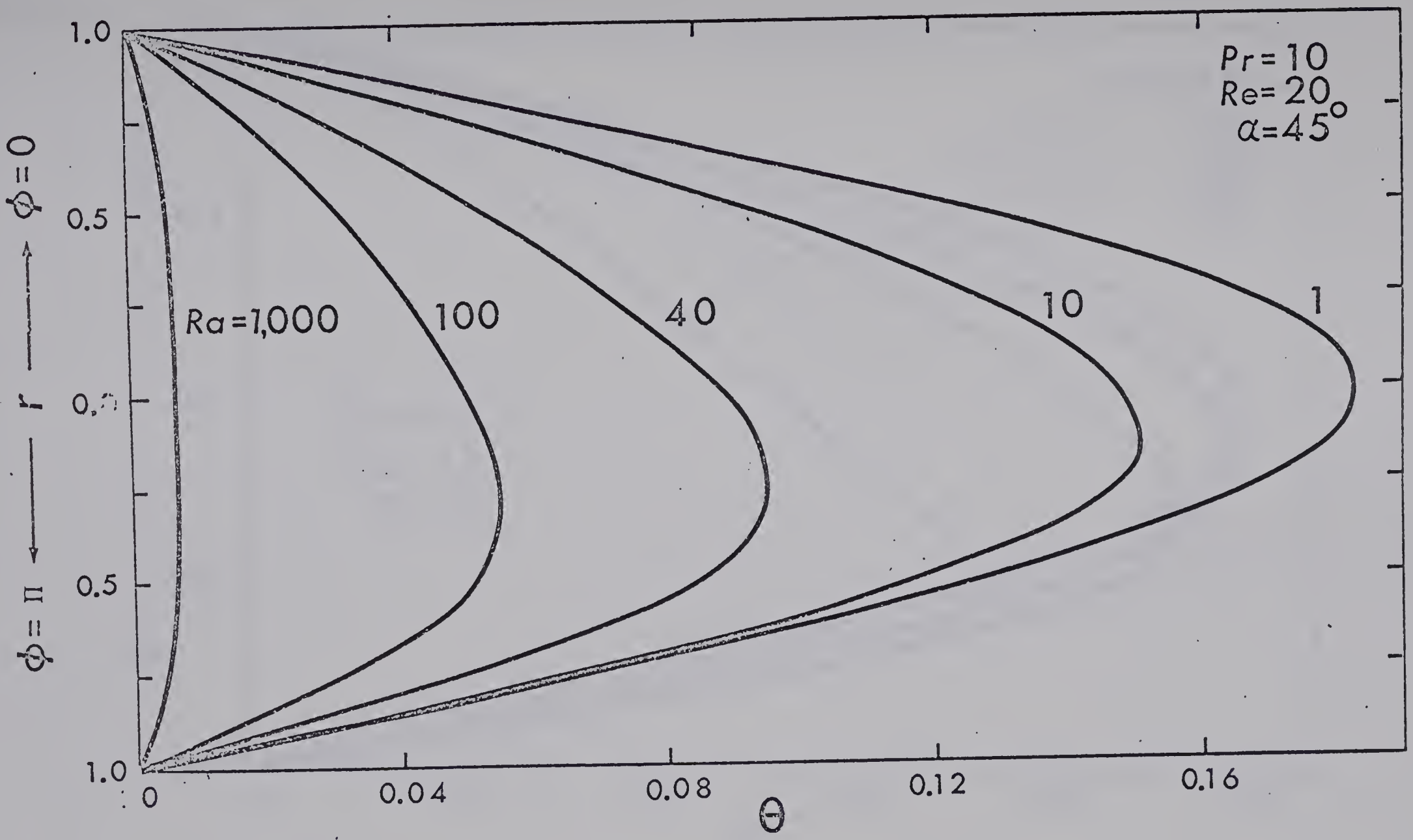

Fig.4(a) Effect of Ra on Temperature profile along the directions $\phi = 0$ and π.

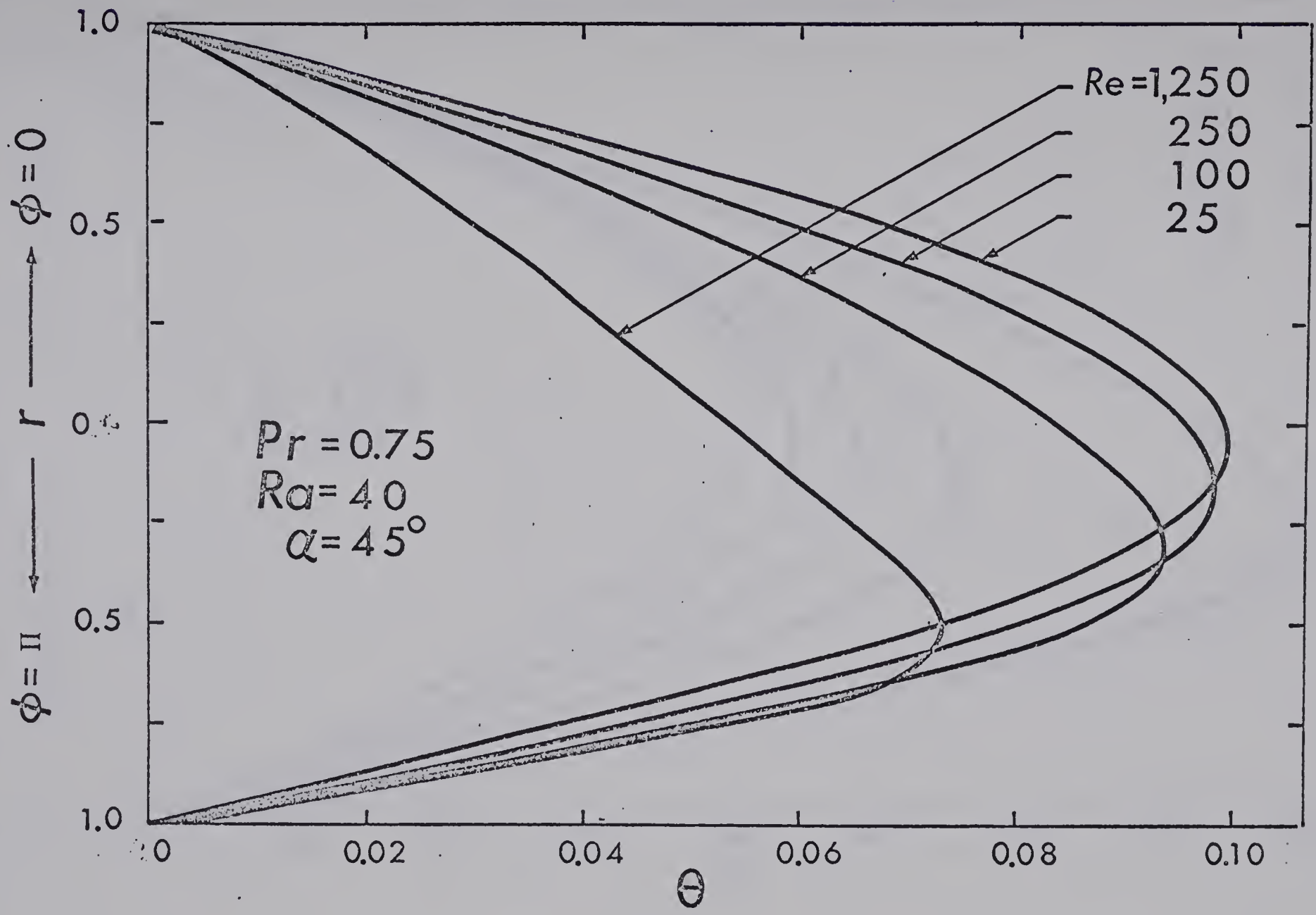

Fig.4(b) Effect of Re on temperature profile along the directions $\phi = 0$ and π.

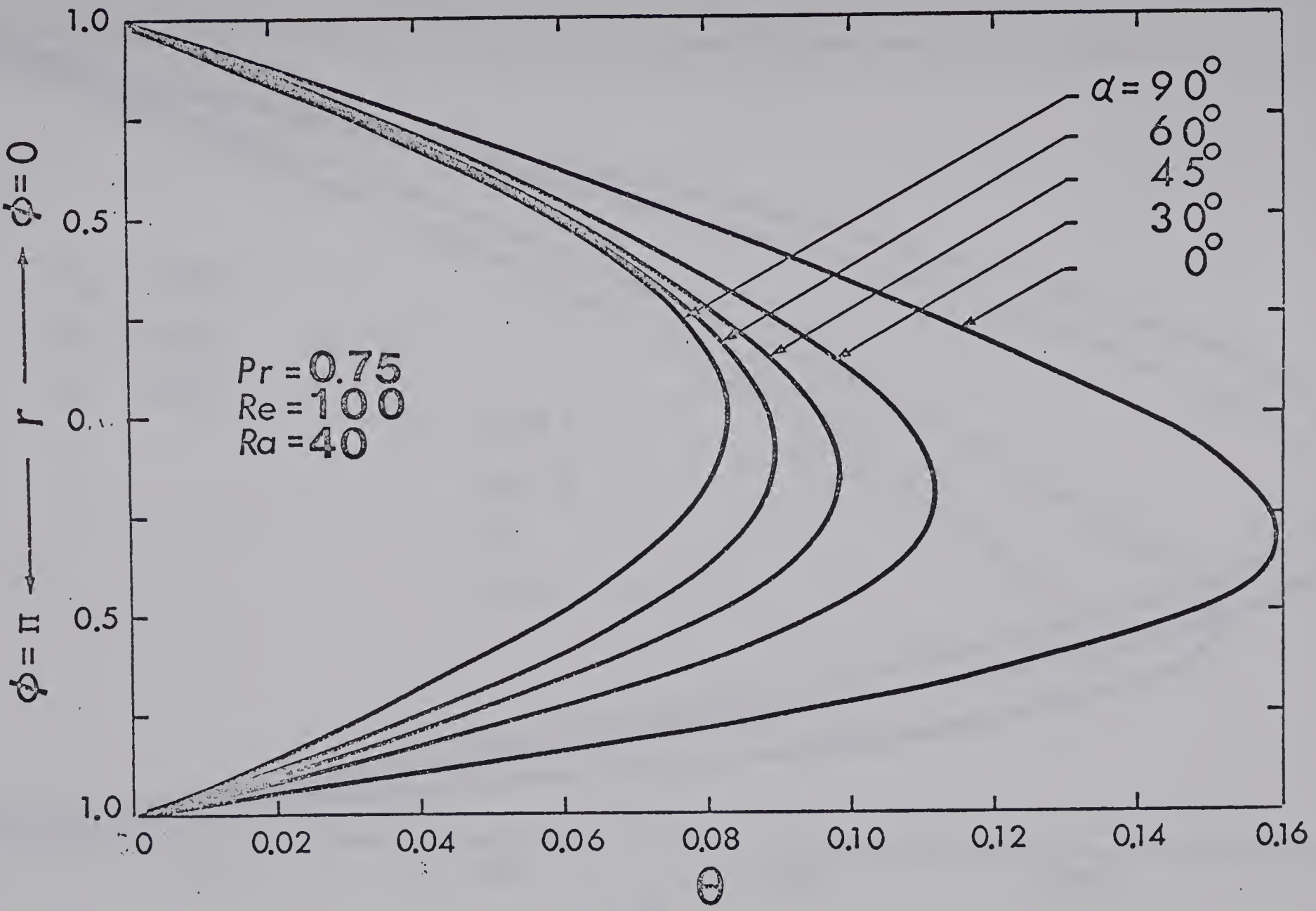

Fig.4(c) Effect of inclination angle on temperature profile along the directions $\phi = 0$ and π.

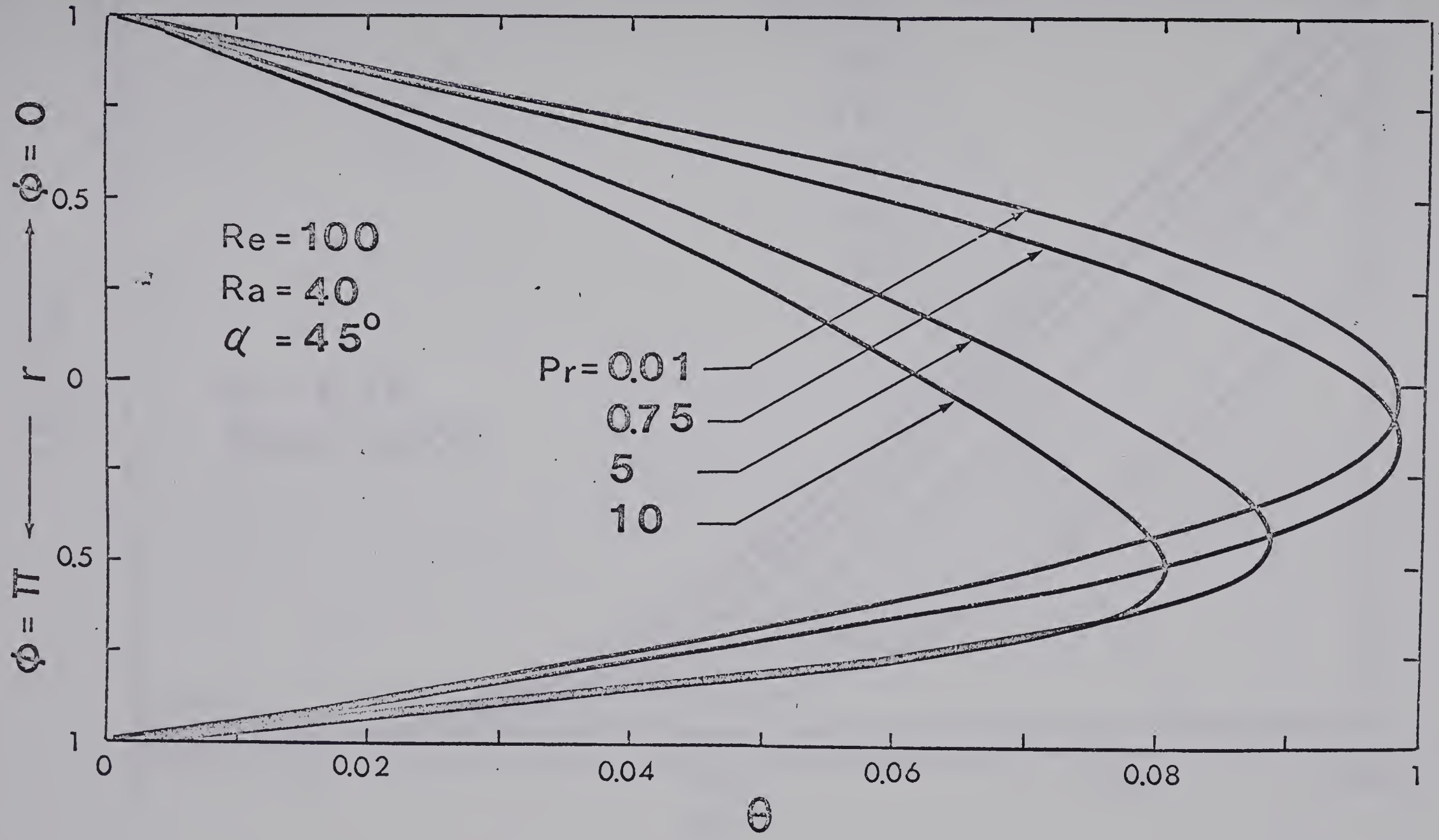

Fig.4(d) Effect of Prandtl number on temperature profile along the directions $\phi = 0$ and π

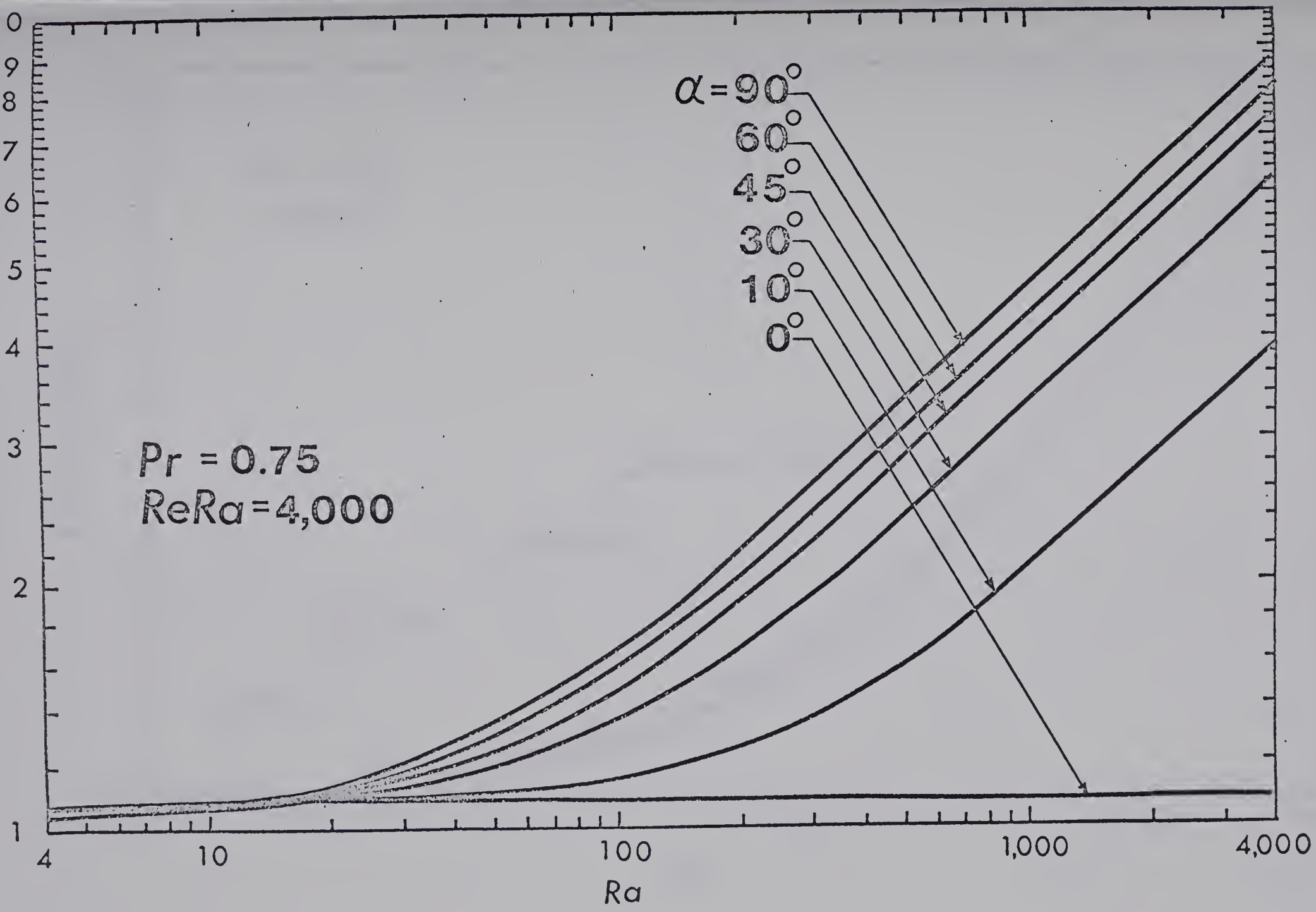

Fig.5 $fRe/(fRe)_0$ versus Ra with α as a parameter for Pr = 0.75 and ReRa = 4,000

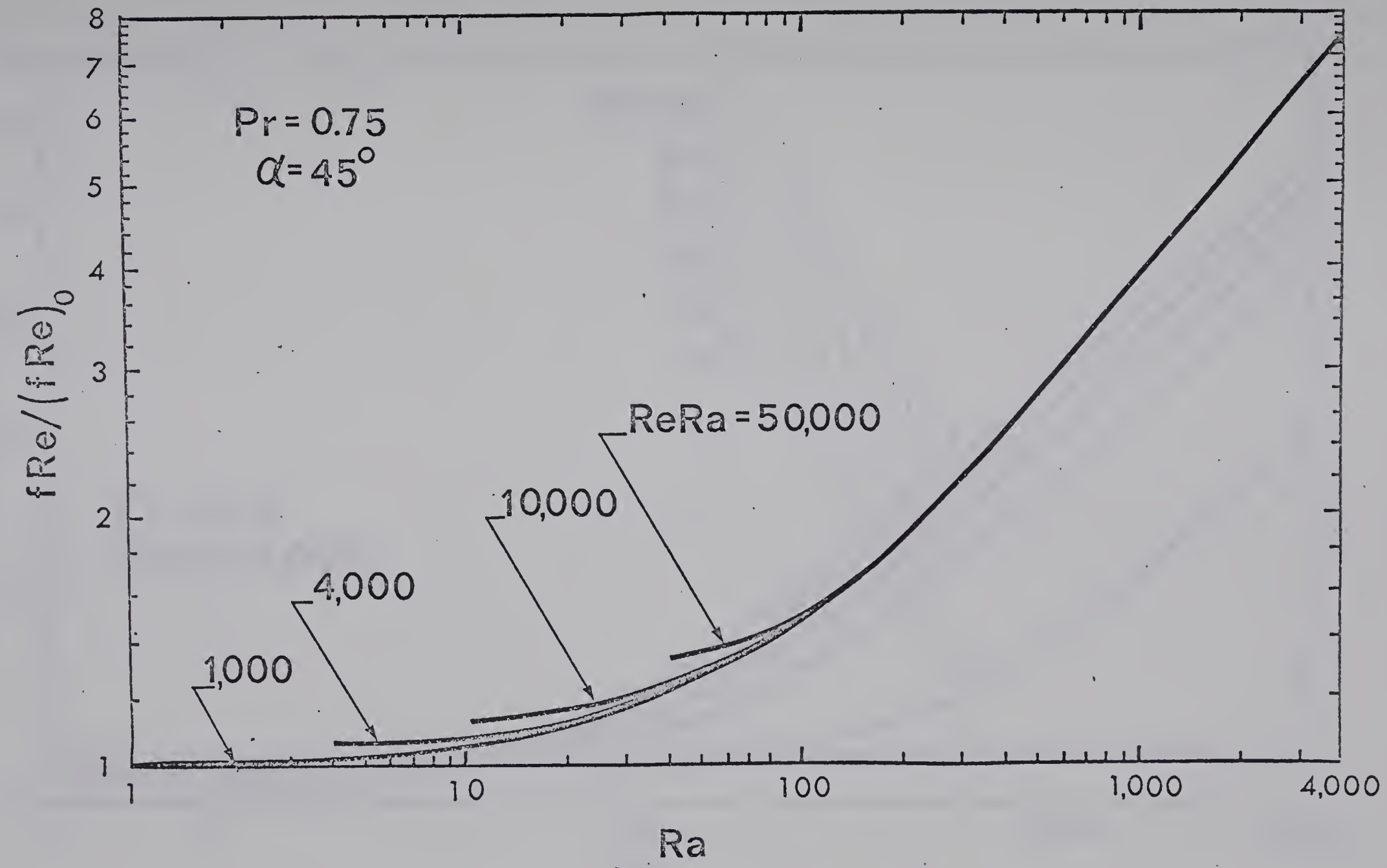

Fig.6 $fRe/(fRe)_0$ versus Ra with ReRa as a parameter for Pr = 0.75 and $\alpha = 45°$.

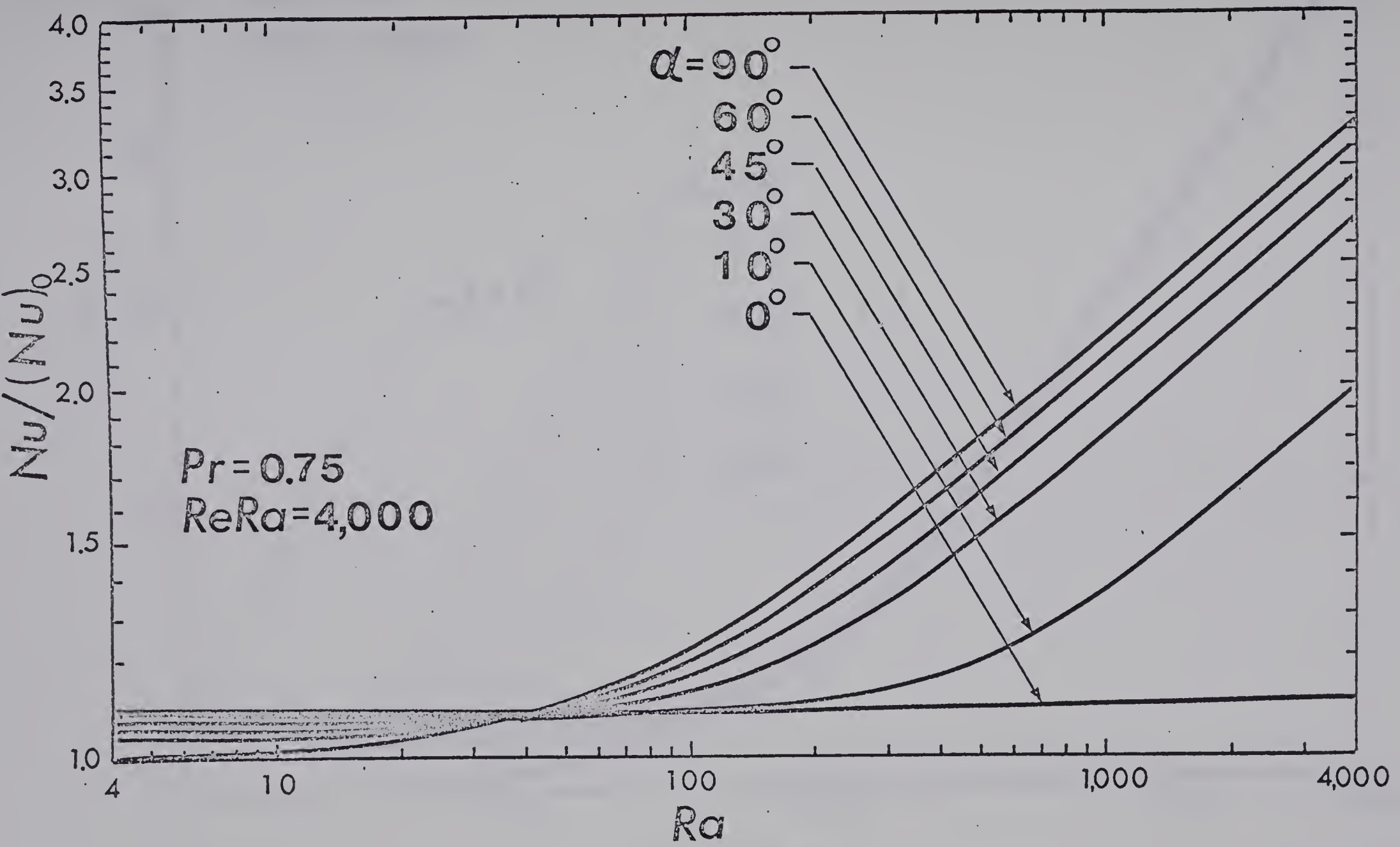

Fig. 7. $Nu/(Nu)_0$ versus Ra with α as a parameter for Pr = 0.75 and Re Ra = 4,000.

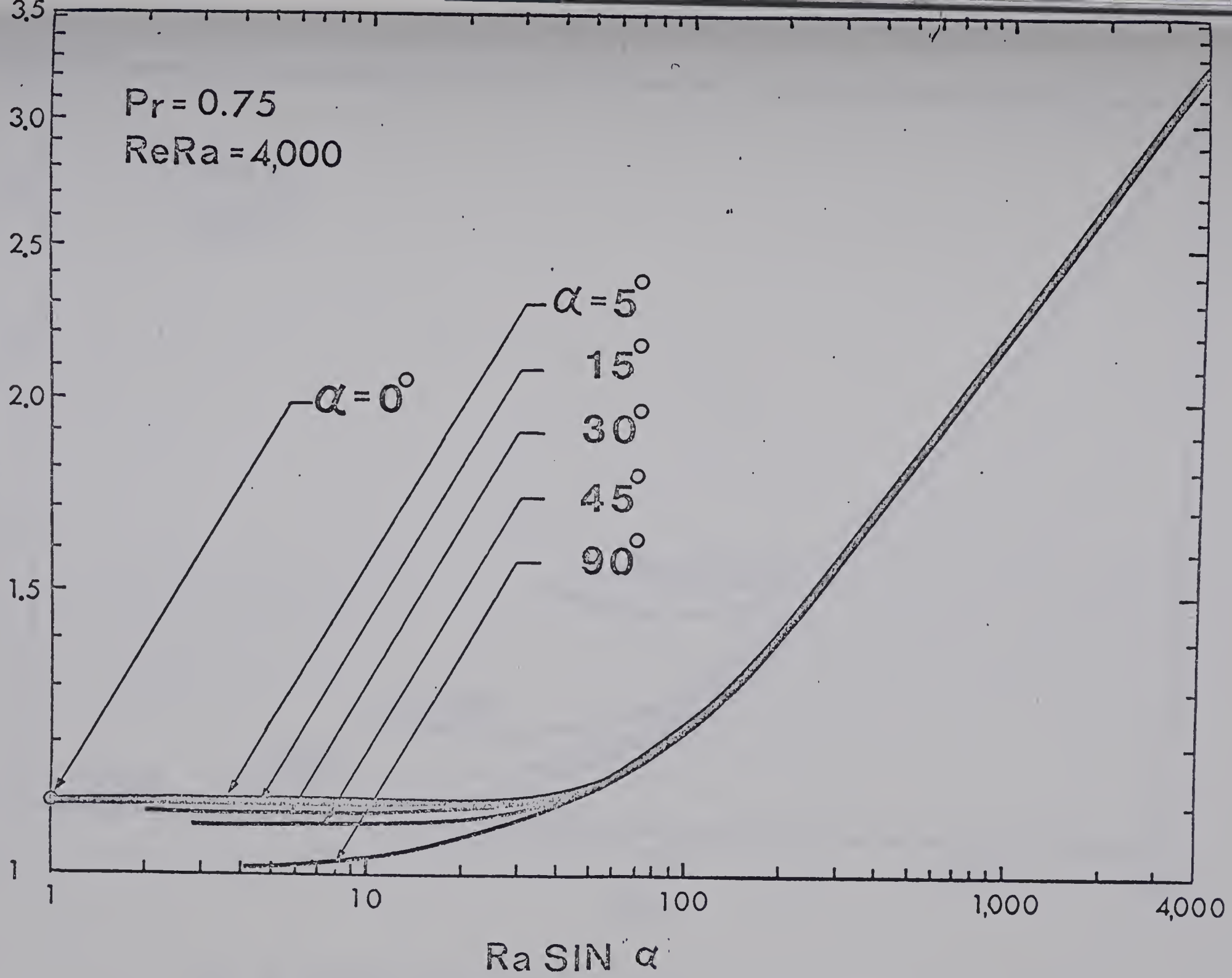

Fig.8 $Nu/(Nu)_0$ versus Ra sin α with α as a parameter for Pr = 0.75 and ReRa = 4,000.

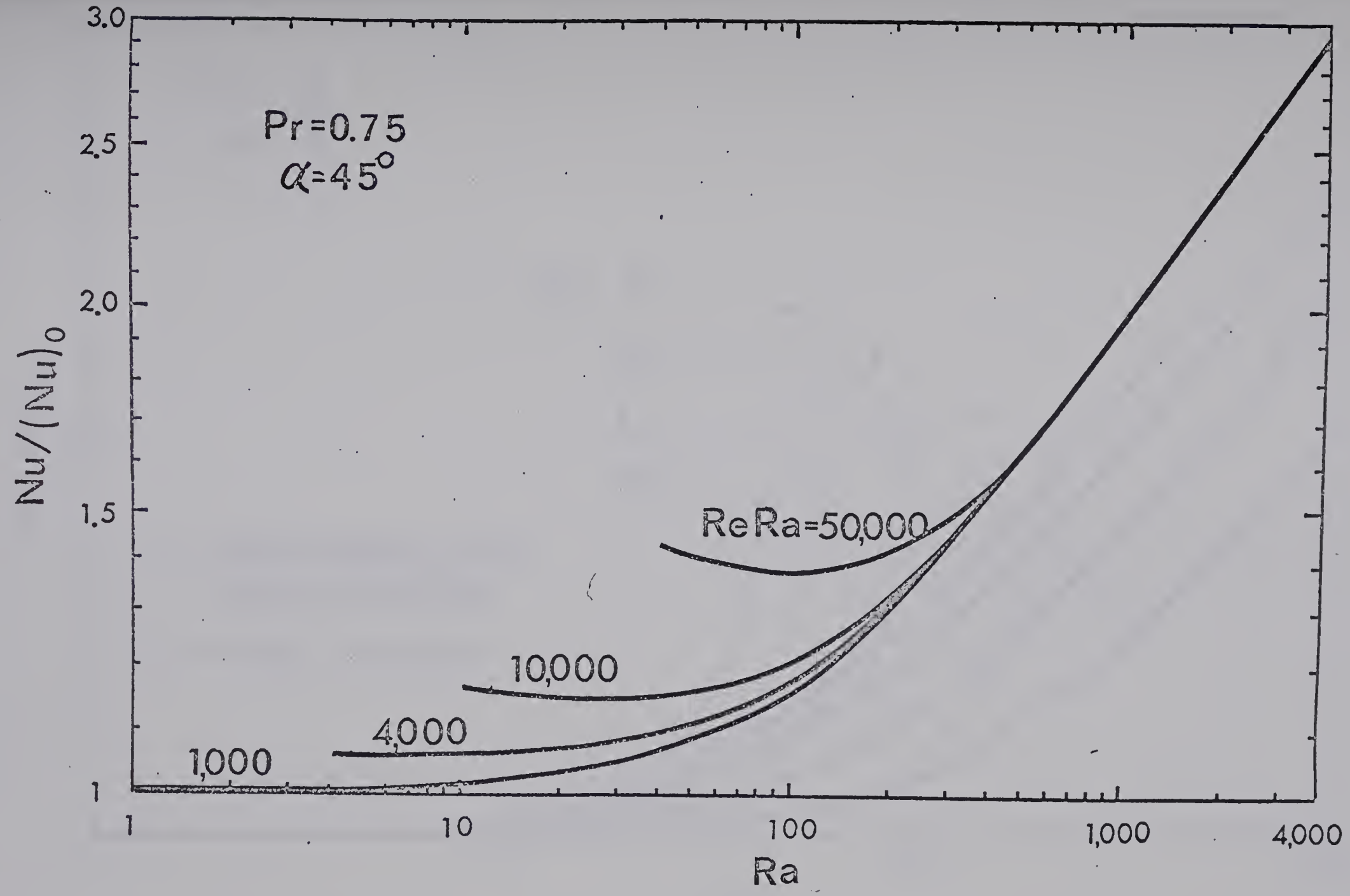

Fig. 9 $Nu/(Nu)_0$ versus Ra with ReRa as a parameter for Pr = 0.75 and $\alpha = 45°$.

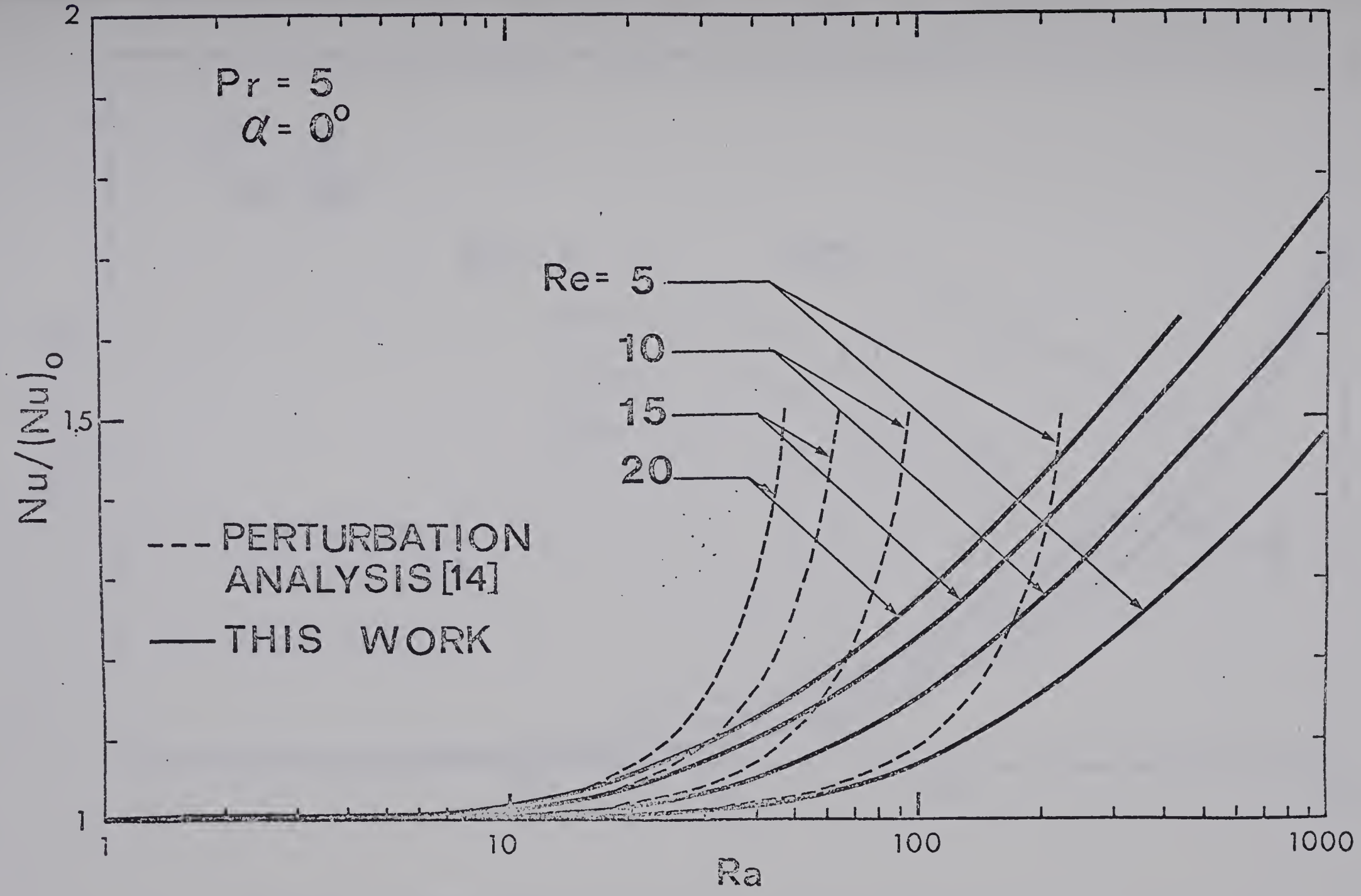

Fig.10 $Nu/(Nu)_0$ versus Ra for Pr = 5 and $\alpha = 0°$ with comparison made against perturbation solution.

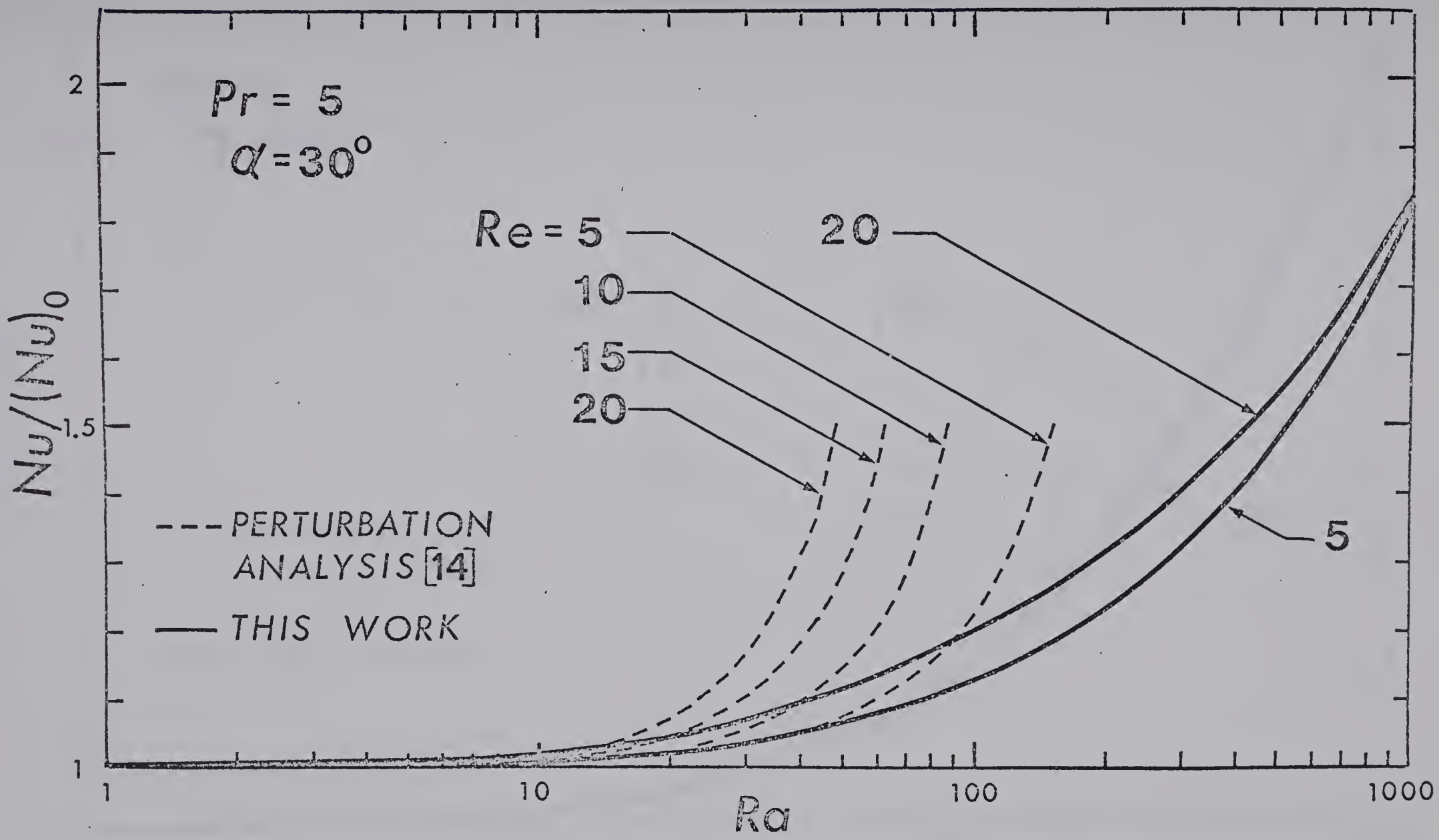

Fig.1.1 $Nu/(Nu)_0$ versus Ra for Pr = 5 and $\alpha = 30°$ with comparison made against perturbation solution.

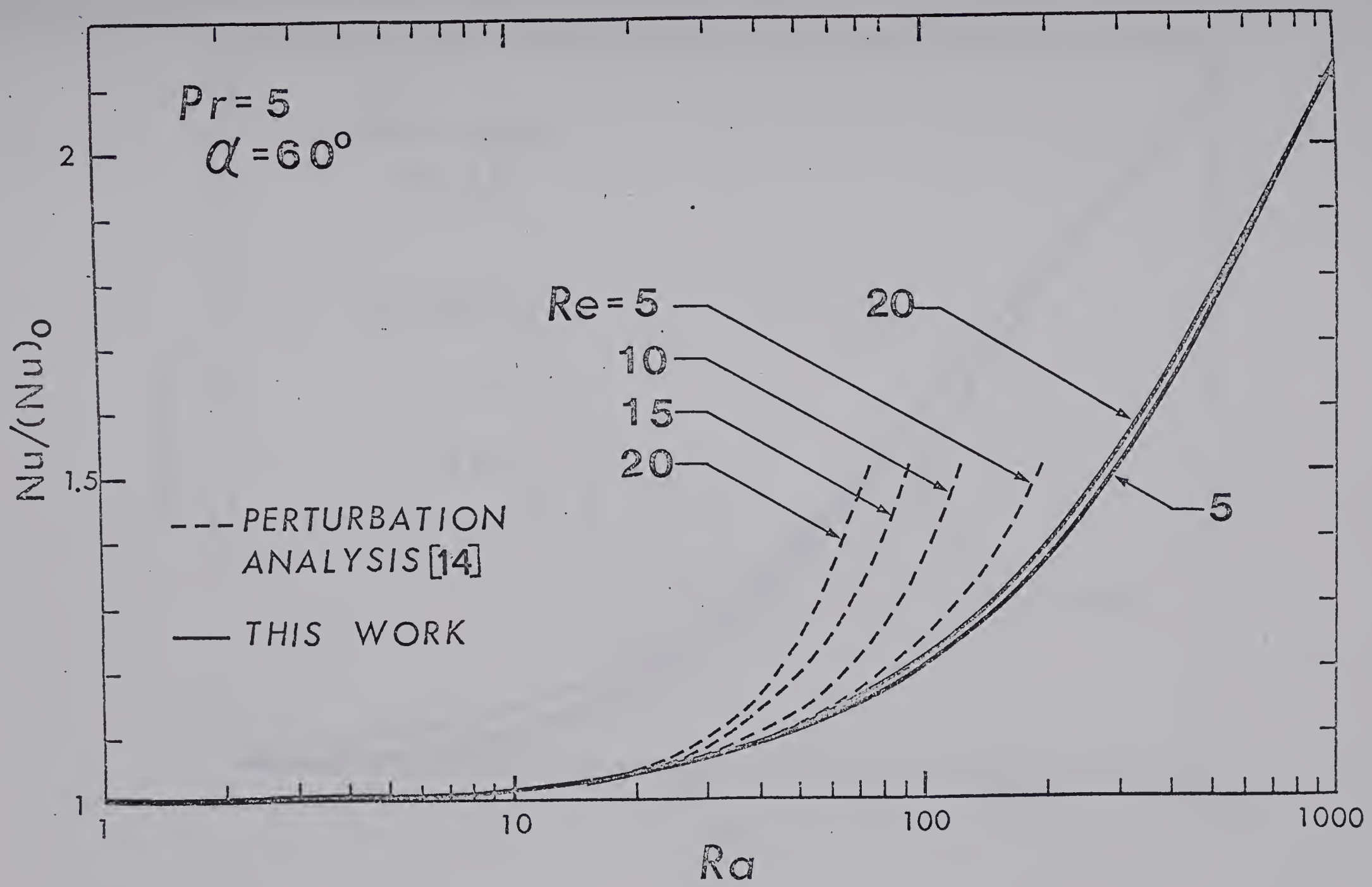

Fig.12 $Nu/(Nu)_0$ versus Ra for Pr = 5 and $\alpha = 60°$ with comparison made against perturbation solution.

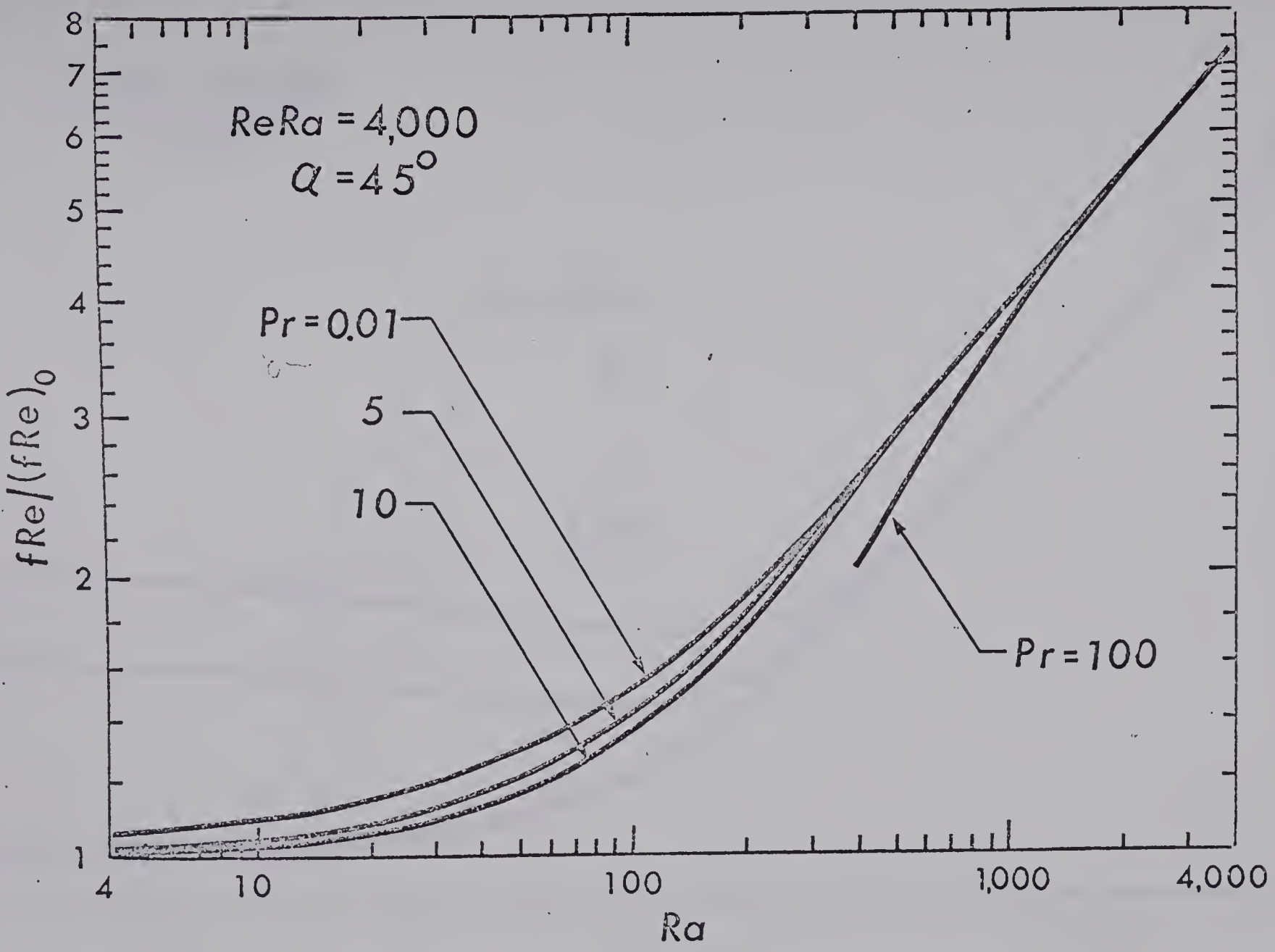

Fig.13 $fRe/(fRe)_0$ versus Ra with Pr as a parameter for ReRa = 4,000 and $\alpha = 45°$

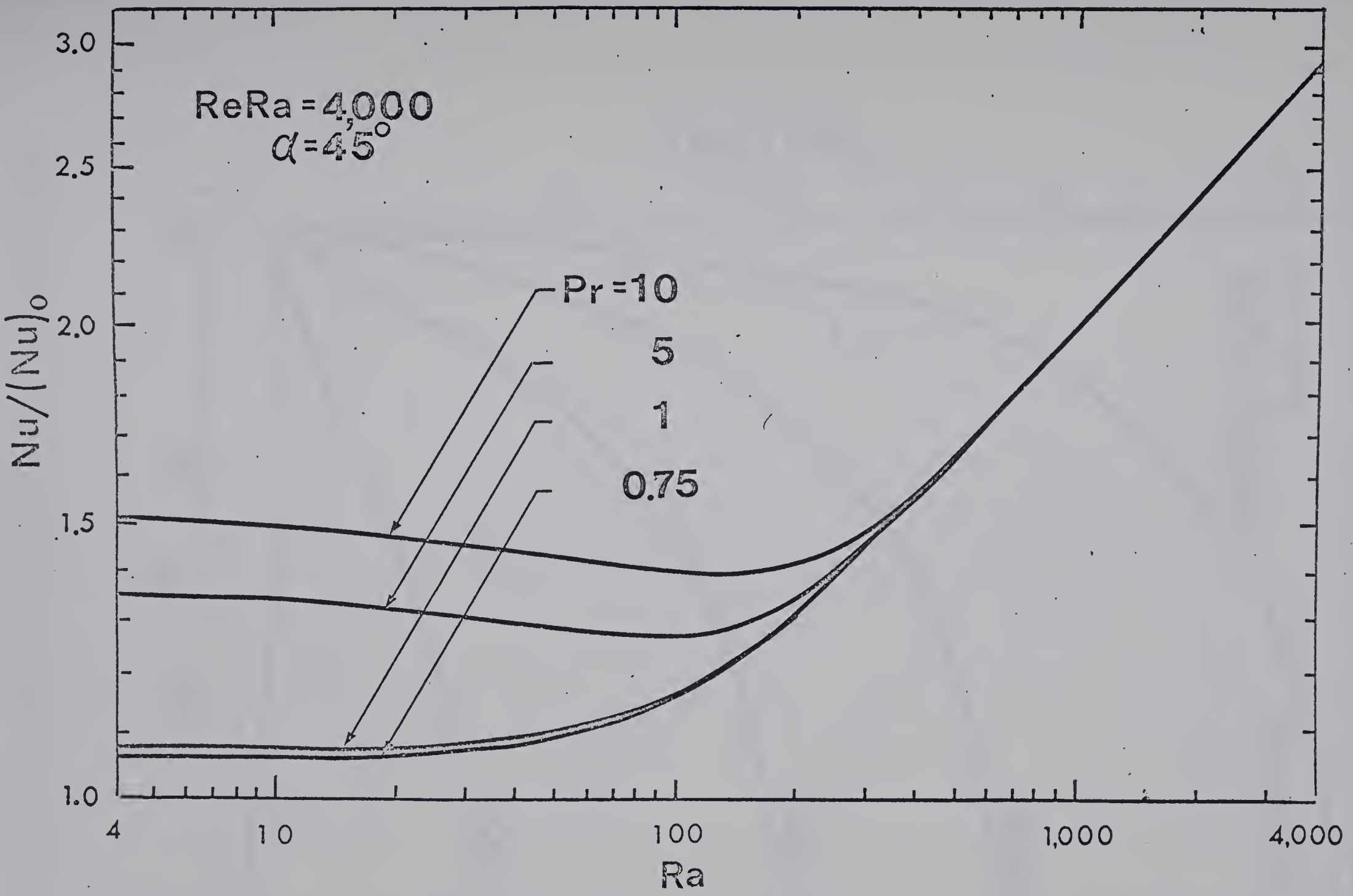

Fig.14 $Nu/(Nu)_0$ versus Ra with Pr as a parameter for ReRa = 4,000 and $\alpha = 45°$.

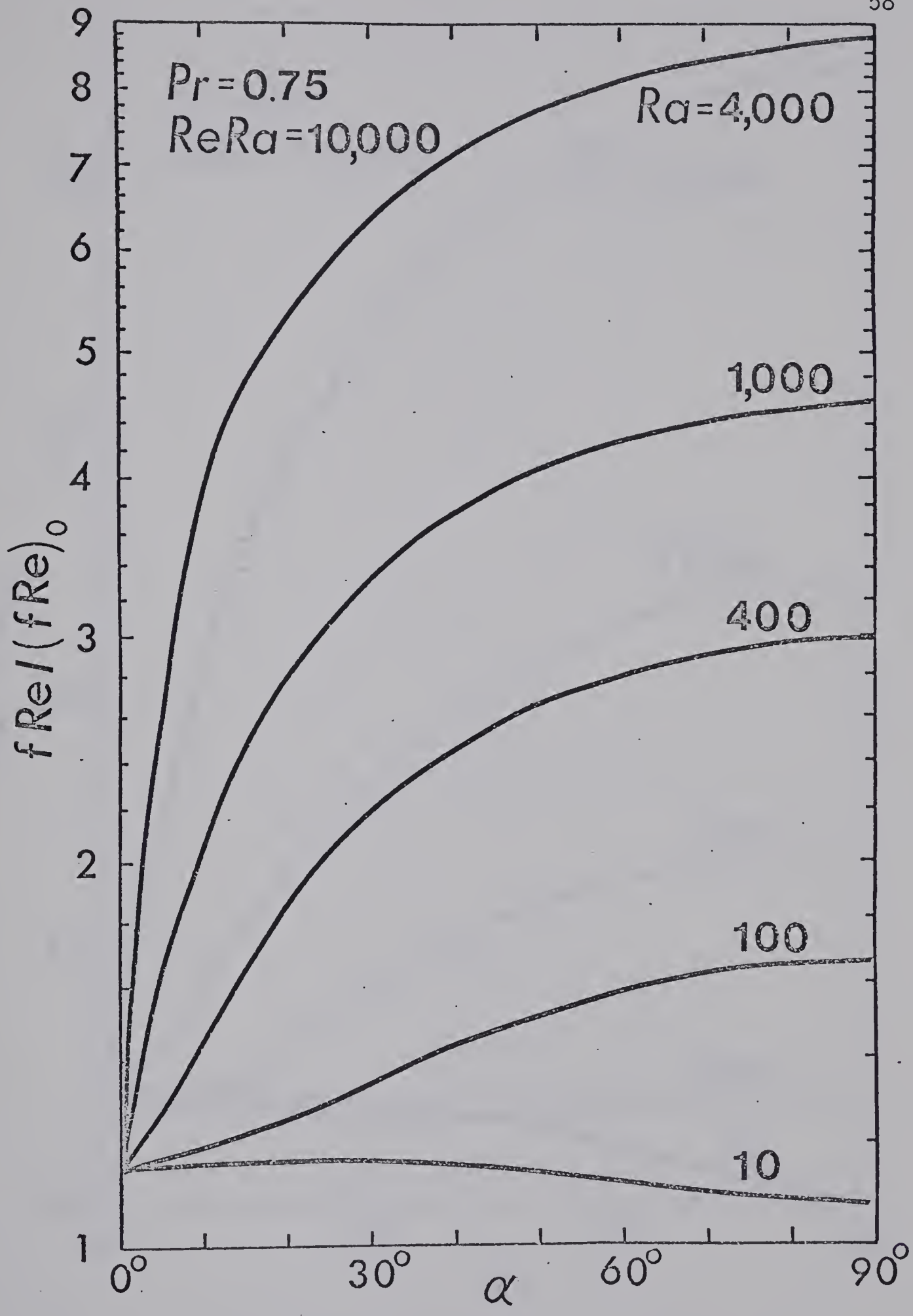

Fig.15 $fRe/(fRe)_0$ versus α with Ra as a parameter for Pr = 0.75 and ReRa = 10,000

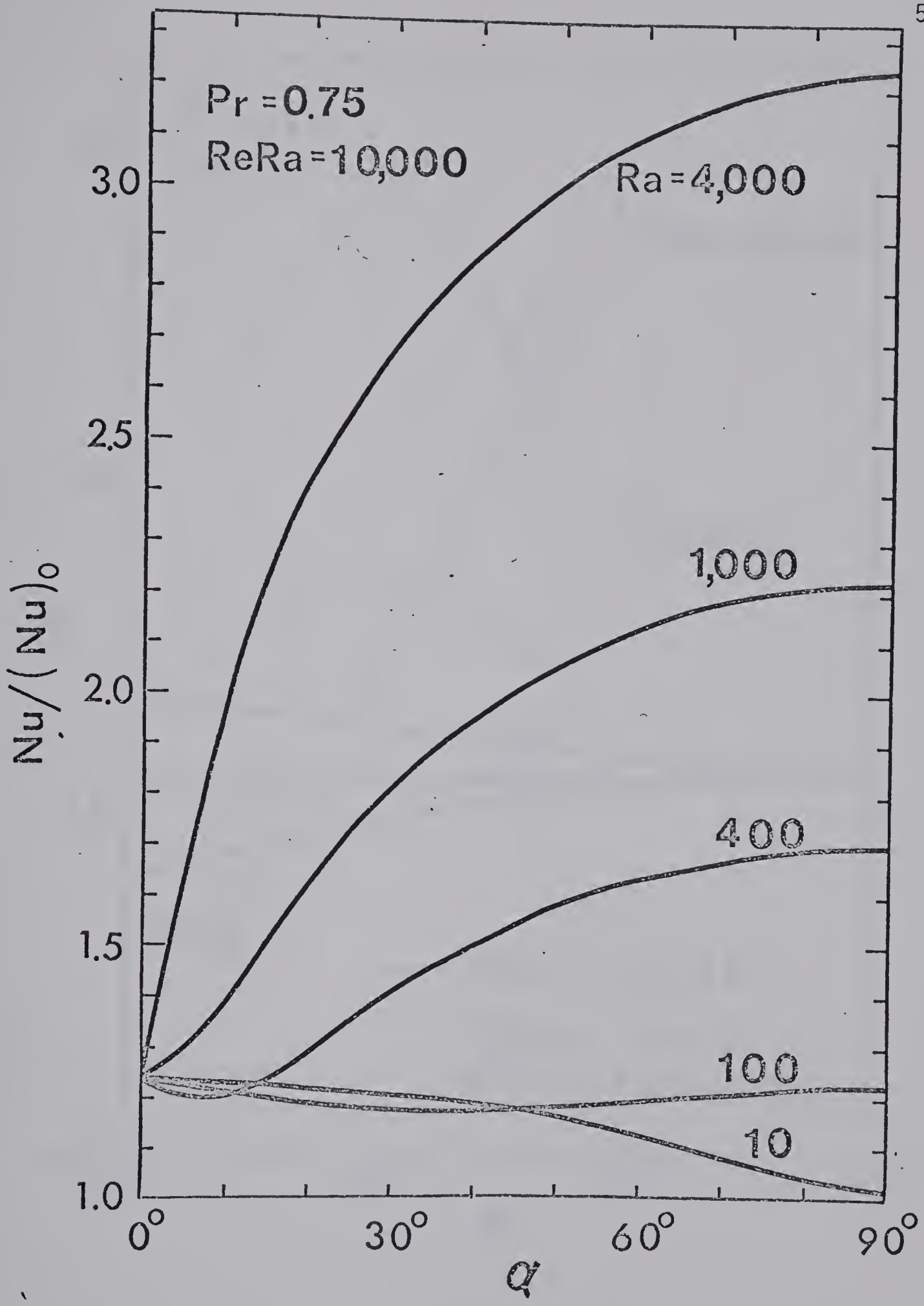

Fig.16 $Nu/(Nu)_0$ versus α with Ra as a parameter for Pr = 0.75 and ReRa = 10,000.

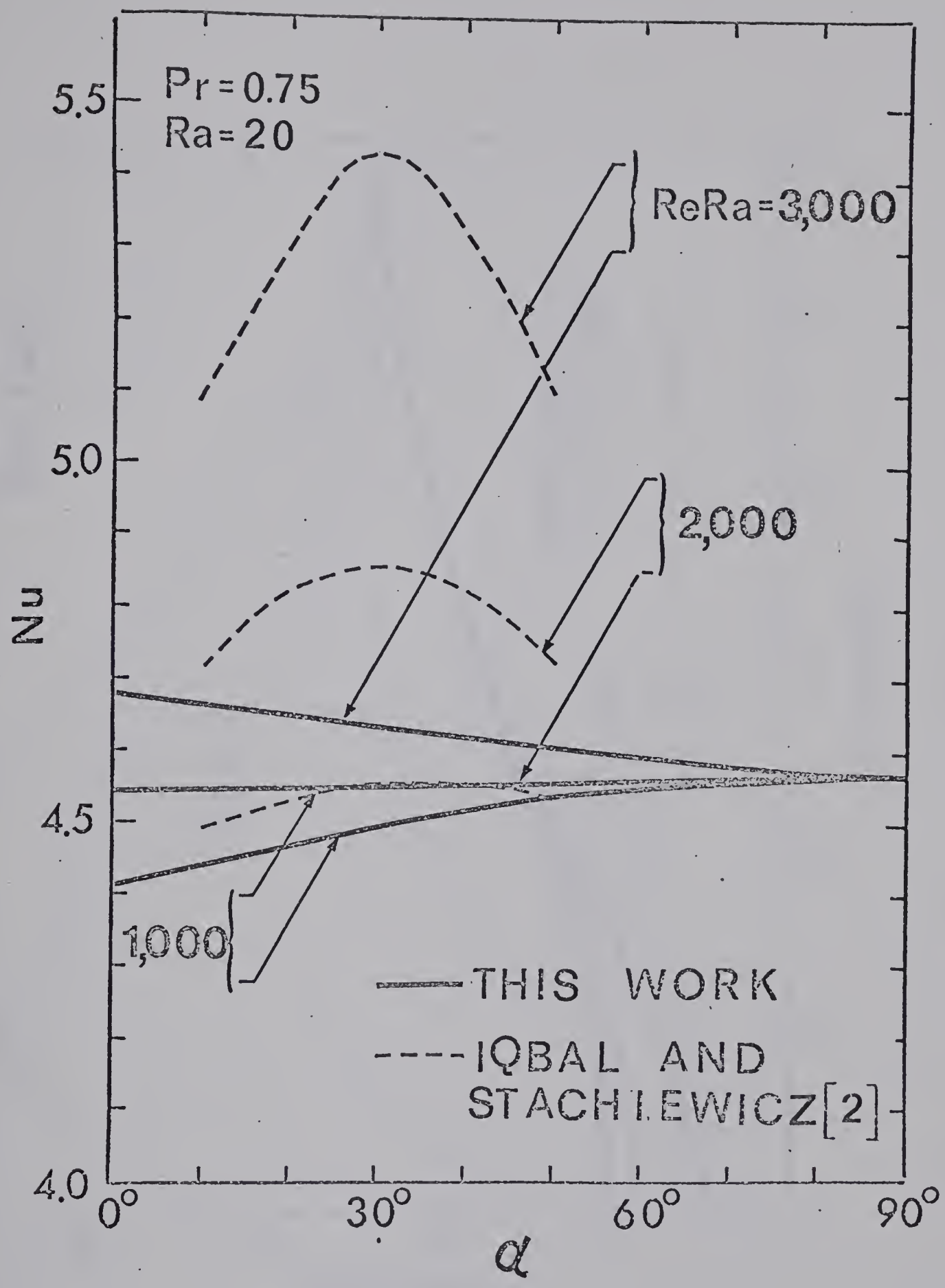

Fig.17 Comparison of heat transfer results from this work with those from perturbation method [2].

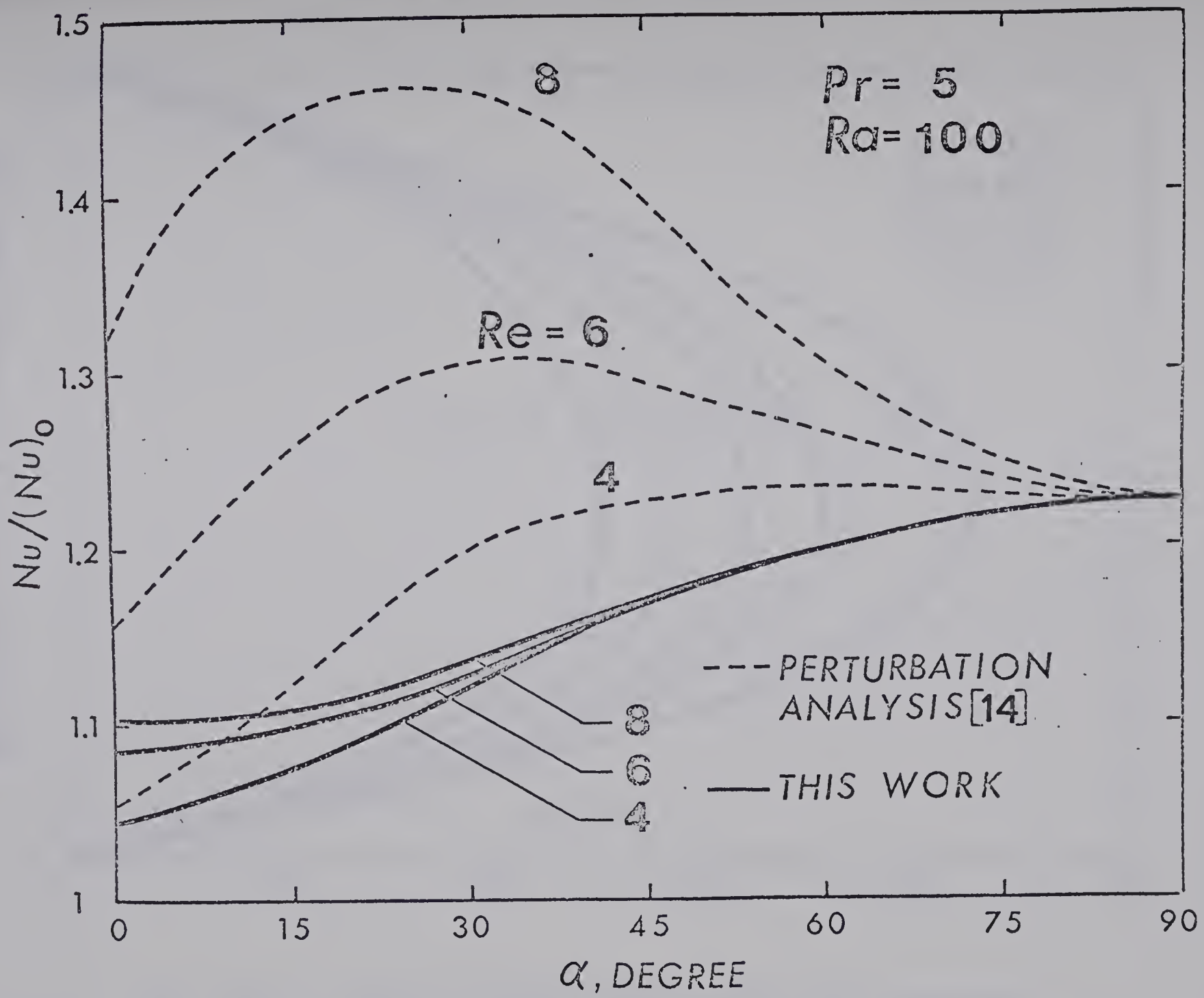

Fig.18 Comparison of heat transfer results from this work with those from perturbation analysis.

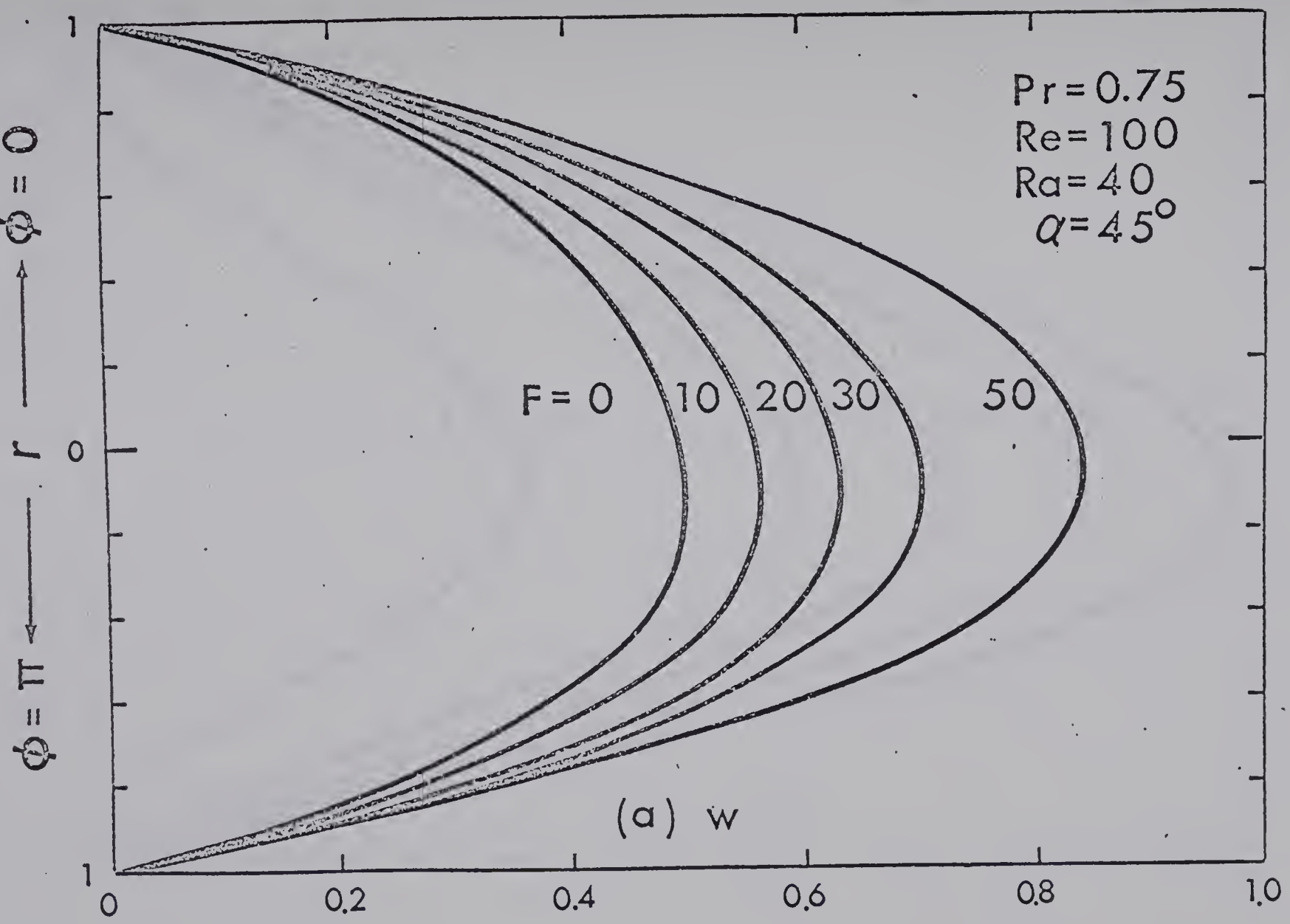

Fig. 19(a) Typical velocity profiles with F as a parameter

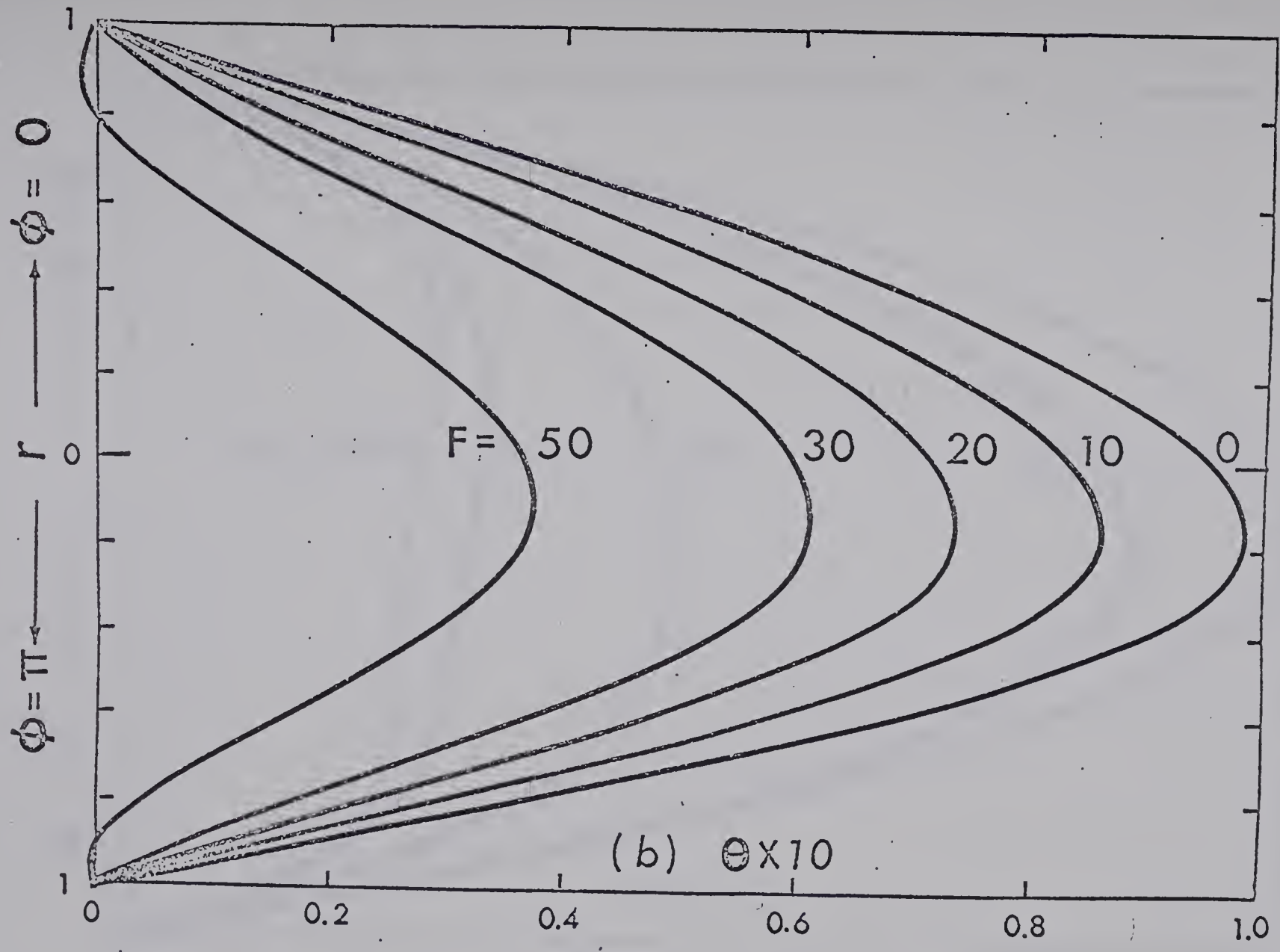

Fig. 19(b) Typical temperature profiles with F as a parameter

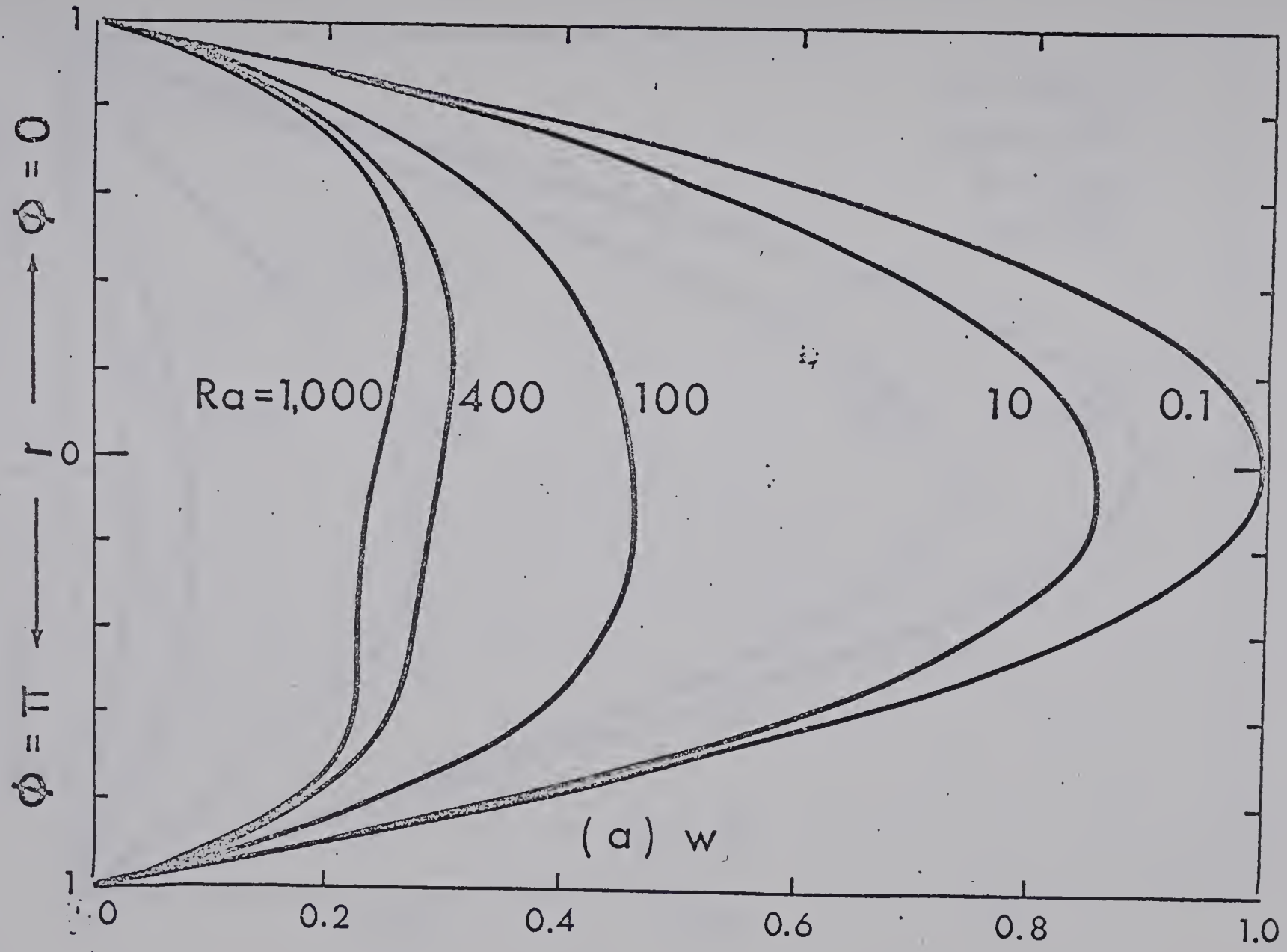

Fig. 20(a) Typical velocity profiles with Ra as a parameter

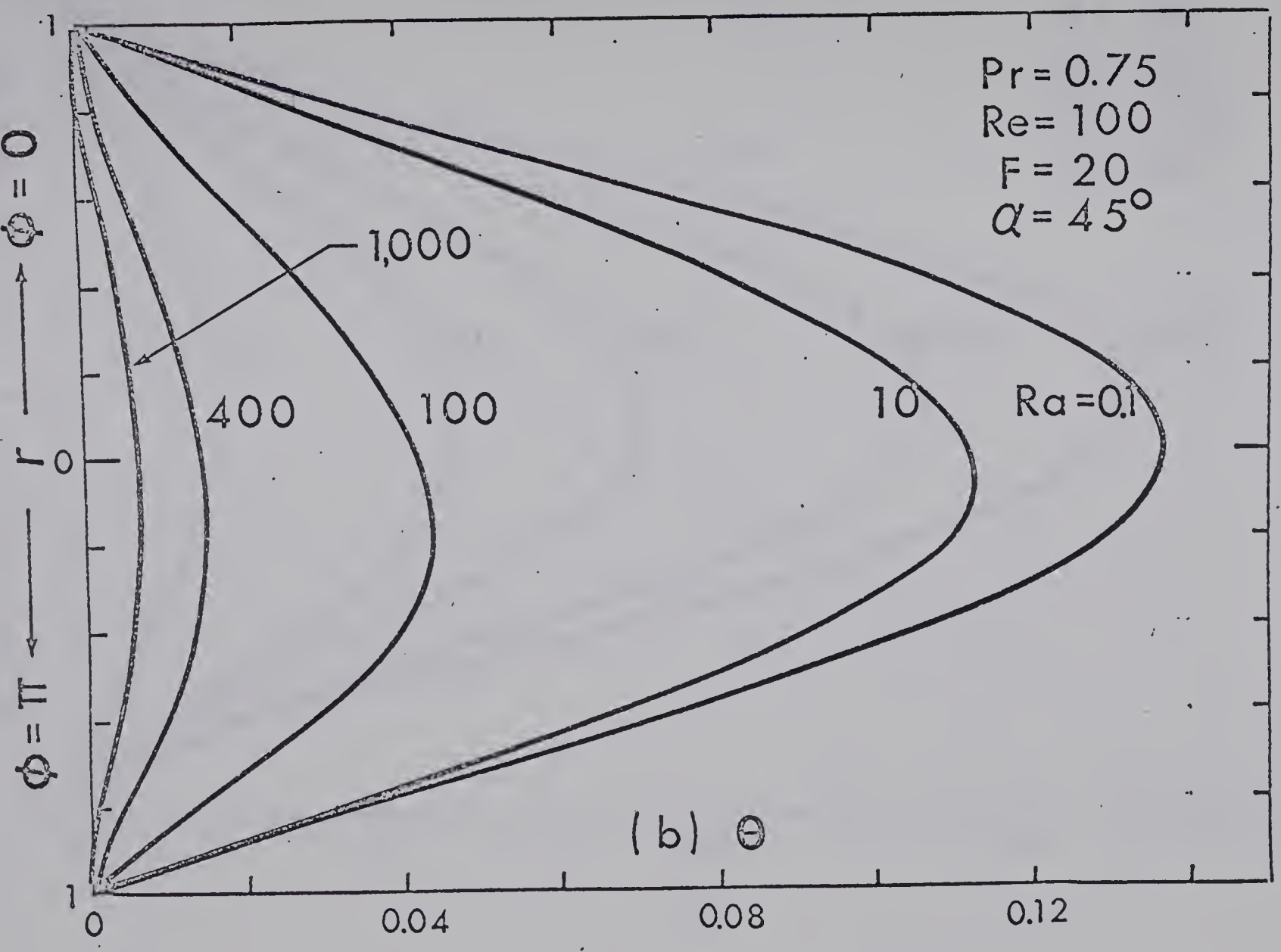

Fig. 20(b) Typical temperature profile with Ra as a parameter

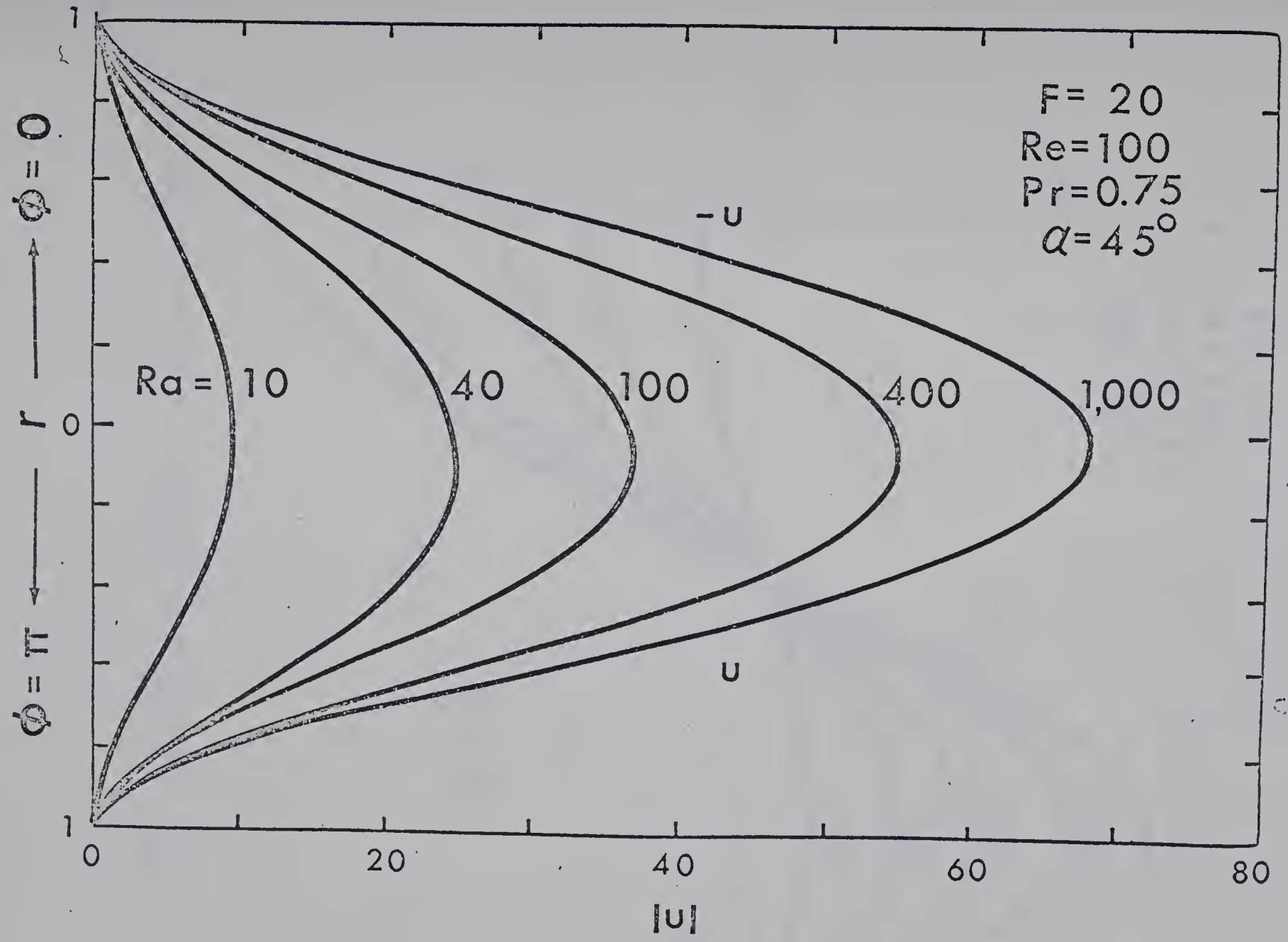

Fig.21(a) Distribution of secondary velocity component u along $\phi = 0$ and π with Ra as a parameter

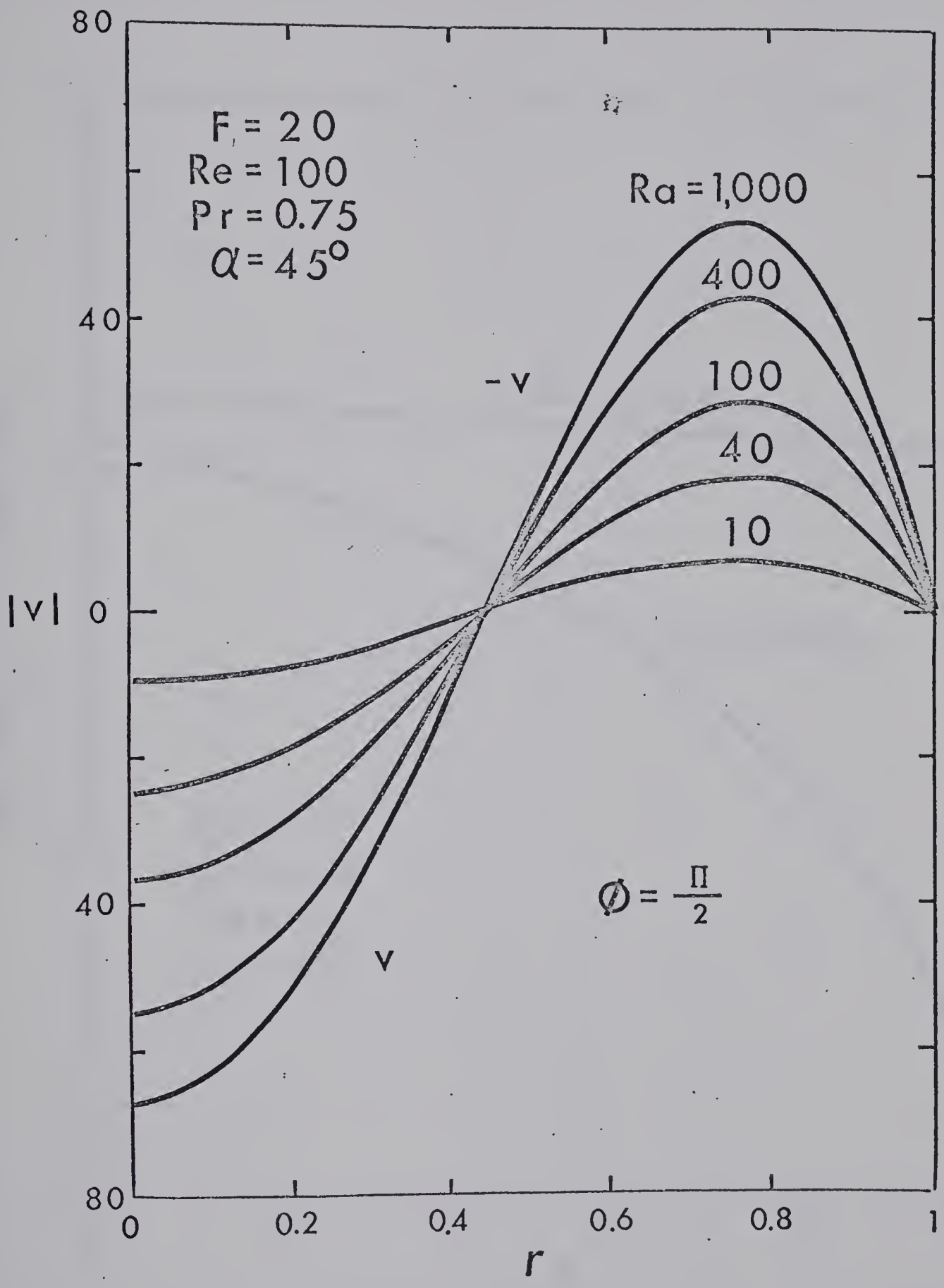

Fig.21(b) Distribution of secondary velocity component v along $\phi = \pi/2$ with Ra as a parameter

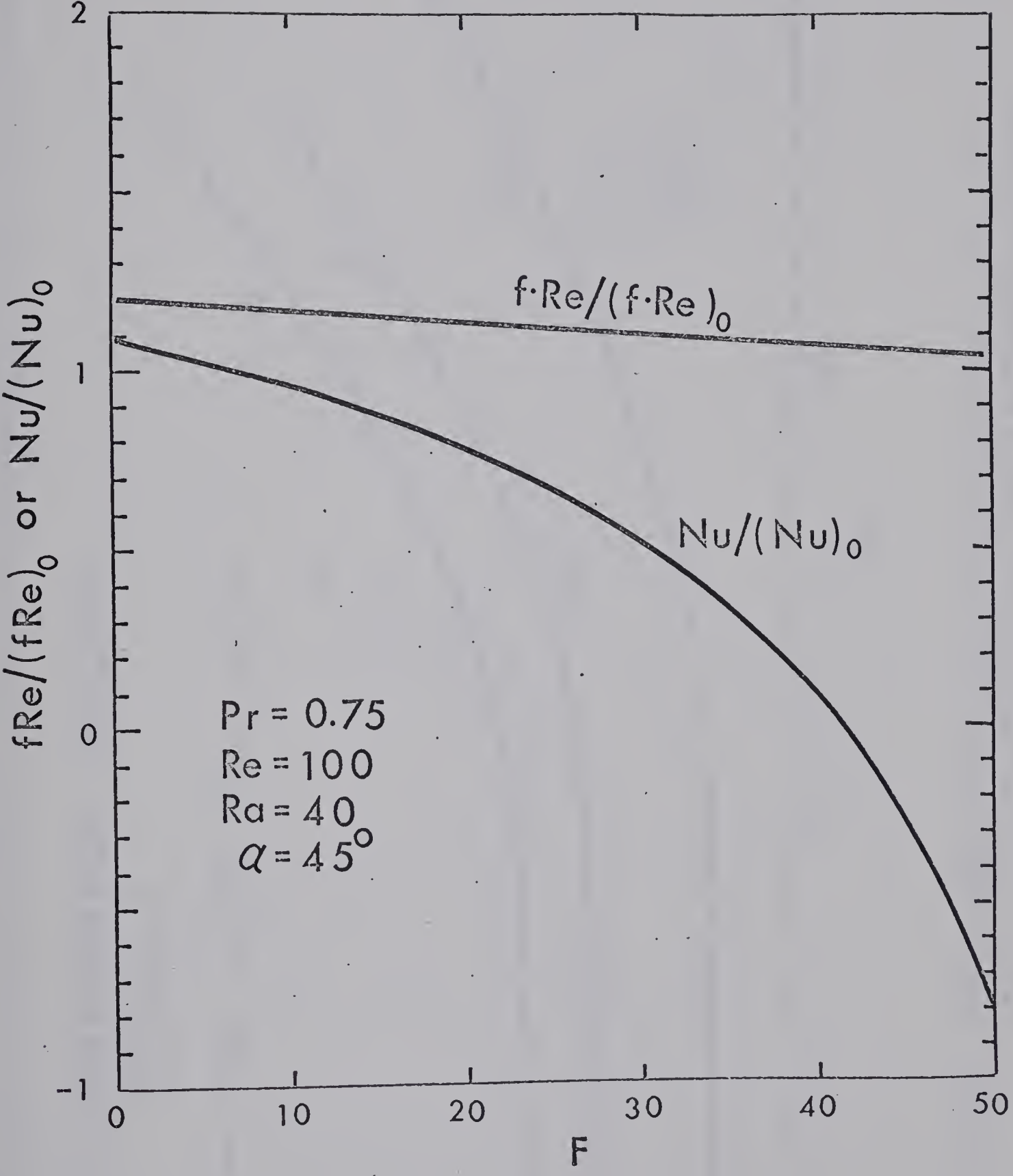

Fig.22 $fRe/(fRe)_0$ or $Nu/(Nu)_0$ versus F.

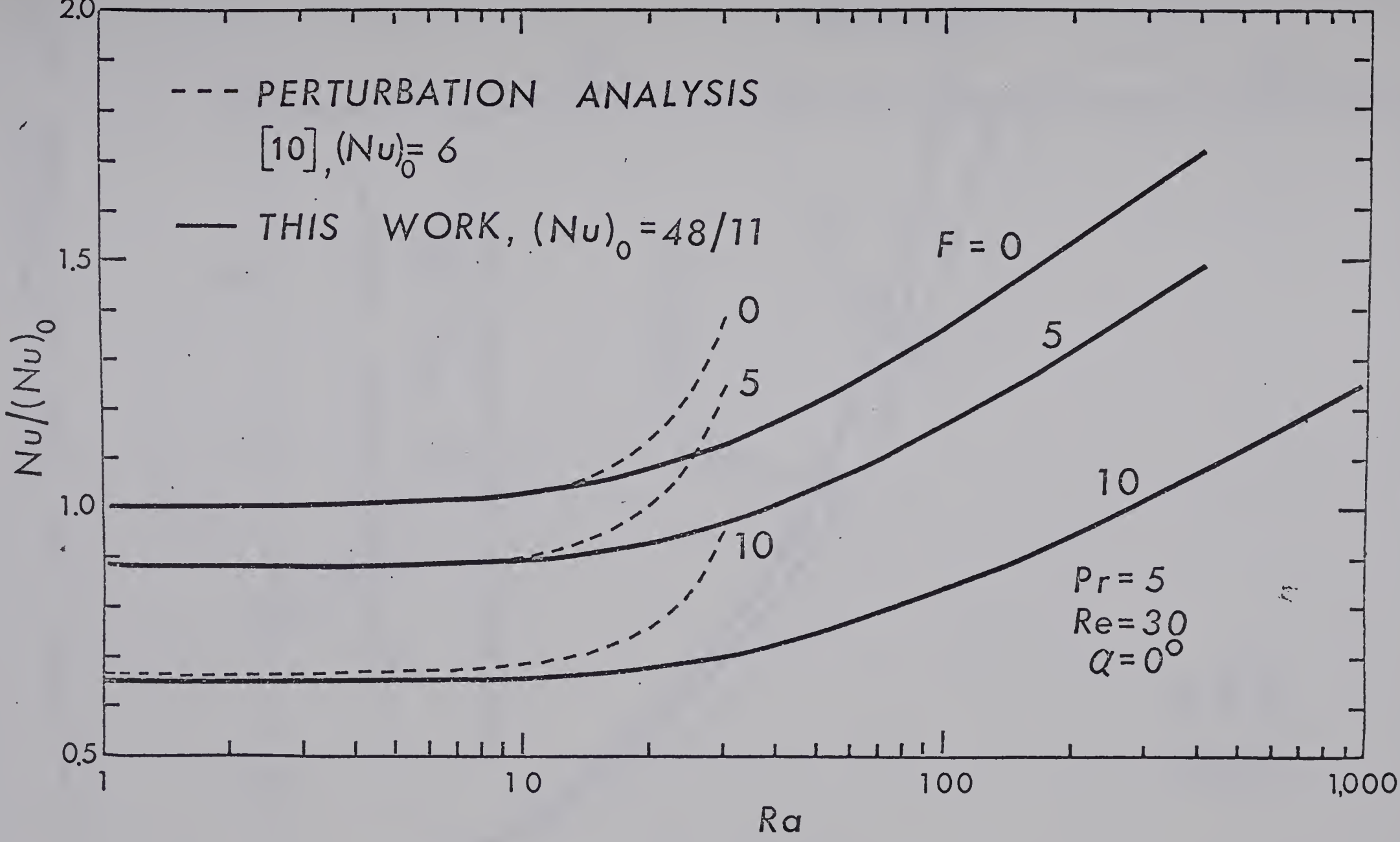

Fig.23 Nusselt number ratio versus Rayleigh number for $\alpha = 0°$, $Pr = 5$ and $Re = 30$ with comparison made against perturbation solution.

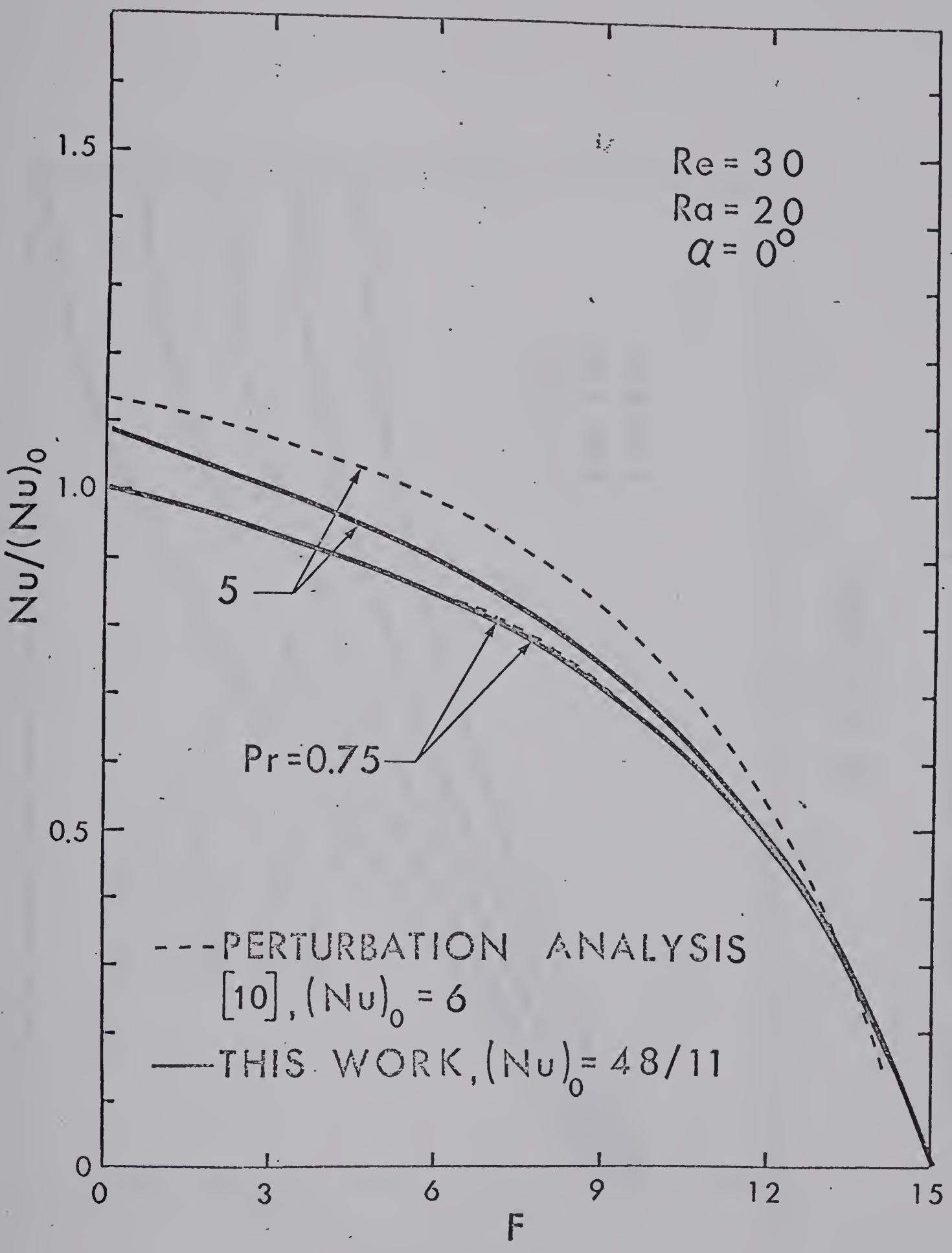

Fig.24 Comparison of heat transfer results between numerical solution and perturbation solution.

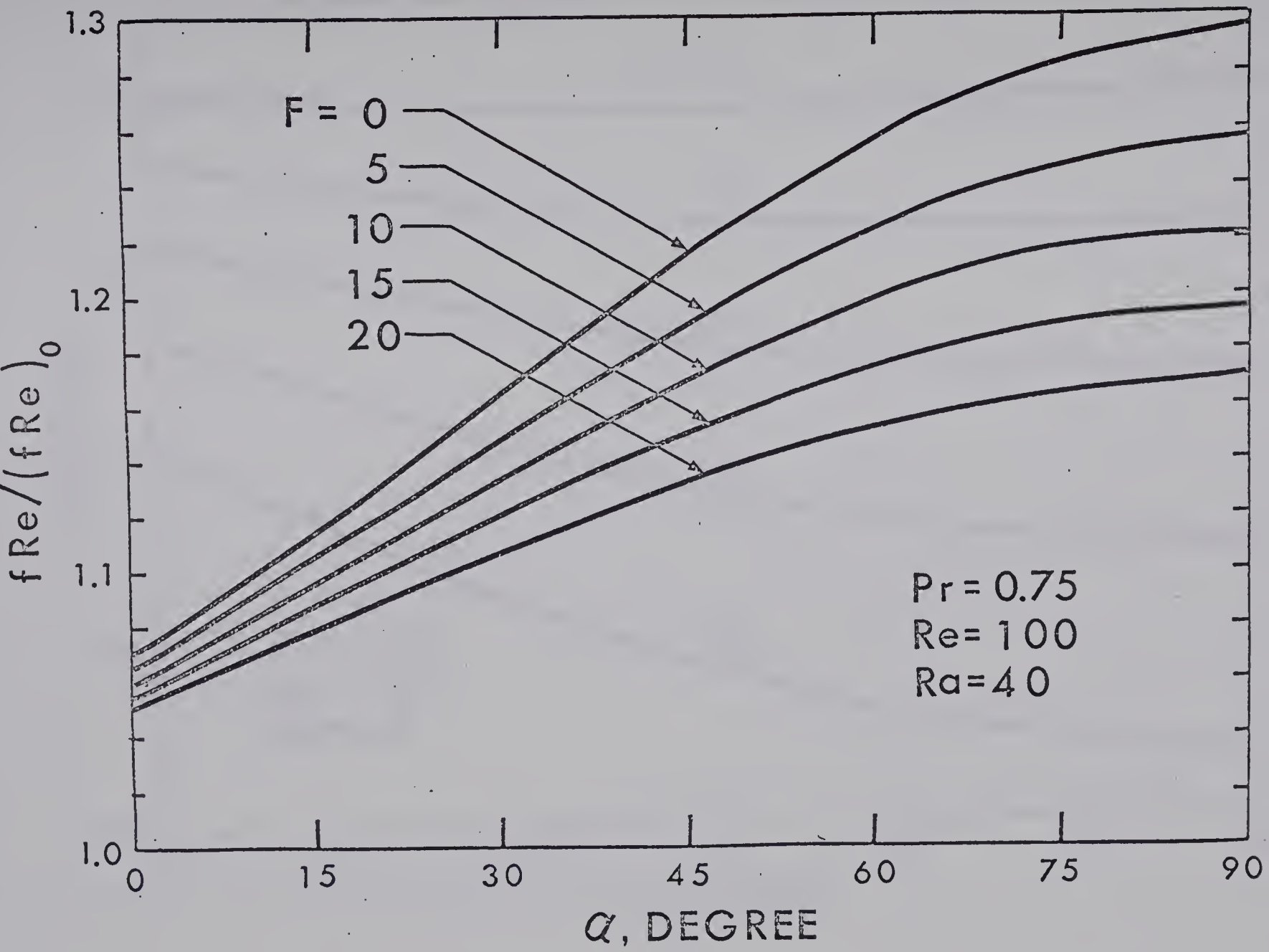

Fig.25 $fRe/(fRe)_0$ versus α with F as a parameter

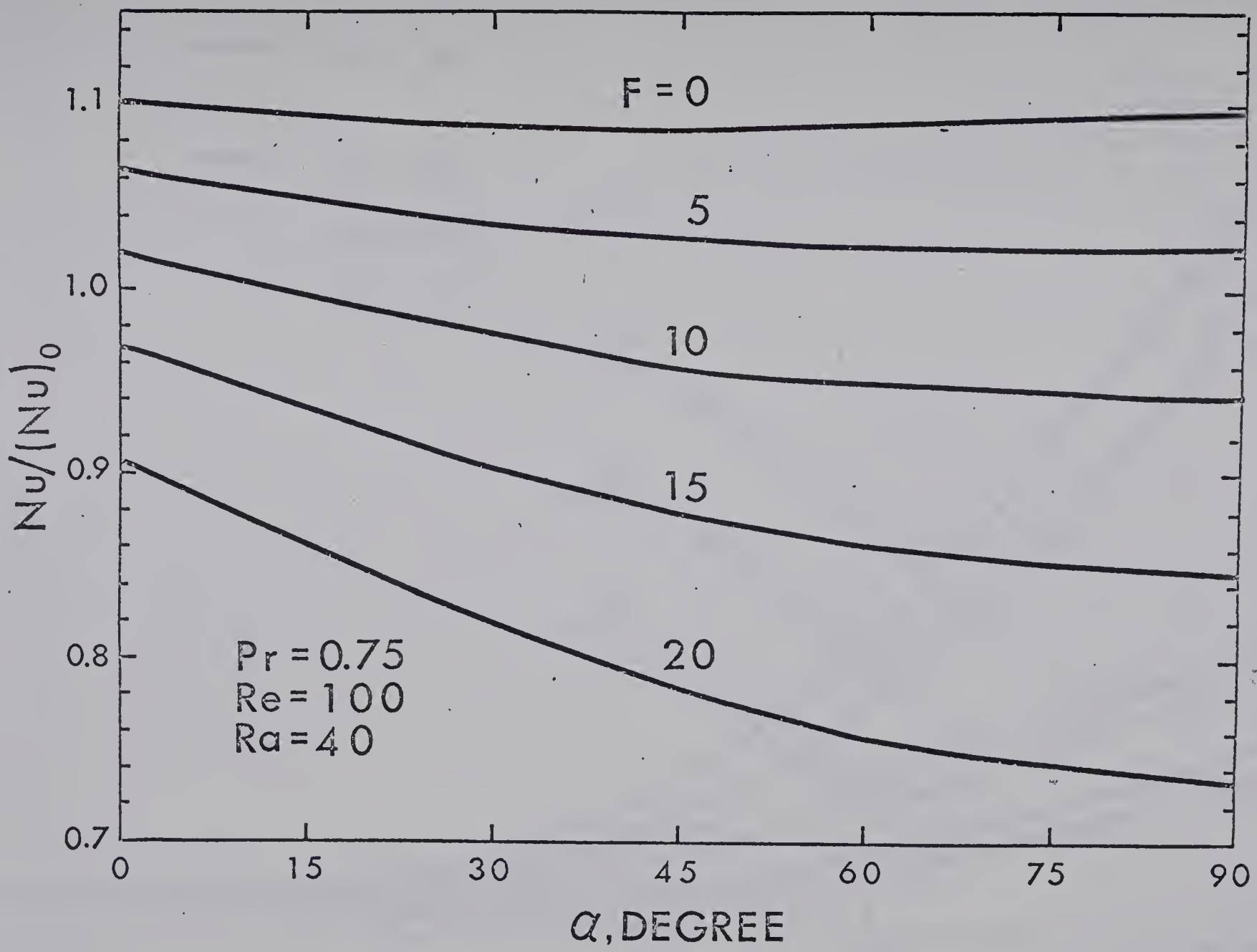

Fig.26 Nusselt number ratio versus α with F as a parameter

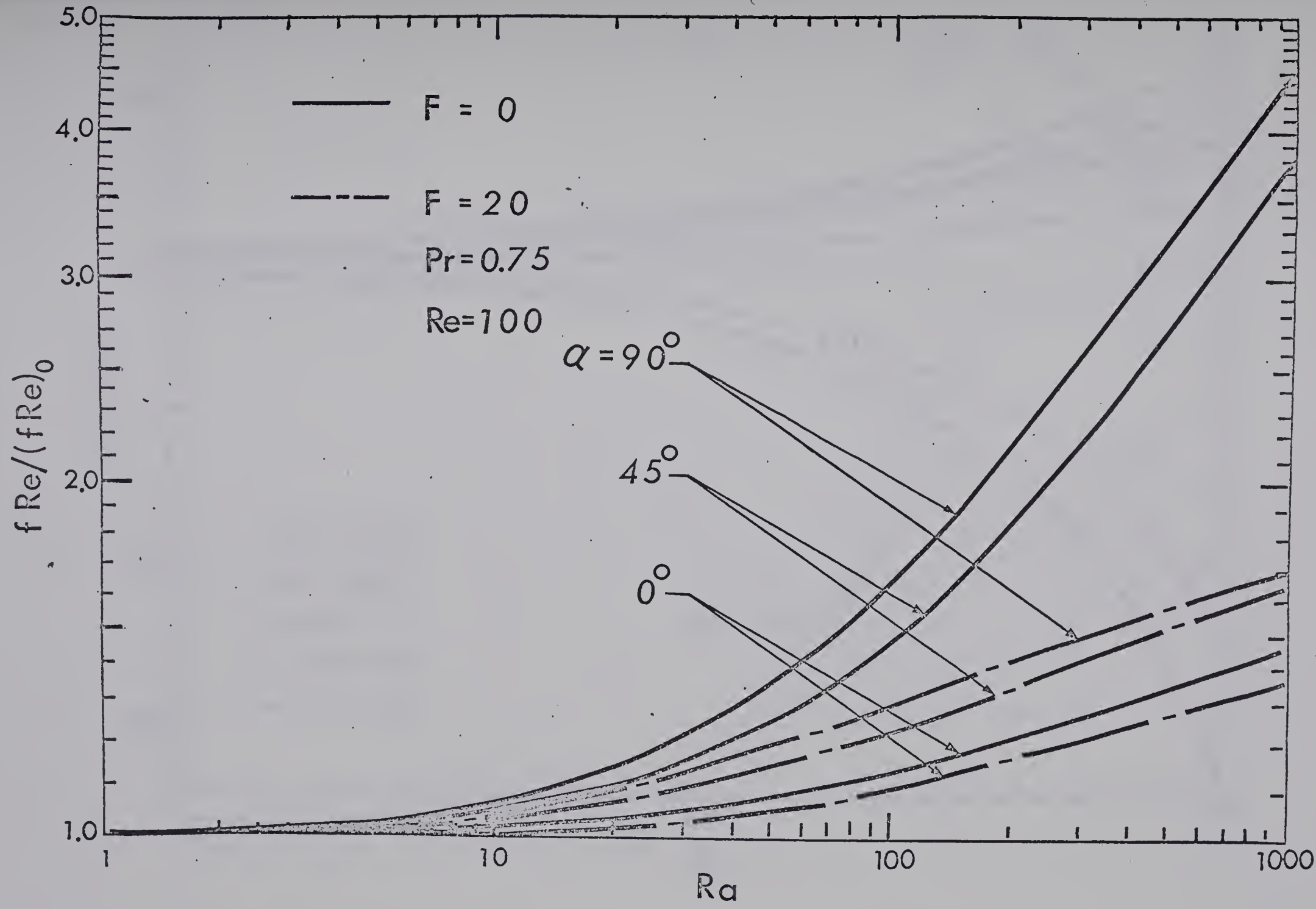

Fig.27 $fRe/(fRe)_0$ versus Ra with F as a parameter for Pr = 0.75 and $\alpha = 0°$, 45° and 90°

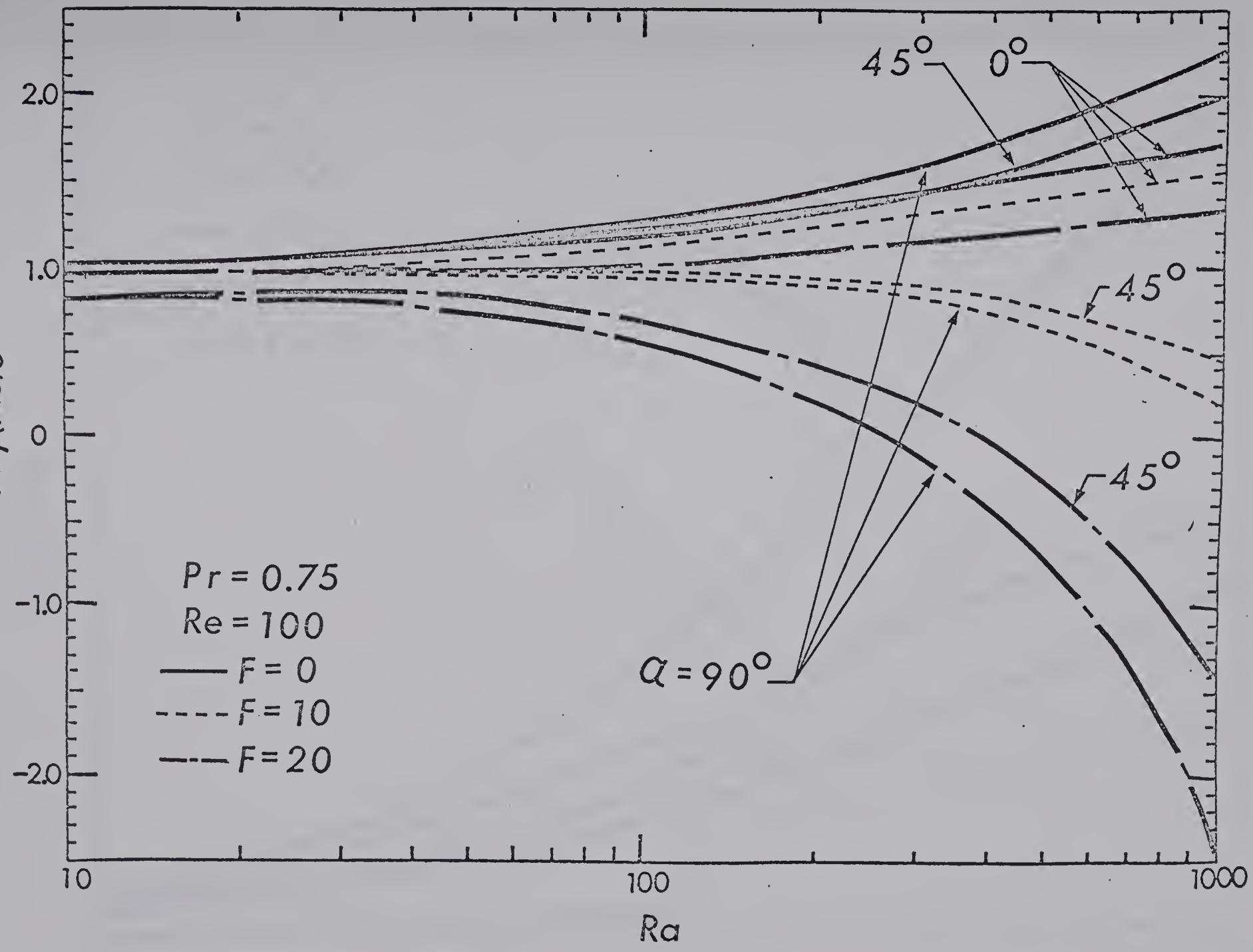

Fig.28 Nusselt number ratio versus Rayleigh number with F as a parameter for Pr = 0.75 and α = 0°, 45° and 90°

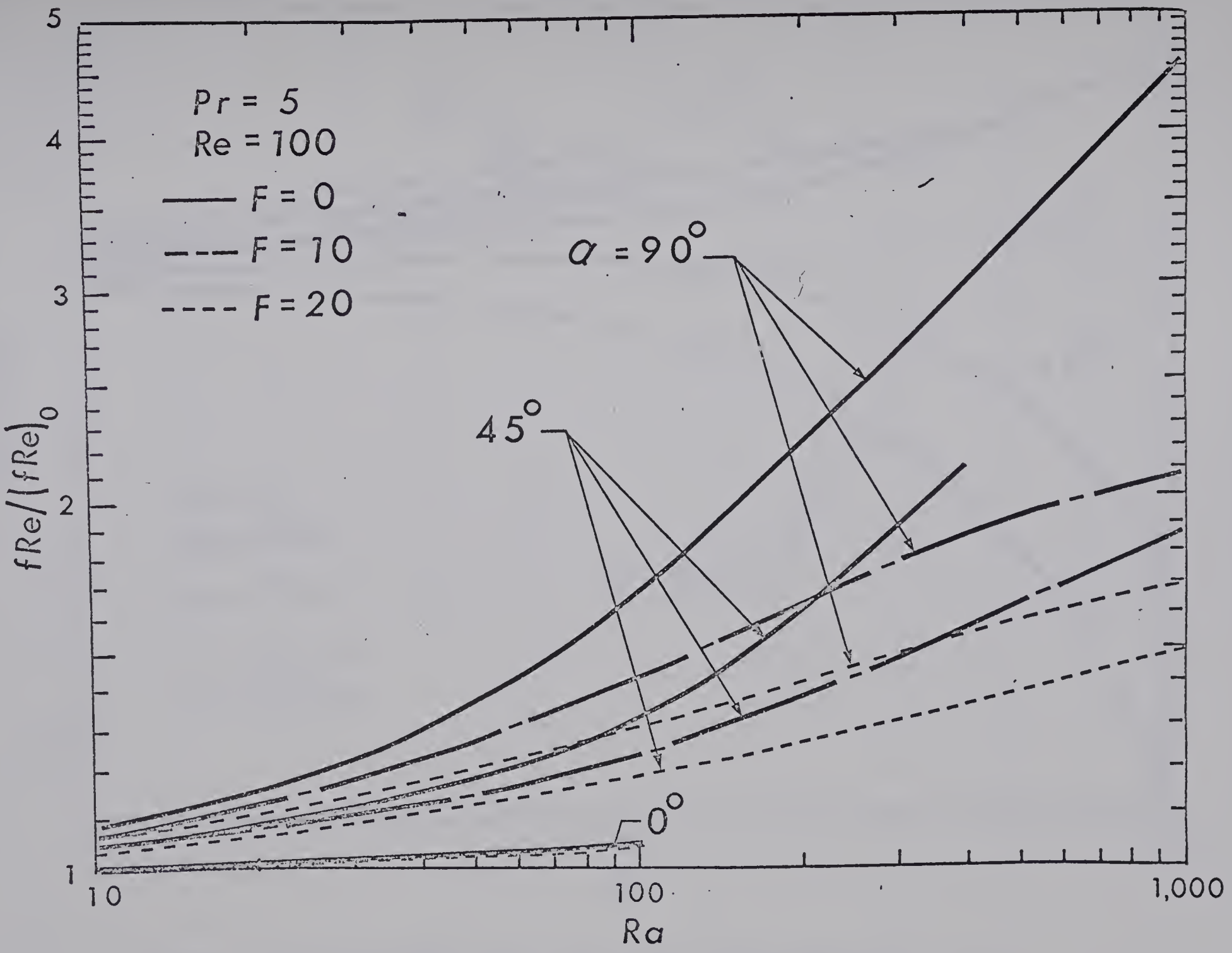

Fig. 29 $fRe/(fRe)_0$ versus α with F as a parameter for Pr = 5 and α = 0°, 45° and 90°

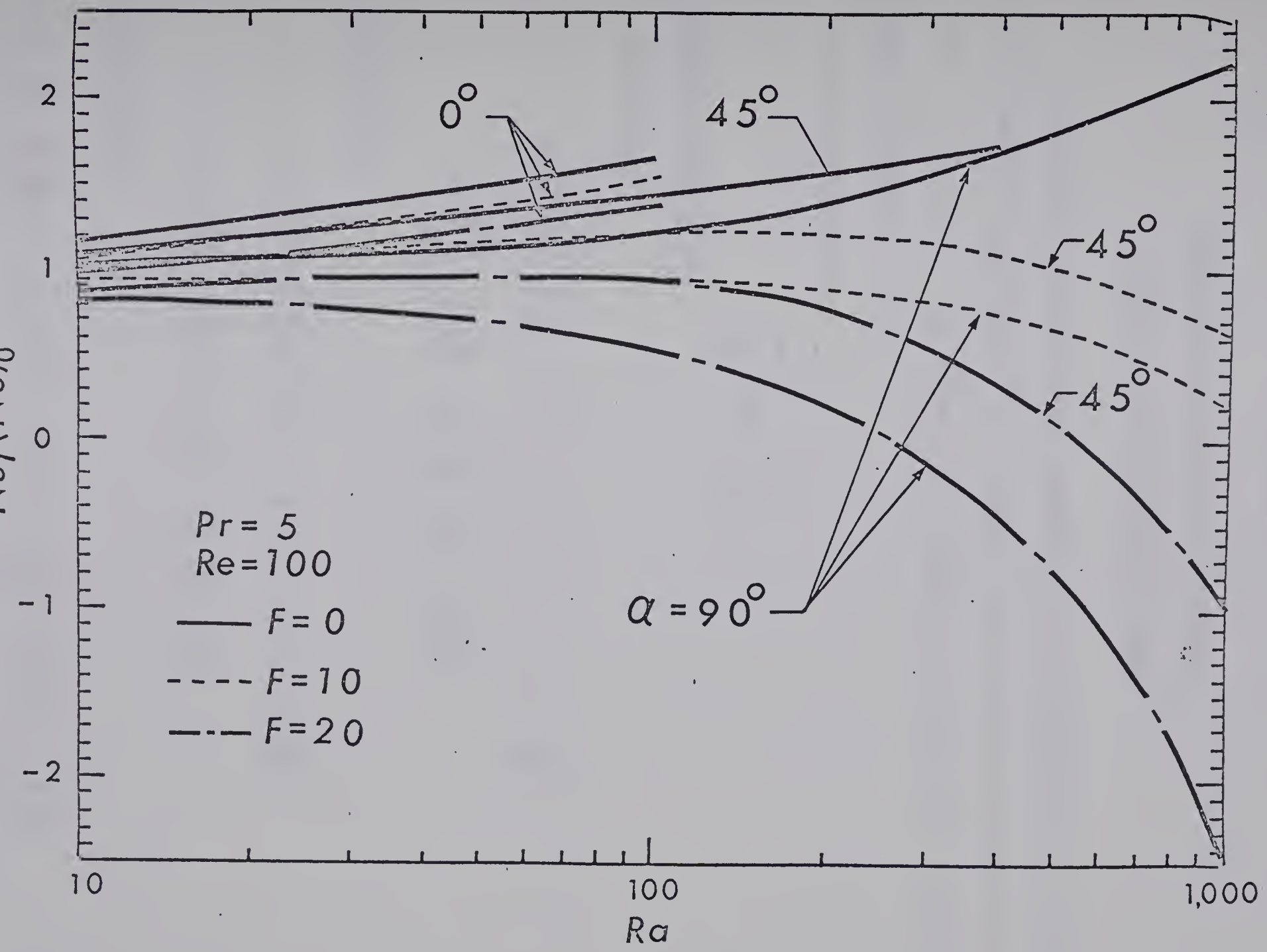

Fig.30 Nusselt number ratio versus Rayleigh number with F as a parameter for Pr = 5 and α = 0°, 45° and 90°

APPENDIX A

REDUCTION OF GOVERNING DIFFERENTIAL EQUATIONS TO DIMENSIONLESS FORM

The governing conservation equations for mass momentum and energy in cylindrical coordinates for a steady fully developed upward laminar flow in an inclined tube (see Fig. 1) using the simplifying assumptions made in Chapter II are:

Continuity equations:

$$\frac{\partial}{\partial R}(RU) + \frac{\partial V}{\partial \phi} = 0 \qquad (A.1)$$

Momentum equations:

R-direction,

$$\rho\left(U\frac{\partial U}{\partial R} + \frac{V}{R}\frac{\partial U}{\partial \phi} - \frac{V^2}{R}\right) = -\rho g \cos\alpha \cos\phi - \frac{\partial P}{\partial R}$$
$$+ \mu\left(\frac{\partial^2 U}{\partial R^2} + \frac{1}{R}\frac{\partial U}{\partial R} + \frac{1}{R^2}\frac{\partial^2 U}{\partial \phi^2} - \frac{U}{R^2} - \frac{2}{R^2}\frac{\partial V}{\partial \phi}\right) \qquad (A.2)$$

ϕ-direction,

$$\rho\left(U\frac{\partial V}{\partial R} + \frac{V}{R}\frac{\partial V}{\partial \phi} + \frac{UV}{R}\right) = \rho g \cos\alpha \sin\phi - \frac{1}{R}\frac{\partial P}{\partial \phi}$$
$$+ \mu\left(\frac{\partial^2 V}{\partial R^2} + \frac{1}{R}\frac{\partial V}{\partial R} + \frac{1}{R^2}\frac{\partial^2 V}{\partial \phi^2} + \frac{2}{R^2}\frac{\partial U}{\partial \phi} - \frac{V}{R^2}\right) \qquad (A.3)$$

Z-direction,

$$\rho\left(U\frac{\partial W}{\partial R} + \frac{V}{R}\frac{\partial W}{\partial \phi}\right) = -\rho g \sin\alpha - \frac{\partial P}{\partial Z} + \mu\left(\frac{\partial^2 W}{\partial R^2} + \frac{1}{R}\frac{\partial W}{\partial R} + \frac{1}{R^2}\frac{\partial^2 W}{\partial \phi^2}\right) \qquad (A.4)$$

Energy equation:

$$\rho C_p \left(U\frac{\partial T}{\partial R} + \frac{V}{R}\frac{\partial T}{\partial \phi} + W\frac{\partial T}{\partial Z}\right) = k\left(\frac{\partial^2 T}{\partial R^2} + \frac{1}{R}\frac{\partial T}{\partial R} + \frac{1}{R^2}\frac{\partial^2 T}{\partial \phi^2} + \frac{\partial^2 T}{\partial Z^2}\right) + Q + \Phi \qquad (A.5)$$

where the viscous dissipation function Φ is defined as

$$\Phi = 2\mu\left\{\left(\frac{\partial U}{\partial R}\right)^2 + \left[\frac{1}{R^2}\left(\frac{\partial V}{\partial \phi} + U\right)\right]^2\right\} + \mu\left\{\left(\frac{1}{R}\frac{\partial W}{\partial \phi}\right)^2 + \left(\frac{\partial W}{\partial R}\right)^2 + \left[\frac{1}{R}\frac{\partial U}{\partial \phi} + R\frac{\partial}{\partial R}\left(\frac{V}{R}\right)\right]^2\right\} \qquad (A.6)$$

and Q is the rate of internal heat generation per unit volume which will be considered to be constant in this study. In order to normalize the governing equations, it is convenient to introduce the following characteristic quantities:

$$U = U_c u, \quad V = V_c v, \quad W = W_c w, \quad R = ar, \quad T_w - T = \theta_c \theta \qquad (A.7)$$

From the continuity equation, the secondary velocity components U and V can be considered as the same order of magnitude as indicated below.

$$\frac{\partial (ru)}{\partial r} + \left[\frac{V_c}{U_c}\right]\frac{\partial v}{\partial \phi} = 0$$

Setting, $V_c = U_c$, the continuity equation is reduced to

$$\frac{\partial (ru)}{\partial r} + \frac{\partial v}{\partial \phi} = 0 \qquad (A.8)$$

Using Boussinesq approximation, the density variation in buoyancy term can be expressed as,

$$\rho = \rho_w\left[1+\beta(T_w - T)\right] = \rho_w\left[1+\beta\,\theta_c\theta\right] \qquad (A.9)$$

It is recalled that the axial pressure gradient is assumed to be constant and the axial temperature gradient is constant due to the imposed thermal

boundary conditions, namely

$$-\left(\frac{\partial P}{\partial Z} + \rho_w g \sin\alpha\right) = A = \text{constant}$$

$$\frac{\partial T}{\partial Z} = c = \text{constant}$$

The characteristic axial velocity W_c can be taken as the maximum velocity in the pure forced convection case, that is,

$$W_c = W_{max} = \frac{a^2 A}{4\mu} = 2\,\overline{W}$$

and Reynolds number Re will be defined using mean velocity as,

$$Re = \frac{\overline{W}\ 2a}{\nu} = \frac{A\ a^3}{4\rho\nu^2} = \frac{W_c\ a}{\nu}$$

By introducing the above characteristic quantities, the axial momentum equation (A.4) can now be written as

$$\nabla^2 w = \left[\frac{aU_c}{\nu}\right]\left(u\frac{\partial w}{\partial r} + \frac{v}{r}\frac{\partial w}{\partial \phi}\right) + \left[\frac{g\ \beta\ \theta_c\ a^2}{\nu\ W_c}\right]\theta_c \sin\alpha - \frac{A\ a^2}{\mu\ W_c} \qquad (A.10)$$

It is possible to set the coefficient of the convective terms to be order one, and we have

$$U_c = \frac{\nu}{a}$$

It is noted that each term of the equation (A.10) is seen to be of the same order of magnitude.

Similarly, equation (A.5) can be written as

$$\nabla^2\theta = \left[\frac{\rho\ C_p\ U_c\ a}{k}\right]\left(u\frac{\partial\theta}{\partial r} + \frac{v}{r}\frac{\partial\theta}{\partial\phi}\right) - \left[\frac{W_c\ C\ \rho\ C_p\ a^2}{k\ \theta_c}\right] w + \frac{Qa^2}{k\theta_c} + \Phi' \qquad (A.11)$$

The conduction terms and the convection term in the energy equation may be considered to be the same order of magnitude leading to:

$$\frac{\rho\ C_p\ U_c\ a}{k} = \frac{\mu\ C_p}{k} = Pr$$

$$\frac{W_c\ C\ \rho\ C_p\ a^2}{k\ \theta_c} = 1, \qquad \theta_c = Re\ C\ a\ Pr \tag{A.12}$$

The dimensionless viscous dissipation function is

$$\Phi' = \frac{a^2\ \Phi}{k\ \theta_c}$$

$$= E_c \left\{ \frac{2}{Re} \left[\left(\frac{\partial u}{\partial r}\right)^2 + \frac{1}{r^2} \left(\frac{\partial v}{\partial \phi} + u\right)^2 \right] + Re \left[\left(\frac{1}{r} \frac{\partial w}{\partial \phi}\right)^2 \right.\right.$$

$$\left.\left. + \left(\frac{\partial w}{\partial R}\right)^2 \right] + \frac{1}{Re} \left[\frac{1}{r} \frac{\partial u}{\partial \phi} + r \frac{\partial}{\partial r} \left(\frac{v}{r}\right) \right]^2 \right\}$$

where $E_c = \dfrac{U_c^2}{C_p\ C\ a}$ = Eckert number.

If $E_c << 1$, the viscous dissipation terms in equation (A.11) can be neglected. The dimensionless heat-source parameter is defined as,

$$F = \frac{Q\ a}{\rho\ C_p\ \nu\ C}$$

Then the normalized energy equation becomes,

$$\nabla^2 \theta = Pr \left(u \frac{\partial \theta}{\partial r} + \frac{v}{r} \frac{\partial \theta}{\partial \phi} \right) - w + \frac{F}{Re} \tag{A.13}$$

Substituting equation (A.12) into equation (A.10), the axial momentum equation becomes

$$\nabla^2 w = u \frac{\partial w}{\partial r} + \frac{v}{r} \frac{\partial w}{\partial \phi} + Ra\ \theta \sin \alpha - 4 \tag{A.14}$$

where $Ra = \beta\ g\ C\ a^4/\nu\kappa$, is Rayleigh number.

The pressure terms in the equations (A.2) and (A.3) can be eliminated by differentiating equation (A.2) with respect to ϕ and equation (A.3) with respect to R, and then reducing them to one equation. Introducing the dimensionless stream function and the vorticity as,

$$u = \frac{\partial \psi}{r \partial \phi}, \qquad v = \frac{\partial \psi}{\partial r}$$

$$\xi = \nabla^2 \psi \tag{A.15}$$

where $\nabla^2 = \frac{\partial}{\partial r} + \frac{1}{r}\frac{\partial}{\partial r} + \frac{1}{r^2}\frac{\partial^2}{\partial \phi^2}$,

the momentum equations (A.2) and (A.3) are reduced to:

$$\nabla^2 \xi = u\frac{\partial \xi}{\partial r} + \frac{v}{r}\frac{\partial \xi}{\partial \phi} + \mathrm{ReRa}\left(\frac{\partial \theta}{\partial r}\sin\phi + \frac{1}{r}\frac{\partial \theta}{\partial \phi}\cos\phi\right)\cos\alpha \tag{A.16}$$

A set of partial differential equations (A.13) to (A.16) is the normalized equations which have been solved numerically in this study. For the problem under consideration, five independent parameters Re, Ra, Pr, α and F appear in the governing dimensionless differential equations.

APPENDIX B

FORTRAN PROGRAM

```
------------------------------------------------------------------

'*' IN COL. 6: THIS LINE IS A PART OF PREVIOUS STATEMENT

------------------------------------------------------------------

C       THIS IS A PROGRAM FOR SOLVING COMBINED FREE AND FORCED
C       CONVECTION WITH HEAT GENERATION IN INCLINED TUBES
C
C
C       EXPLANATION OF SYMBOLS IN THIS PROGRAM
C
C       FN      : HEAT GENERATION PARAMENT NUMBER
C       M       : NO. OF DIVISION IN THE R-DIRECTION
C       N       : NO. OF DIVISION IN THE CITA DIRECTION
C       PR      : PRANDTL NUMBER
C       RA      : RAYLEIGH NUMBER
C       RE      : REYNOLDS NUMBER
C       S       : STREAM FUNCTION
C       VC      : VELOCITY IN THE CITA DIRECTION
C       VO      : VOTICITY FUNCTION
C       VR      : VELOCITY IN THE RADIAL DIRECTION
C       VX      : VELOCITY IN THE AXIAL DIRECTION
C
C
        DIMENSION VX(31,31),T(31,31),VR(31,31),VC(31,31),BVTS(
       *  31,31),
       1AVX(31,31),CVX(31,31),PVX(31,31),S(31,31),VC(31,31),AT
       *  (31,31),
       3CT(31,31),PT(31,31),AS(31,31),CS(31,31),PS(31,31),TT(3
       *  1,31),
       CCITA(31),R(31),ZA(31),ZB(31),ZC(31),VVX(31,31),SS(31,3
       *  1)
        INTEGER*4 M,N,MI,NI,ND,MD,MSTD,NO
        COMMON HR,HR2,HC,HC2,AF,RAC,RA,PR,STD,OK,ZA,ZB,ZC,R,CI
       *  TA,EVIS,
       1VX,T,VR,VC,OMEG1,OMES
        COMMON M,N,MI,NI,ND,MD,MSTD,NO
    99  READ(5,100,END=150) M,N,STD,OK
C
C       READ IN THE GIVEN VALUE
        READ(5,201) RE,RA,AF,PR,FN
C
        RAC=RE*RA
```

```
      FM=FN/RE
      READ(5,250) CMEG1,CMES,NSTD,MO
      PI=3.1415927
      AG=AF
      AF=PI*AF/180
   33 MD=M-1
      MI=M+1
      ND=N-1
      NI=N+1
      NO=0
      NOO=50
      MO=MO+1
      IF(M.GT.21.OR.MO.GT.1) GO TO 34
      DO 10 J=1,NI
      DO 10 I=1,MI
      VX(I,J)=0.0
      VVX(I,J)=0.0
       T(I,J)=0.0
      TT(I,J)=0.0
       S(I,J)=0.0
      SS(I,J)=0.0
      VO(I,J)=0.0
      VR(I,J)=0.0
      VC(I,J)=0.0
   10 CONTINUE
C
C     READ IN THE INITIAL VALUES
C
      READ(5,200) ((VX(I,J),I=1,MI),J=1,NI)
      READ(5,200) ((VVX(I,J),I=1,MI),J=1,NI)
      READ(5,200) (( T(I,J),I=1,MI),J=1,NI)
      READ(5,200) ((TT(I,J),I=1,MI),J=1,NI)
      READ(5,200) (( S(I,J),I=1,MI),J=1,NI)
      READ(5,200) ((SS(I,J),I=1,MI),J=1,NI)
      READ(5,200) ((VO(I,J),I=1,MI),J=1,NI)
      READ(5,200) ((VR(I,J),I=1,MI),J=1,NI)
      READ(5,200) ((VC(I,J),I=1,MI),J=1,NI)
   34 HR=1.0/M
      HR2=HR**2
      F=FM*HR2
      HC=PI/N
      HC2=HC**2
      CITA(1)=0.0
      DO 9 J=2,NI
    9 CITA(J)=CITA(J-1)+HC
      R(1)=0.0
      DO 8 I=2,MI
      R(I)=R(I-1)+HR
      ZA(I)=HR/(2*R(I))
      ZB(I)=(HR/(HC*R(I)))**2
      ZC(I)=HR**2/(2*R(I)*HC)
    8 CONTINUE
```

```
      DO 7 J=1,NI
      DO 7 I=2,MI
      BVTS(I,J)=(1+ZE(I))*(-2)
      AS(I,J)=1-ZA(I)
      CS(I,J)=1+ZA(I)
    7 CONTINUE
      IF(M.LT.21) GO TO 1
      DO 23 J=1,NI,2
      DO 23 I=2,M,2
      VX(I,J)=0.5*(VX(I-1,J)+VX(I+1,J))
      VVX(I,J)=0.5*(VVX(I-1,J)+VVX(I+1,J))
       T(I,J)=0.5*( T(I-1,J)+ T(I+1,J))
      TT(I,J)=0.5*(TT(I-1,J)+TT(I+1,J))
       S(I,J)=0.5*( S(I-1,J)+ S(I+1,J))
      SS(I,J)=0.5*(SS(I-1,J)+SS(I+1,J))
      VO(I,J)=0.5*(VO(I-1,J)+VO(I+1,J))
      VR(I,J)=0.5*(VR(I-1,J)+VR(I+1,J))
      VC(I,J)=0.5*(VC(I-1,J)+VC(I+1,J))
   23 CONTINUE
      DO 24 I=1,MI
      DO 24 J=2,N,2
      VX(I,J)=0.5*(VX(I,J-1)+VX(I,J+1))
      VVX(I,J)=0.5*(VVX(I,J-1)+VVX(I,J+1))
       T(I,J)=0.5*( T(I,J-1)+ T(I,J+1))
      TT(I,J)=0.5*(TT(I,J-1)+TT(I,J+1))
       S(I,J)=0.5*( S(I,J-1)+ S(I,J+1))
      SS(I,J)=0.5*(SS(I,J-1)+SS(I,J+1))
      VO(I,J)=0.5*(VO(I,J-1)+VO(I,J+1))
      VR(I,J)=0.5*(VR(I,J-1)+VR(I,J+1))
      VC(I,J)=0.5*(VC(I,J-1)+VC(I,J+1))
   24 CONTINUE
    1 IM=1
C
C     DO LOOP OF 25 IS TO CALCULATE THE COEFFICIENT OF LINE
C     ITERATION
C
      DO 25 J=1,NI
      AS(MI,J)=2.0
      AVX(2,J)=1-ZA(2)+0.5*HR*VR(2,J)
      CVX(2,J)=1+ZA(2)-HR*VR(2,J)/2
      PVX(2,J)=CVX(2,J)/BVTS(2,J)
      AT(2,J)=1-ZA(2)+0.5*PR*HR*VR(2,J)
      CT(2,J)=1+ZA(2)-HR*PR*VR(2,J)*0.5
      PT(2,J)=CT(2,J)/BVTS(2,J)
      PS(2,J)=CS(2,J)/BVTS(2,J)
      DO 25 I=3,M
      AVX(I,J)=1-ZA(I)+0.5*HR*VR(I,J)
      CVX(I,J)=1+ZA(I)-0.5*HR*VR(I,J)
      PVX(I,J)=CVX(I,J)/(BVTS(I,J)-AVX(I,J)*PVX(I-1,J))
      AT(I,J)=1-ZA(I)+0.5*HR*PR*VR(I,J)
      CT(I,J)=1+ZA(I)-0.5*HR*PR*VR(I,J)
      PT(I,J)=CT(I,J)/(BVTS(I,J)-AT(I,J)*PT(I-1,J))
```

```
      PS(I,J)=CS(I,J)/(BVTS(I,J)-AS(I,J)*PS(I-1,J))
25    CONTINUE
      CALL SUBVX(VVX,AVX,CVX,PVX)
      CALL SUBT(TT,AT,CT,PT,F)
      CALL SUBVS(S,VO,SS,AS,CS,PS,AVX,CVX,PVX)
      CALL SUBVRC(S,ERROR)
      IF(ERROR.LT.CK.OR.NC.GT.MSTD) GO TO 60
      NO=NC+1
      IF(NC.NE.NCO) GO TO 1
      WRITE(6,101) ERROR
      WRITE(6,116) NO
      NCC=NCC+50
      GO TO 1
60    CALL TANK(SVXP,SVXT,SGT,SGVX,BUKT,FRE1,FRE2,UN1,UN2,RE
     *  RA,RFE1,
     CRFE2,RNU1,RNU2,ARNU,STP,FRE3,AVEN,AVEF,RFE12,RFE3,FM)
      IF(M.LT.20) GO TO 5
      WRITE(6,105)
      WRITE(6,113) ((VX(I,J),I=1,M),J=1,NI)
      WRITE(6,106)
      WRITE(6,113) ((T(I,J),I=1,M),J=1,NI)
      WRITE(6,107)
      WRITE(6,113) ((VO(I,J),I=2,MI),J=1,NI)
      WRITE(6,108)
      WRITE(6,113) ((S(I,J),I=2,MI),J=1,NI)
      WRITE(6,109)
      WRITE(6,113) ((VR(I,J),I=1,M),J=1,NI)
      WRITE(6,110)
      WRITE(6,113) ((VC(I,J),I=1,M),J=1,NI)
5     IM=5
      WRITE(6,202) M,N
      WRITE(6,203) STD,OK
      WRITE(6,204) RAC,RA,PR,RE,FN
      WRITE(6,104) AG
      WRITE(6,101) ERROR
      WRITE(6,116) NC
      WRITE(6,205) OMEG1,OMES
      WRITE(6,210)
      WRITE(6,111) BUKT
      WRITE(6,212) STP
      WRITE(6,112) SVXP
      WRITE(6,114) FRE1,FRE2
      WRITE(6,121) RFE1,RFE2
      WRITE(6,215) RFE12
      WRITE(6,214) FRE3,RFE3
      WRITE(6,115) UN1,UN2
      WRITE(6,213) AVEN,AVEF
      WRITE(6,122) RNU1,RNU2,ARNU
      WRITE(6,120) SVXT,SGT,SGVX
      WRITE(6,117) RERA
      WRITE(6,211)
      IF(MC.LT.5.OR.M.GT.21) GO TO 75
```

```
      WRITE(7,200) ((VX(I,J),I=1,MI),J=1,NI)
      WRITE(7,200) ((VVX(I,J),I=1,MI),J=1,NI)
      WRITE(7,200) (( T(I,J),I=1,MI),J=1,NI)
      WRITE(7,200) ((TT(I,J),I=1,MI),J=1,NI)
      WRITE(7,200) (( S(I,J),I=1,MI),J=1,NI)
      WRITE(7,200) ((SS(I,J),I=1,MI),J=1,NI)
      WRITE(7,200) ((VO(I,J),I=1,MI),J=1,NI)
      WRITE(7,200) ((VR(I,J),I=1,MI),J=1,NI)
      WRITE(7,200) ((VC(I,J),I=1,MI),J=1,NI)
   75 IM=2
C
      IF(M.GT.21) GO TO 40
C
      DO 31 J=1,NI
      L=2*(NI-J)+1
      JJ=NI+1-J
      DO 31 I=1,MI
      K=2*(MI-I)+1
      II=MI+1-I
      VX(K,L)=VX(II,JJ)
      VVX(K,L)=VVX(II,JJ)
       T(K,L)= T(II,JJ)
      TT(K,L)=TT(II,JJ)
       S(K,L)= S(II,JJ)
      SS(K,L)=SS(II,JJ)
      VO(K,L)=VO(II,JJ)
      VR(K,L)=VR(II,JJ)
      VC(K,L)=VC(II,JJ)
   31 CONTINUE
C
C     ENLARGE THE MESH SIZE
C
      M=2*M
      N=2*N
      GO TO 33
   40 DO 41 J=1,NI,2
      L=(J+1)/2
      DO 41 I=1,MI,2
      K=(I+1)/2
      VX(K,L)=VX(I,J)
      VVX(K,L)=VVX(I,J)
       T(K,L)= T(I,J)
      TT(K,L)=TT(I,J)
       S(K,L)= S(I,J)
      SS(K,L)=SS(I,J)
      VO(K,L)=VO(I,J)
      VR(K,L)=VR(I,J)
      VC(K,L)=VC(I,J)
   41 CONTINUE
      GO TO 99
  100 FORMAT(2I4,2F10.6)
  101 FORMAT('0',50X,'ERROR'15X,E14.6)
```

```
104 FORMAT('C',40X,'ANGLE IN DEGREE',F10.1)
105 FORMAT('1',' AXIAL VELOCIYY',3X,'I FROM 1 TO M J FROM
   *  1 TC N')
107 FORMAT('1',' VOTICITY')
106 FORMAT('1',' TEMPERATURE')
108 FORMAT('1',' STREAM FUNCTION')
109 FORMAT('1',' SECONDARY VELOCITY IN R-DIRECTION  VR')
110 FORMAT('1',' SECONDARY VELOCITY IN CITA-DIRECTION  VC'
   *  )
111 FORMAT('C',10X,'BULK TEMPERATURE...   ...   ...   ...
   *    ...   ...'
   C,F15.6)
112 FORMAT('0',10X,'AVERAGE VELOCITY IN AXIAL DIRECTION...
   *  ..........'
   C,F15.6)
113 FORMAT(' ',7E18.7)
114 FORMAT('0',10X,'FRE1  FRE2...   ...   ...   ...   ...
   *    ...   ...'
   C,F15.6,F25.6)
115 FORMAT('C',10X,'NUSSELT NUMBER NU1  NU2...   ...   ...
   *     ...   ..'
   C,F15.6,F25.6)
116 FORMAT('0',45X,'NUMBER OF ITERATIONS',10X,I10)
117 FORMAT('C',10X,'RERA...   ...   ...   ...   ...   ...
   *    ...   ...'
   C,F15.6)
120 FORMAT('C',10X,'SVXT GRADIENT OF T AND V AT WALL.....
   *  ..........'
   C,F15.6,2F25.6)
121 FORMAT('0',10X,'FRE1/FREC  FRE2/FRE0 ...   ...   ...
   *   ...   ... '
   C,F15.6,F25.6)
122 FORMAT('C',10X,'NU1/NU0  NU2/NU0  AVERAGE OF THEM.....
   *  ..........'
   C,F15.6,2F25.6)
200 FORMAT(20A4)
201 FORMAT(3F10.1,F10.4,F10.4)
202 FORMAT('1',/////,40X,'MESH SIZE',I5,2X,'BY',I5)
203 FORMAT('0',30X,'ERROR LIMITED',2E20.6)
204 FORMAT('0',25X,'RAC',F10.1,5X,'RA',F10.1,5X,'PR',F10.4
   *  ,5X,'RE',
   CF10.1,5X,'F',F10.4)
205 FORMAT('0',40X,'REDUCING FACTOR IN V AND T',5X,F5.2,5X
   *  ,'IN S',5X,
   CF5.2)
210 FORMAT('0',///,'**********************************
   *  **      HEAT
   CTRANSFER RESULT      **********************************
   *  *****',///)
211 FORMAT('C',///,'**********************************
   *  *******
   CEND       **********************************
   *  *',/////)
```

```
212 FORMAT('0',10X,'MEAN TEMPERATURE...   ...   ...   ...
   *    ...   ...'
   C,F15.6)
213 FORMAT('0',10X,'AVERAGE NUSSELT NO AND FRICTION FACTOR
   *  ..........'
   C,F15.6,F25.6)
214 FORMAT('0',10X,'PRESSURE DROP AND IT RATIO.............
   *  ..........'
   C,F15.6,F25.6)
215 FORMAT('0',10X,'AVERAGE OF FRE1/FRE0 AND FRE2/FRE0....
   *  ..........'
   C,F15.6,F25.6)
250 FORMAT(2F5.2,2I5)
150 STOP
    END
```

```
C      SUBROUTINE SUBVX IS TO SOLVE THE MOMENTUM EQUATION OF
C      (2-9) IN CHAPTER 2
C
C
C
      SUBROUTINE SUBVX(VVX,AVX,CVX,PVX)
      DIMENSION VX(31,31),T(31,31),VR(31,31),VC(31,31),BVTS(
     *  31,31),
     1AVX(31,31),CVX(31,31),PVX(31,31),QVX(31,31),DVX(31,31)
     *  ,
     CCITA(31),R(31),ZA(31),ZB(31),ZC(31),VVX(31,31)
      INTEGER*4 M,N,MI,NI,ND,MD,MSTD,NO
      COMMON HR,HR2,HC,HC2,AF,RAC,RA,PR,STD,CK,ZA,ZB,ZC,R,CI
     *  TA,BVTS,
     1VX,T,VR,VC,OMEG1,OMES
      COMMON M,N,MI,NI,ND,MD,MSTD,NO
      VVX(1,1)=0.25*((1-HR*VR(1,1)/2)*VX(2,1)+(1+HR*VR(1,1)/
     *  2)*VX(2,NI)
     C+2*VX(2,N/2+1)+(4-RA*T(1,1)*SIN(AF))*HR2)
      DO 9 J=1,NI
      VVX(1,J)=VVX(1,1)
      IF(J.EQ.1.OR.J.EQ.NI) GO TO 6
      DVX(2,J)=(RA*T(2,J)*SIN(AF)-4)*HR2-(ZB(2)+ZC(2)*VC(2,J
     *  ))*VVX(2,J-1
     C)-(ZB(2)-ZC(2)*VC(2,J))*VVX(2,J+1)-AVX(2,J)*VVX(1,J)
    6 IF(J.EQ.1) DVX(2,J)=(RA*T(2,J)*SIN(AF)-4)*HR2-2*ZB(2)*
     *  VVX(2,J+1)-
     CVVX(1,J)*AVX(2,J)
      IF(J.EQ.NI) DVX(2,J)=(RA*T(2,J)*SIN(AF)-4)*HR2-2*ZB(2)
     *  *VVX(2,J-1)
     C-VVX(1,J)*AVX(2,J)
      QVX(2,J)=DVX(2,J)/BVTS(2,J)
      DO 10 I=3,M
      IF(J.EQ.1.OR.J.EQ.NI) GO TO 7
      DVX(I,J)=(RA*SIN(AF)*T(I,J)-4)*HR2-(ZB(I)+ZC(I)*VC(I,J
     *  ))*VVX(I,J-1
     C)-(ZB(I)-ZC(I)*VC(I,J))*VVX(I,J+1)
    7 IF(J.EQ.1) DVX(I,J)=(RA*T(I,J)*SIN(AF)-4)*HR2-2*ZB(I)*
     *  VVX(I,J+1)
      IF(J.EQ.NI)DVX(I,J)=(RA*T(I,J)*SIN(AF)-4)*HR2-2*ZB(I)*
     *  VVX(I,J-1)
      QVX(I,J)=(DVX(I,J)-AVX(I,J)*QVX(I-1,J))/(BVTS(1,J)-AVX
     *  (I,J)*PVX(
     CI-1,J))
   10 CONTINUE
      VVX(M,J)=QVX(M,J)
      DO 4 II=2,MD
      I=MI-II
    4 VVX(I,J)=QVX(I,J)-PVX(I,J)*VVX(I+1,J)
    9 CONTINUE
      DO 8 J=1,NI
      DO 8 I=1,M
```

```
      DI=OMEG1*(VVX(I,J)-VX(I,J))
      VX(I,J)=VX(I,J)+DI
    8 CONTINUE
      RETURN
      END
```

```
C      SUBROUTINE SUBT IS TO SOLVE THE ENERGY EQUATION (2-10)
C
C
C
C
      SUBROUTINE SUBT(TT,AT,CT,PT,F)
      DIMENSION VX(31,31),T(31,31),VR(31,31),VC(31,31),BVTS(
     *  31,31),
     1AT(31,31),CT(31,31),DT(31,31),PT(31,31),QT(31,31),TT(3
     *  1,31),
     CCITA(31),R(31),ZA(31),ZB(31),ZC(31)
      INTEGER*4 M,N,MI,NI,ND,MD,MSTD,NO
      COMMON HR,HR2,HC,HC2,AF,RAC,RA,PR,STD,OK,ZA,ZB,ZC,R,CI
     *  TA,BVTS,
     1VX,T,VR,VC,OMEG1,OMES
      COMMON M,N,MI,NI,ND,MD,MSTD,NO
      TT(1,1)=0.25*(TT(2,1)*(1-HR*VR(1,1)*PR/2)+2*TT(2,N/2+1
     *  )+TT(2,NI)*
     C(1+HR*VR(1,1)*PR/2)+HR2*VX(1,1)-F)
      DO 55 J=2,N
      TT(1,J)=TT(1,1)
      TT(1,NI)=TT(1,1)
      DT(2,1 )=(-2)*ZB(2)*TT(2,2)-VX(2,1 )*HR2-TT(1,1)*AT(2,
     *  1)+F
      DT(2,J)=(-1)*(ZB(2)+ZC(2)*PR*VC(2,J))*TT(2,J-1)-(ZB(2)
     *  -ZC(2)*
     CPR*VC(2,J))*TT(2,J+1)-VX(2,J)*HR2-TT(1,J)*AT(2,J)+F
      DT(2,NI)=(-2)*ZB(2)*TT(2,N)-VX(2,NI)*HR2-TT(1,1)*AT(2,
     *  NI)+F
      QT(2,1 )=CT(2,1 )/BVTS(2,1 )
      QT(2,J)=DT(2,J)/BVTS(2,J)
      QT(2,NI)=DT(2,NI)/BVTS(2,NI)
      DO 99 I=3,M
      DT(I,1 )=(-2)*ZB(I)*TT(I,2)-VX(I,1 )*HR2+F
      DT(I,J)=(ZC(I)*PR*VC(I,J)-ZB(I))*TT(I,J+1)-(ZB(I)+ZC(I
     *  )*PR*VC(I,J)
     C)*TT(I,J-1)-VX(I,J)*HR2+F
      DT(I,NI)=(-2)*ZB(I)*TT(I,N)-VX(I,NI)*HR2+F
      QT(I,1 )=(DT(I,1 )-AT(I,1 )*QT(I-1,1 ))/(BVTS(I,1 )-AT
     *  (I,1 )*
     CPT(I-1,1))
      QT(I,J)=(DT(I,J)-AT(I,J)*QT(I-1,J))/(BVTS(I,J)-AT(I,J)
     *  *PT(I-1,J))
      QT(I,NI)=(DT(I,NI)-AT(I,NI)*QT(I-1,NI))/(BVTS(I,NI)-AT
     *  (I,NI)*
     CPT(I-1,NI))
   99 CONTINUE
      TT(M,1 )=QT(M,1)
      TT(M,J)=QT(M,J)
      TT(M,NI)=QT(M,NI)
      DO 3 II=2,MD
      I=MI-II
      TT(I,1 )=QT(I,1 )-PT(I,1 )*TT(I+1,1 )
```

```
      TT(I,J)=GT(I,J)-PT(I,J)*TT(I+1,J)
    3 TT(I,NI)=GT(I,NI)-PT(I,NI)*TT(I+1,NI)
   55 CONTINUE
      DO 77 J=1,NI
      DO 77 I=1,M
      DTT=OMEGA*(TT(I,J)-T(I,J))
      T(I,J)=T(I,J)+DTT
   77 CONTINUE
      RETURN
      END
```

```
C      SUBROUTINE SUEVS IS TO SOLVE THE VORTICITY EQUATION
C      AND MOMENTUM EQUATION FOR SECONDARY FLOW IN EQ. (2-7)
C      AND (2-8) USING BOUNDARY VORTICITY METHOD
C
C
C
      SUBROUTINE SUEVS(S,VO,SS,AS,CS,PS,AVX,CVX,PVX)
      DIMENSION VX(31,31),T(31,31),VR(31,31),VO(31,31),BVTS(
     *  31,31),
     2AS(31,31),CS(31,31),PS(31,31),QS(31,31),AVX(31,31),CVX
     *  (31,31),
     3PVX(31,31),QVO(31,31),VO(31,31),DS(31,31),SMI(3),VMI(3
     *  ),
     CCITA(31),R(31),ZA(31),ZB(31),ZC(31),DVO(31,31),TRA(31,
     *  31)
     4,SS(31,31),S(31,31)
      INTEGER*4 M,N,MI,NI,ND,MD,MSTD,NO
      COMMON HR,HR2,HC,HC2,AF,RAC,RA,PR,STD,CK,ZA,ZB,ZC,R,CI
     *  TA,BVTS,
     1VX,T,VR,VO,OMEG1,OMES
      COMMON M,N,MI,NI,ND,MD,MSTD,NC
      DO 17 J=2,N
      DO 10 I=2,M
      TRA(I,J)=RAC*COS(AF)*(SIN(CITA(J))*(T(I+1,J)-T(I-1,J))
     *  *(HR/2)+
     COS(CITA(J))*(T(I,J+1)-T(I,J-1))*ZC(I))
 10   CONTINUE
      K=0
      VMI(1)=0.0
 20   K=K+1
      VO(MI,J)=VMI(K)
      DO 9 I=2,M
      DVO(I,J)=TRA(I,J)-(ZB(I)+ZC(I)*VC(I,J))*VO(I,J-1)-(ZB(
     *  I)-
     CZC(I)*VC(I,J))*VC(I,J+1)
      IF(I.EQ.M) DVO(I,J)=TRA(I,J)-(ZB(I)+ZC(I)*VC(I,J))*VO(
     *  I,J-1)-(ZB(I
     C)-ZC(I)*VC(I,J))*VO(I,J+1)-CVX(I,J)*VO(MI,J)
  9   CONTINUE
      QVO(2,J)=DVO(2,J)/BVTS(2,J)
      DO 8 I=3,M
  8   QVO(I,J)=(DVO(I,J)-AVX(I,J)*QVO(I-1,J))/(BVTS(I,J)-AVX
     *  (I,J)*
     CPVX(I-1,J))
      VO(M,J)=QVC(M,J)
      DO 4 II=2,MD
      I=MI-II
  4   VO(I,J)=QVO(I,J)-PVX(I,J)*VO(I+1,J)
      DO 3 I=2,M
      DS(I,J)=(-1)*(ZB(I)*(SS(I,J-1)+SS(I,J+1)))+HR2*VO(I,J)
      IF(I.EQ.2) GO TO 2
      QS(I,J)=(DS(I,J)-AS(I,J)*QS(I-1,J))/(BVTS(I,J)-AS(I,J)
     *  *PS(I-1,J))
```

```
 2 QS(2,J)=DS(2,J)/EVTS(2,J)
 3 CONTINUE
   DS(MI,J)=(-1)*(ZE(MI)*(SS(MI,J-1)+SS(MI,J+1)))+HR2*VO(
  *  MI,J)
   QS(MI,J)=(DS(MI,J)-AS(MI,J)*QS(M,J))/(BVTS(MI,J)-AS(MI
  *  ,J)*PS(M,J))
   SMI(K)=QS(MI,J)
   IF(K-2) 50,51,52
50 VMI(2)=-100.0
   GO TO 20
51 VMI(3)=100*SMI(1)/(SMI(2)-SMI(1))
   GO TO 20
52 SS(MI,J)=SMI(K)
   DO 18 II=1,MD
   I=MI-II
18 SS(I,J)=QS(I,J)-PS(I,J)*SS(I+1,J)
17 CONTINUE
   DO 78 J=2,N
   DO 78 I=2,MI
   DI=OMES*(SS(I,J)-S(I,J))
   S(I,J)=S(I,J)+DI
78 CONTINUE
   RETURN
   END
```

```
C      SUBROUTINE SUBVRC TO TO SOLVE THE SECONDARY VELOCITY U
C      AND V FROM THE DEFINITION OF STREAM FUNCTION
C
C
C
      SUBROUTINE SUBVRC(S,ERROR)
      DIMENSION VX(31,31),T(31,31),VR(31,31),VC(31,31),BVTS(
     *  31,31),
     CCITA(31),R(31),ZA(31),ZB(31),ZC(31),VVR(31,31),VVC(31,
     *  31)
     2,S(31,31)
      INTEGER*4 M,N,MI,NI,ND,MC,MSTD,NO
      COMMON HR,HR2,HC,HC2,AF,FAC,RA,PR,STD,DK,ZA,ZB,ZC,R,CI
     *  TA,BVTS,
     1VX,T,VR,VC,CNEG1,ONES
      COMMON M,N,MI,NI,ND,MD,MSTD,NO
      DO 10 I=2,M
      RH6=R(I)*HC*6
      RH12=R(I)*HC*12
      VVR(I,1)=(8*S(I,2)-S(I,3))/RH6
      VVR(I,2)=(-S(I,2)+8*S(I,3)-S(I,4))/RH12
      VVR(I,NI)=(S(I,ND)-8*S(I,N))/RH6
      VVR(I,N)=(S(I,N-2)-8*S(I,ND)+S(I,N))/RH12
      DO 10 J=3,ND
      VVR(I,J)=(S(I,J-2)-8*S(I,J-1)+8*S(I,J+1)-S(I,J+2))/RH1
     *  2
   10 CONTINUE
      HR12=HR*12
      DO 9 J=2,N
      VVC(2,J)=(10*S(2,J)-18*S(3,J)+6*S(4,J)-S(5,J))/HR12
      VVC(M,J)=(S(M-3,J)-6*S(M-2,J)+18*S(M-1,J)-10*S(M,J)-3*
     *  S(M+1,J))/
     CHR12
      DO 9 I=3,MD
      VVC(I,J)=(S(I+2,J)-8*S(I+1,J)+8*S(I-1,J)-S(I-2,J))/HR1
     *  2
    9 CONTINUE
      VVR(1,1)=(8*S(2,N/2+1)-S(3,N/2+1))/(6*HR)
      DO 8 J=1,NI
      VVC(1,J)=0.0
    8 VVR(1,J)=VVR(1,1)
      DO 7 I=2,M
      VVC(I,1)=0.0
    7 VVC(I,NI)=0.0
      SD=0.0
      SUM=0.0
      DO 6 I=1,M
      DO 6 J=1,NI
      DVR=VVR(I,J)-VR(I,J)
      DVC=VVC(I,J)-VC(I,J)
      SD=SD+ABS(DVR)+ABS(DVC)
      SUM=SUM+ABS(VVC(I,J))+ABS(VVR(I,J))
```

```
      VR(I,J)=VVR(I,J)
      VC(I,J)=VVC(I,J)
    6 CONTINUE
      ERROR=SC/SUM
      RETURN
      END
```

```
C      SUBROUTINE TANK IS TO CALCULATE THE NUSSELT NUMBER,
C      FRICTION FACTOR
C
C
C
C      BUKT: BULK TEMPERATURE
C      FRE1: PRODUCTION OF FRICTION FACTOR AND REYNOLDS NO.
C            OF 1ST EXPRESSION
C      FRE2: PRODUCTION OF FRICTION FACTOR AND REYNOLDS NO.
C            OF 2ND EXPRESSION
C      NU1 : NUSSELT NUMBER OF 1ST EXPRESSION
C      NU2 : NUSSELT NUMBER OF 2ND EXPRESSION
C      SGT : GRADIENT OF TEMPERATURE ALONG WALL
C      SGVX: GRADIENT OF AXIAL VELOCITY ALONG WALL
C      STP : AVERAGE TEMPERATURE
C      SVXP: AVERAGE AXIAL VELOCITY
C
       SUBROUTINE TANK(SVXP,SVXT,SGT,SGVX,BUKT,FRE1,FRE2,UN1,
     *  UN2,RERA,
     CRFE1,RFE2,RNU1,RNU2,ARNU,STP,FRE3,AVEN,AVEF,RFE12,RFE3
     *  ,FM)
       DIMENSION VX(31,31),T(31,31),VR(31,31),VC(31,31),BVTS(
     *  31,31),
     2GT(31),GVX(31),VXP(31),VXT(31),TS(31),
     CCITA(31),R(31),ZA(31),ZB(31),ZC(31)
       INTEGER*4 M,N,MI,NI,ND,MD,MSTD,NO
       COMMON HR,HR2,HC,HC2,AF,RAC,RA,PR,STD,CK,ZA,ZB,ZC,R,CI
     *  TA,BVTS,
     1VX,T,VR,VC,CMEG1,CMES
       COMMON M,N,MI,NI,ND,MD,MSTD,NO
       PI=3.1415927
       DO 10 J=1,NI
       GT(J)=-(T(M-3,J)/4-4*T(M-2,J)/3+3*T(MD,J)-4*T(M,J))/HR
       GVX(J)=-(VX(M-3,J)/4-4*VX(M-2,J)/3+3*VX(MD,J)-4*VX(M,J
     *  ))/HR
    10 CONTINUE
       SGT=GT(1)+GT(NI)
       SGVX=GVX(1)+GVX(NI)
       DO 9 J=2,N,2
       SGT=SGT+GT(J)*4
       SGVX=SGVX+GVX(J)*4
     9 CONTINUE
       DO 8 J=3,ND,2
       SGT=SGT+GT(J)*2
     8 SGVX=SGVX+GVX(J)*2
       SGT=HC*SGT/(3*PI)
       SGVX=HC*SGVX/(3*PI)
       DO 7 I=2,M
       VXT(I)=VX(I,1)*T(I,1)+VX(I,NI)*T(I,NI)
       TS(I)=T(I,1)+T(I,NI)
       VXP(I)=VX(I,1)+VX(I,NI)
       DO 6 J=2,N,2
```

```
      VXT(I)=VXT(I)+VX(I,J)*T(I,J)*4
      TS(I)=TS(I)+T(I,J)*4
    6 VXP(I)=VXP(I)+VX(I,J)*4
      DO 5 J=3,ND,2
      VXT(I)=VXT(I)+VX(I,J)*T(I,J)*2
      TS(I)=TS(I)+T(I,J)*2
    5 VXP(I)=VXP(I)+VX(I,J)*2
      VXT(I)=HC*VXT(I)/3
      TS(I)=HC*TS(I)/3
      VXP(I)=HC*VXP(I)/3
    7 CONTINUE
      SVXT=0.0
      STP=0.0
      SVXP=0.0
      DO 4 I=2,M,2
      SVXT=SVXT+VXT(I)*R(I)*4
      STP=STP+TS(I)*R(I)*4
    4 SVXP=SVXP+VXP(I)*R(I)*4
      DO 3 I=3,MD,2
      SVXT=SVXT+VXT(I)*R(I)*2
      STP=STP+TS(I)*R(I)*2
    3 SVXP=SVXP+VXP(I)*R(I)*2
      SVXT=HR*SVXT*2/(3*PI)
      STP=HR*STP*2/(3*PI)
      SVXP=HR*SVXP*2/(3*PI)
      BUKT=SVXT/SVXP
      FRE1=4*SQVX/SVXP
      FRE2=8*(1-SIN(AF)*RA*STP/4)/SVXP
      FRE3=8.0/SVXP
      UN1=2*SVXP*SGT/SVXT
      UN2=SVXP**2/SVXT-FM*(1/BUKT)
      RERA=2*SVXP*RAC
      RFE1=FRE1/16
      RFE2=FRE2/16
      RFE3=FRE3/16
      RNU1=UN1*11/48
      RNU2=UN2*11/48
      ARNU=(RNU1+RNU2)/2
      AVEN=(UN1+UN2)/2
      AVEF=(FRE1+FRE2)/2
      RFE12=(RFE1+RFE2)/2
      RETURN
      END
```

APPENDIX C

NUMERICAL RESULTS

Table 1 Numerical Results for Pr = 0.75, ReRa = 4,000 and F = 0 with $(fRe)_0 = 16$, $(Nu)_0 = 48/11$

α	Ra	$\bar{w}$	$\bar{\theta} \times 10$	f Re	$fRe/(fRe)_0$	Nu	$Nu/(Nu)_0$
0°	any value	0.4669	0.7115	17.13	1.071	4.814	1.103
10°	4	0.4606	0.7038	17.15	1.072	4.803	1.101
	10	0.4509	0.6904	17.21	1.076	4.798	1.100
	40	0.4057	0.6268	17.57	1.098	4.781	1.096
	100	0.3352	0.5241	18.42	1.151	4.779	1.095
	400	0.1768	0.2741	23.70	1.481	5.097	1.168
	1,000	0.0961	0.1388	33.06	2.066	5.967	1.367
	4,000	0.0358	0.0416	61.75	3.860	8.756	2.007
	7,000	0.0240	0.0250	80.05	5.003	10.262	2.352
20°	4	0.4554	0.6999	17.14	1.071	4.777	1.095
	10	0.4365	0.6732	17.27	1.079	4.770	1.093
	40	0.3579	0.5596	18.07	1.129	4.758	1.090
	100	0.2593	0.4087	20.06	1.254	4.830	1.107
	400	0.1134	0.1678	30.03	1.877	5.670	1.299
	1,000	0.0594	0.0782	44.56	2.785	7.120	1.632
	4,000	0.0221	0.0224	84.58	5.286	10.600	2.429
	10,000	0.0114	0.0095	129.96	8.122	13.543	3.104

Table 1 - continued Pr = 0.75, ReRa = 4,000 and F = 0

α	Ra	$\bar{w}$	$\bar{\theta}$ x 10	f Re	$fRe/(fRe)_0$	Nu	$Nu/(Nu)_0$
30°	4	0.4515	0.6997	17.10	1.068	4.737	1.086
	10	0.4238	0.6600	17.31	1.082	4.730	1.084
	40	0.3209	0.5066	18.61	1.163	4.744	1.087
	100	0.2136	0.3357	21.72	1.357	4.929	1.130
	400	0.0870	0.1236	35.11	2.195	6.171	1.414
	1,000	0.0453	0.0560	53.04	3.315	7.951	1.822
	4,000	0.0168	0.0158	100.96	6.310	11.742	2.691
	10,000	0.0087	0.0067	155.66	9.729	14.978	3.432
45°	4	0.4479	0.7062	16.96	1.060	4.654	1.066
	10	0.4090	0.6478	17.32	1.082	4.654	1.066
	40	0.2812	0.4479	19.43	1.214	4.744	1.087
	100	0.1744	0.2710	23.88	1.493	5.093	1.167
	400	0.0680	0.0922	40.89	2.556	6.752	1.547
	1,000	0.0354	0.0410	62.27	3,892	8.801	2.017
	4,000	0.0130	0.0114	119.97	7.498	12.902	2.957
60°	4	0.4469	0.7199	16.78	1.049	4.550	1.043
	10	0.3979	0.6425	17.30	1.081	4.5691	1.047
	40	0.2564	0.4100	20.11	1.257	4.759	1.091
	100	0.1535	0.2359	25.49	1.593	5.231	1.199
	400	0.0589	0.0774	44.82	2.801	7.146	1.638

Table 1 - continued Pr = 0.75, ReRa = 4,000 and F = 0

α	Ra	$\bar{w}$	$\bar{\theta}$ x 10	f Re	$fRe/(fRe)_0$	Nu	$Nu/(Nu)_0$
60°	1,000	0.0306	0.0341	68.40	4.275	9.331	2.138
	4,000	0.0113	0.0094	130.74	8.171	13.589	3.114
75°	4	0.4476	0.7368	16.60	1.037	4.449	1.019
	10	0.3914	0.6421	17.26	1.079	4.497	1.031
	40	0.2428	0.3888	20.56	1.285	4.773	1.094
	100	0.1430	0.2181	26.46	1.654	5.319	1.219
	400	0.0544	0.0703	47.11	2.945	7.374	1.690
	1,000	0.0283	0.0309	71.95	4.497	9.624	2.206
	4,000	0.0104	0.0085	137.69	8.605	13.989	3.206
90°	1	0.4858	0.8097	16.13	1.008	4.373	1.002
	4	0.4485	0.7450	16.51	1.032	4.405	1.010
	10	0.3892	0.6428	17.25	1.078	4.468	1.024
	40	0.2385	0.3821	20.72	1.295	4.779	1.095
	100	0.1398	0.2127	26.79	1.674	5.349	1.226
	400	0.0531	0.0682	47.87	2.992	7.449	1.707
	1,000	0.0276	0.0299	73.12	4.570	9.719	2.227
	4,000	0.0102	0.0082	139.98	8.749	14.118	3.235

Table 2 Numerical Results for Pr = 0.75, ReRa = 10,000 and F = 0

α	Ra	$\bar{w}$	$\bar{\theta}$ x 10	f Re	$fRe/(fRe)_0$	Nu	$Nu/(Nu)_0$
0°	any	0.4330	0.5952	18.47	1.154	5.402	1.238
10°	4	0.4287	0.5913	18.46	1.154	5.384	1.234
	10	0.4216	0.5831	18.49	1.156	5.374	1.232
	40	0.3879	0.5428	18.67	1.167	5.332	1.222
	100	0.3319	0.4743	19.14	1.196	5.264	1.206
	400	0.1811	0.2725	23.25	1.453	5.243	1.201
	1,000	0.0964	0.1391	32.85	2.053	5.957	1.365
	4,000	0.0358	0.0417	61.74	3.859	8.754	2.006
	10,000	0.0186	0.0180	94.51	5.907	11.30	2.591
20°	4	0.4256	0.5914	18.41	1.151	5.344	1.225
	10	0.4118	0.5750	18.47	1.154	5.325	1.220
	40	0.3507	0.5004	18.90	1.181	5.254	1.204
	100	0.2642	0.3895	20.18	1.261	5.177	1.186
	400	0.1141	0.1684	29.72	1.857	5.671	1.300
	1,000	0.0594	0.0783	44.53	2.783	7.112	1.630
	4,000	0.0221	0.0224	84.57	5,286	10.600	2.429
	10,000	0.0114	0.0095	129.96	8.122	13.54	3.104
30°	4	0.4240	0.5959	18.30	1.144	5.279	1.210
	10	0.4033	0.5708	18.41	1.151	5.255	1.204
	40	0.3200	0.4663	19.16	1.200	5.167	1.184

Table 2 - continued Pr = 0.75, ReRa = 10,000 and F = 0

α	Ra	$\bar{w}$	$\bar{\theta}$ x 10	f Re	$fRe/(fRe)_0$	Nu	$Nu/(Nu)_0$
30°	100	0.2187	0.3295	21.50	1.344	5.140	1.178
	400	0.0871	0.1238	34.99	2.187	6.160	1.412
	1,000	0.0453	0.0560	53.05	3.315	7.949	1.822
	4,000	0.0168	0.0158	100.95	6.310	11.742	2.691
45°	4	0.4244	0.6122	18.03	1.127	5.132	1.176
	10	0.3946	0.5746	18.21	1.138	5.102	1.169
	40	0.2842	0.4281	19.61	1.226	5.031	1.153
	100	0.1769	0.2704	23.60	1.475	5.169	1.185
	400	0.0680	0.0922	40.86	2.554	6.746	1.546
	1,000	0.0354	0.0410	62.27	3.892	8.801	2.017
	4,000	0.0131	0.0114	118.80	7.425	12.88	2.951
60°	4	0.4291	0.6439	17.60	1.100	4.915	1.126
	10	0.3896	0.5906	17.90	1.119	4.891	1.121
	40	0.2590	0.4023	20.11	1.257	4.905	1.124
	100	0.1543	0.2360	25.34	1.584	5.251	1.203
	400	0.0588	0.0774	44.82	2.801	7.145	1.637
	1,000	0.0306	0.0341	68.40	4.275	9.331	2.138
	4,000	0.0113	0.0094	130.74	8.171	13.59	3.114
75°	4	0.4393	0.6978	16.98	1.061	4.622	1.059
	10	0.3884	0.6197	17.51	1.094	4.635	1.062

Table 2 - continued Pr = 0.75, ReRa = 10,000 and F = 0

α	Ra	$\bar{w}$	$\bar{\Theta}$ x 10	f Re	$fRe/(fRe)_0$	Nu	$Nu/(Nu)_0$
75°	40	0.2437	0.3872	20.54	1.284	4.812	1.103
	100	0.1431	0.2182	26.43	1.652	5.323	1.220
	400	0.0544	0.0703	47.11	2.945	7.374	1.690
	1,000	0.0283	0.0309	71.95	4.497	9.624	2.206
	4,000	0.0104	0.0085	137.69	8.605	13.988	3.206

Table 3 Numerical Results for Pr = 0.75, α = 45° and F = 0

ReRa	Ra	$\bar{w}$	θ x 10	f Re	$fRe/(fRe)_0$	Nu	$Nu/(Nu)_0$
1,000	1	0.4879	0.8085	16.16	1.010	4.398	1.008
	4	0.4479	0.7062	16.78	1.049	4.427	1.015
	10	0.4154	0.6852	16.92	1.058	4.456	1.021
	40	0.2798	0.4525	19.42	1.214	4.670	1.070
	100	0.1738	0.2709	23.96	1.497	5.080	1.164
	400	0.0680	0.0922	40.90	2.556	6.753	1.548
	1,000	0.0354	0.0410	62.26	3.891	8.801	2.017
	4,000	0.0131	0.0114	118.80	7.425	12.877	2.951
$5x10^4$	10	0.3550	0.4226	20.85	1.303	6.403	1.467
	40	0.2834	0.3491	21.26	1.329	6.252	1.433
	100	0.1936	0.2526	22.86	1.429	6.048	1.386
	400	0.0682	0.0932	39.95	2.497	6.626	1.518
	1,000	0.0353	0.0410	62.28	3.893	8.791	2.015
	4,000	0.0131	0.0114	118.80	7.425	12.877	2.951

Table 4 Numerical Results for $\alpha = 0°$, Pr = 0.75 and F = 0

$Re Ra \times 10^3$	$\bar{w}$	$\bar{\theta} \times 10$	$\overline{w\theta}/\bar{w}$	f Re	$fRe/(fRe)_0$	Nu	$Nu/(Nu)_0$
0.1	0.4997	0.8335	0.1146	16.01	1.001	4.364	1.000
0.4	0.4990	0.8314	0.1143	16.03	1.002	4.370	1.001
1	0.4953	0.8170	0.1122	16.15	1.009	4.416	1.012
4	0.4669	0.7115	0.0970	17.13	1.071	4.814	1.103
10	0.4330	0.5952	0.0801	18.47	1.154	5.402	1.238
40	0.3804	0.4406	0.0579	21.03	1.315	6.577	1.507
80	0.3549	0.3766	0.0489	22.55	1.409	7.267	1.665
100	0.3466	0.3571	0.0462	23.09	1.443	7.505	1.720

Table 5 Numerical Results for $\alpha = 90°$ and $F = 0$

Ra	$\bar{w}$	$\bar{\theta} \times 10$	$\overline{w\theta}/\bar{w}$	f Re	$fRe/(fRe)_0$	Nu	$Nu/(Nu)_0$
1	0.4858	0.8097	0.1112	16.13	1.008	4.373	1.002
4	0.4485	0.7450	0.1019	16.51	1.032	4.405	1.010
10	0.3892	0.6428	0.0872	17.25	1.078	4.468	1.024
40	0.2385	0.3821	0.0499	20.72	1.295	4.779	1.095
100	0.1398	0.2127	0.0261	26.78	1.674	5.349	1.226
400	0.0531	0.0682	0.0071	47.87	2.992	7.449	1.707
1,000	0.0276	0.0299	0.0028	73.12	4.570	9.719	2.227
4,000	0.0102	0.0082	0.0007	139.98	8.749	14.176	3.235

Note: The numerical result is independent of Pr and Re for $\alpha = 90°$.

Table 6 Numerical Results for Pr = 10, Re = 20 and F = 0

Ra	α	$\bar{w}$	$\bar{\theta}$ x 10	f Re	$fRe/(fRe)_0$	Nu	$Nu/(Nu)_0$
1	0	0.4997	0.8333	16.01	1.000	4.365	1.000
	15	0.4960	0.8269	16.04	1.002	4.368	1.001
	30	0.4927	0.8211	16.07	1.004	4.370	1.001
	45	0.4899	0.8170	16.09	1.006	4.369	1.001
	60	0.4877	0.8133	16.11	1.007	4.370	1.001
	75	0.4864	0.8111	16.13	1.008	4.371	1.002
4	0	0.4997	0.8275	16.01	1.000	4.403	1.009
	15	0.4854	0.8038	16.13	1.008	4.408	1.010
	30	0.4728	0.7834	16.25	1.016	4.410	1.011
	45	0.4625	0.7670	16.36	1.022	4.409	1.010
	60	0.4548	0.7551	16.44	1.027	4.406	1.010
	75	0.4500	0.7479	16.49	1.031	4.404	1.009
10	0	0.4996	0.8019	16.01	1.001	4.570	1.047
	15	0.4665	0.7518	16.31	1.020	4.562	1.046
	30	0.4389	0.7115	16.60	1.038	4.543	1.041
	45	0.4172	0.6809	16.86	1.054	4.517	1.035
	60	0.4017	0.6596	17.07	1.067	4.492	1.029
	75	0.3923	0.6470	17.20	1.075	4.474	1.025
40	0	0,4986	0.6955	16.04	1.003	5.402	1.238
	15	0.4006	0.5768	16.99	1.062	5.266	1.207
	30	0.3340	0.4960	18.01	1.125	5.131	1.176

Table 6 - continued Pr = 10, Re = 20 and F = 0

Ra	α	$\bar{w}$	$\bar{\theta}$ x 10	f Re	$fRe/(fRe)_0$	Nu	$Nu/(Nu)_0$
40	45	0.2892	0.4419	19.01	1.188	5.003	1.147
	60	0.2602	0.4074	19.89	1.243	4.891	1.121
	75	0.2437	0.3881	20.50	1.281	4.809	1.102
100	0	0.4962	0.6097	16.12	1.007	6.269	1.437
	15	0.3222	0.4239	18.02	1.126	5.946	1.363
	30	0.2337	0.3245	20.34	1.271	5.715	1.310
	45	0.1851	0.2678	22.75	1.422	5.548	1.272
	60	0.1580	0.2351	24.85	1.553	5.436	1.246
	75	0.1440	0.2180	26.29	1.643	5.372	1.231
400	0	0.4900	0.4903	16.32	1.020	7.936	1.819
	15	0.1694	0.2026	22.47	1.404	7.017	1.608
	30	0.0967	0.1247	31.14	1.946	6.833	1.566
	45	0.0707	0.0928	38.92	2.433	6.967	1.597
	60	0.0595	0.0775	44.14	2.759	7.203	1.651
	75	0.0546	0.0703	46.97	2.936	7,384	1.692
1,000	15	0.0876	0.1015	31.33	1.958	7.806	1.789
	30	0.0471	0.0564	49.93	3.121	8.167	1.871
	45	0.0356	0.0411	61.51	3.844	8.849	2.028
	60	0.0307	0.341	68.22	4.264	9.344	2.141
	75	0.0283	0.0309	71.92	4.495	9.627	2.206

Table 7 Numerical Results for Pr = 0.75, Re = 100 and F = 0

α	Ra	$\bar{w}$	$\bar{\theta}$ x 10	f Re	$fRe/(fRe)_0$	Nu	$Nu/(Nu)_0$
0°	1	0.4997	0.8335	16.01	1.001	4.363	1.000
	4	0.4989	0.8305	16.03	1.002	4.372	1.002
	10	0.4951	0.8165	16.15	1.010	4.418	1.013
	40	0.4667	0.7102	17.13	1.071	4.819	1.104
	100	0.4318	0.5932	18.51	1.157	5.413	1.239
	400	0.3803	0.4403	21.03	1.315	6.578	1.508
	1,000	0.3436	0.3514	23.17	1.448	7.528	1.725
45°	1	0.4898	0.8164	16.10	1.006	4.370	1.002
	4	0.4621	0.7683	16.37	1.023	4.398	1.007
	10	0.4153	0.6853	16.92	1.058	4.455	1.021
	40	0.2811	0.4474	19.44	1.215	4.748	1.088
	100	0.1768	0.2703	23.60	1.475	5.170	1.185
	400	0.0681	0.0929	40.32	2.520	6.664	1.527
	1,000	0.0352	0.0410	62.33	3.896	8.756	2.007

Table 8 Numerical Results for Pr = 0.75, Re = 100 and F = 10

α	Ra	$\bar{w}$	$\bar{\theta}$ x 10	f Re	$fRe/(fRe)_0$	Nu	$Nu/(Nu)_0$
0°	1	0.4997	0.7086	16.01	1.000	4.084	0.9359
	4	0.4992	0.7073	16.02	1.001	4.088	0.9369
	10	0.4961	0.6959	16.12	1.007	4.125	0.9452
	40	0.4713	0.6069	16.96	1.060	4.453	1.0205
	100	0.4402	0.5039	18.17	1.136	4.963	1.1373
	400	0.3872	0.3578	20.61	1.288	6.024	1.3805
	1,000	0.3567	0.2859	22.43	1.402	6.837	1.5668
45°	1	0.4912	0.6940	16.08	1.005	4.085	0.9361
	4	0.4675	0.6530	16.32	1.020	4.089	0.9371
	10	0.4275	0.5820	16.78	1.049	4.107	0.9412
	40	0.3126	0.3777	18.74	1.171	4.191	0.9604
	100	0.2243	0.2260	21.40	1.338	4.214	0.9658
	400	0.1338	0.0758	27.76	1.735	3.637	0.8335
	1,000	0.1077	0.0323	31.94	1.996	2.025	0.4641
90°	1	0.4879	0.6882	16.11	1.007	4.085	0.9361
	4	0.4559	0.6333	16.43	1.027	4.088	0.9368
	10	0.4053	0.5455	17.04	1.065	4.096	0.9387
	40	0.2767	0.3224	19.58	1.224	4.115	0.9431
	100	0.1929	0.1777	23.03	1.440	4.069	0.9325
	400	0.1213	0.0549	29.72	1.858	3.225	0.7390
	1,000	0.1023	0.0230	33.26	2.079	0.894	0.2049

Table 9 Numerical Results for Pr = 0.75, Re = 100 and F = 20

α	Ra	$\bar{w}$	$\bar{\theta}$ x 10	f Re	$fRe/(fRe)_0$	Nu	$Nu/(Nu)_0$
0°	1	0.4997	0.5838	16.01	1.000	3.690	0.8457
	4	0,4994	0.5828	16.02	1.001	3.693	0.8464
	10	0.4970	0.5746	16.09	1.006	3.717	0.8519
	40	0.4764	0.5032	16.78	1.049	3.958	0.9071
	100	0.4479	0.4479	17.86	1.116	4.362	0.9996
	400	0.3995	0.2825	20.02	1.251	5.207	1.1932
	1,000	0.3669	0.2120	21.72	1.358	5.832	1.3365
45°	1	0.4927	0.5716	16.07	1.004	3.683	0.8439
	4	0.4730	0.5376	16.27	1.017	3.659	0.8386
	10	0.4398	0.4788	16.65	1.040	3.620	0.8296
	40	0.3443	0.3085	18.16	1.135	3.422	0.7841
	100	0.2717	0.1821	19.96	1.247	2.927	0.6708
	400	0.1991	0.0587	23.51	1.469	- 0.051	- 0.0116
	1,000	0.1799	0.0236	26.01	1.625	- 1.402	- 1.4396
90°	1	0.4899	0.5668	16.10	1.006	3.679	0.8431
	4	0.4633	0.5211	16.36	1.023	3.644	0.8352
	10	0.4213	0.4481	16.86	1.053	3.577	0.8196
	40	0.3149	0.2631	18.71	1.170	3.211	0.7359
	100	0.2461	0.1428	20.89	1.306	2.414	0.5531
	400	0.1895	0.0416	24.63	1.540	- 0.430	- 0.4348
	1,000	0.1767	0.0161	27.13	1.695	-10.665	- 2.4441

Table 10 Comparison of Numerical Results Using Two Alternative Expressions for fRe and Nu with Pr = 5, Re = 100 and F = 10

α	Ra	$\bar{w}$	$\overline{w\theta}$ x 10	$(fRe)_1$	$(fRe)_2$	$(Nu)_1$	$(Nu)_2$
0°	10	0.4974	0.8529	16.075	16.082	4.6566	4.6597
	40	0.4899	0.6745	16.326	16.331	5.7797	5.7807
	100	0.4799	0.5642	16.665	16.670	6.7364	6.7333
45°	10	0.4320	0.7566	16.688	16.695	4.3874	4.3877
	40	0.3328	0.4657	17.997	18.003	4.9980	4.9992
	100	0.2475	0.2781	19.797	19,802	5.3060	5.3026
	400	0.1441	0.0932	25.012	25.052	4.7932	4.7786
	1,000	0.1107	0.0394	29.736	29.736	2.7678	2.7660
90°	10	0.4054	0.7460	17.034	17.041	4.1005	4.0940
	40	0.2766	0.4296	19.570	19.593	4.1180	4.1128
	100	0.1929	0.2285	23.019	23.045	4.0719	4.0667
	400	0.1213	0.0663	29.713	29.732	3.2361	3.2313
	1,000	0.1021	0.0271	33.398	33.358	1.0049	0.9057

Table 11 Comparison of Numerical Results Using Two Alternative Expressions for fRe and Nu with ReRa = 4,000, $\alpha = 45°$ and F = 0.

(a) Pr = 0.01

Ra	$(fRe)_1$	$(fRe)_2$	$fRe/(fRe)_0$	$(Nu)_1$	$(Nu)_2$	$Nu/(Nu)_0$
4	17.101	17.113	1.069	4.5011	4.4955	1.031
10	17.470	17.486	1.092	4.5259	4.5208	1.037
40	19.584	19.608	1.225	4.6933	4.6905	1.075
100	23.965	23.999	1.499	5.0851	5.0832	1.165
400	40.864	40.929	2.556	6.7569	6.7488	1.548
1,000	62.200	62.321	3.892	8.8130	8.7891	2.017
4,000	118.51	119.08	7.425	12.921	12.833	2.951
(b) Pr = 1.0						
4	16.903	16.908	1.057	4.7441	4.7412	1.087
10	17.255	17.265	1.079	4.7353	4.7316	1.085
40	19.348	19.376	1.210	4.7890	4.7867	1.097
100	23.817	23.850	1.490	5.1057	5.1038	1.170
400	40.857	40.920	2.556	6.7563	6.7478	1.547
1,000	62.203	62.308	3,892	8.8134	8.7892	2.017
4,000	118.51	119.08	7.425	12.921	12.833	2.951
(c) Pr = 5						
4	16.456	16.465	1.029	5.8655	5.8626	1.344
10	16.735	16.736	1.046	5.8154	5.8105	1.332

Table 11 - continued fRe and Nu with ReRa = 4,000, α = 45° and F = 0

(c) Pr = 5 cont.

Ra	$(fRe)_1$	$(fRe)_2$	$fRe/(fRe)_0$	$(Nu)_1$	$(Nu)_2$	$Nu/(Nu)_0$
40	18.435	18.441	1.152	5.6337	5.6288	1.290
100	22.649	22.671	1.416	5.5412	5.5369	1.269
400	40.699	40.760	2.546	6.7699	6.7612	1.550
1,000	62.196	62.321	3.891	8.8139	8.7896	2.017
4,000	118.52	119.08	7.425	12.921	12.833	2.951
(d) Pr = 10						
4	16.307	16.318	1.020	6.6022	6.6003	1.513
10	16.545	16.543	1.034	6.5452	6.5405	1.499
40	17.990	17.991	1.124	6.3181	6.3122	1.447
100	21.630	21.640	1.352	6.0887	6.0821	1.395
400	40.256	40.308	2.518	6.8187	6.8091	1.562
1,000	62.171	62.296	3.890	8.8156	8.7913	2.017
4,000	118.52	119.08	7.425	12.922	12.833	2.951
(e) Pr = 100						
400	32.178	32.198	2.012	8.3058	8.2865	1.901
1,000	59.564	59.674	3.726	9.0183	8.9933	2.064
4,000	118.49	119.06	7.423	12.879	12.835	2.952